Comparison of concentration performance and energy consumption by Reverse Osmosis, Electrodialysis and Vacuum Membrane Distillation for brine treatment

Master Thesis

Monique Woen

Delft University of Technology

TU Delft Delft University of Technology

Challenge the future

Comparison of concentration performance and energy consumption by Reverse Osmosis, Electrodialysis and Vacuum Membrane Distillation for brine treatment

Master Thesis

by

Monique Woen

in partial fulfillment of the requirements for the degree of

Master of Science in Civil Engineering

at the Delft University of Technology

This thesis is confidential and cannot be made public until August 26, 2024.

Student number:	4362942		
Thesis committee:	Dr. ir. S.G.J. Heijman,	chair and supervisor	TU Delft, Sanitary Engineering
	Dr. ir. N. van Linden,	daily supervisor	Lenntech
	Dr. ir. H. Spanjers,	supervisor	TU Delft, Sanitary Engineering
	Dr. ir. D.A. Vermaas,	external supervisor	TU Delft, Chemical Engineering

TU Delft

LENNTECH
WATER TREATMENT

Summary

The scarcity on clean freshwater and the growing need for potable and industrial process water is a universal concern that must be resolved by implementing strategies such as desalination. While seawater desalination has been a practice for a long time, brine producing industries progressively become the center of attention as they carry greater environmental consequences. Additional to water production, minimizing the production of waste in treatment of industrial brines must be targeted. Efficient membrane and thermal based technologies, or a combination of both, have been developed and are continuously improved for better performance. Despite the extensive literature that can be found on desalination performance per technology, limited information is available about the practical comparison of the technologies with regards to the brine concentration performance and associated energy consumption. This thesis study aims to contribute to bridging this knowledge gap by comparing reverse osmosis (RO), electrodialysis (ED) and vacuum membrane distillation (VMD), due to their relevance and potential in current industrial water treatment practices. A literature review was conducted to understand the principles of the different technologies, identify their key parameters that influence the brine performance and provide theoretical basis for the experimental design and work.

RO was studied by simulations using WAVE software, which is widely applied in practice, while ED and VMD were studied by performing lab-scale experiments. The concentration performance was assessed by the achieved concentration factor (CF). The energy consumption was expressed as kWh per m^3 concentrate production. The experimental performances of ED and VMD provided results close to reality. This allows drawing conclusions with more certainty compared to simulation methods. Therefore, this study contributes to engineering by industrial scale representation on lab-scale practices.

By performing RO simulations, the effect of feed concentration and net driving pressures on achieved concentration factors and energy consumption were examined. The WAVE simulation results show that the achieved CF was greatly influenced by the feed concentration. Applying higher net driving pressures results in higher recoveries and thus CF. Highest recoveries were achieved at the lowest feed concentration, whilst the lowest recoveries were achieved at the highest feed concentration.

By performing VMD experiments, the effect of feed concentration, operating temperatures and unsteady flow condition on achieved permeate fluxes, energy consumption and their distribution were examined. The associated vapour pressure for each test condition was simulated using the PHREEQC software. Increasing the operating temperature led to an increase in pure water permeate flux and a similar trend was observed using different feed concentration. However, a decrease in permeate flux was observed with increasing solute content in the feed, which is related to the vapour pressure lowering phenomena. Comparison of the pure water permeate flux and permeate fluxes obtained using synthetic NaCl solutions showed that the effect of operating temperature on permeate flux is greater than the effect of the feed concentration. Condensation contributed to the highest energy consumption (81%), followed by the vacuum pump (18.9%). In practice, efficient heating and cooling pumps result in a significant energy consumption decrease. Coefficient of performance (COP) values were considered for the thermal energy components, which reduced the overall energy consumption by 41%.

By performing ED experiments, the effect of feed concentration, applied current density (CD), cross-flow velocity and volume ratios on achieved concentration factors, mass transfer and its distribution, and energy consumption were examined. The operating principle of the ED experiments was 50% salt removal from the feed stream. Results show that increased salt concentration and cross-flow velocities resulted in higher limiting current densities. Furthermore, lower applied partial CD prolonged the operational time. Applying different CD did not influence the concentration factor, meaning that it is more advantageous to apply lower CD to achieve the same desalination from an energy saving point of view. Furthermore, the CF decreased with increasing feed concentration. This trend intensifies with increasing volume ratios. Results show that the dilution factors of the diluate were not equal to the concentration factors of the concentrate, which is related to the osmotic, electro-osmotic and salt mass transfer and its distribution. Results show that the osmotic water transport contribution decreased with increasing feed concentrations. However, the effect of absolute water transport became more significant at higher feed concentrations. This resulted in overall dilution of the concentrate stream and subsequently lower CF. The distribution of mass transport was similar for different volume ratios, meaning that higher CF can be achieved by applying higher volume ratios. Higher energy consumption was related to higher feed concentration, due to larger amount of salt transport. Furthermore,

higher volume ratios resulted in higher energy consumption due to the reduced concentrate volume.

RO, VMD and ED proved to be suitable technologies for concentrating NaCl feed solutions of between 20 and 80 g/L. RO and ED showed very similar concentration performance and energy consumption. A maximum salt concentration of 118 g/L was achieved by RO, whilst ED was able to reach a maximum salt concentration of 140 g/L. A notable difference is that RO was able to achieve higher CF with lower energy consumption compared to ED at feed concentrations lower than 60 g/L, while ED outperformed RO in terms of concentration performance and energy efficiency at higher feed concentrations. The overall energy consumption of ED and RO can be reduced by applying a multi-stage configuration. The VMD results showed that the average energy consumption to achieve a similar CF as RO and ED, increased by a factor of 61. The energy consumption by VMD is governed by the amount of water to be evaporation and thus this application is more advantageous at higher feed concentrations and even more so when waste heat is available. Considering all streams involved in these technologies, VMD and RO are suitable for cases that require high quality permeate whereas ED is not. As such, the technologies could also be applied together to minimize waste production, whilst prioritizing concentration.

Key limiting factors and their relation to energy consumption for brine concentration of RO, ED and VMD were successfully identified in this study. Furthermore, lab-scale experiments and simulations for a NaCl concentration range between 20 and 80 g/L were conducted to quantify and assess the different technologies based on concentration performance and associated energy consumption. This study serves as a foundation to broaden the current knowledge on brine treatment for the technologies RO, ED and VMD, and its results can be used case-by-case as a decision support tool for selecting a suitable brine treatment in larger treatment schemes.

Preface

This thesis was written as the final assignment required for completing my masters degree in civil engineering at the Delft University of Technology. The goal of this thesis was the comparison of membrane techniques with different driving forces with regard to their brine concentration and energy performances and was carried out in collaboration with Lenntech Water Treatment Solutions in Delfgauw. I want to express my sincere gratitude to Lenntech for giving me the opportunity and freedom to explore the practical application of water treatment technologies. Thank you for everyone at Lenntech who guided, supported, and kept me grounded through this journey. I would also like to thank my committee members for providing constructive feedback and expert opinions. I would like to give special thanks to the chair of the committee Bas Heijman for his patience and guidance throughout my thesis process. Furthermore, I would like to thank my daily supervisor Niels van Linden for your advises, discussions and trust. Finally, I want to thank my parents, family and friends who were always there to support me and always providing me with happiness and laughter. I owe thanks to a very special person, Maurice, for his continued support, patience and understanding during my pursuit of a MSc degree, which made the completion of this thesis possible.

Monique Woen
Delft, August 2022

Contents

List of Figures vii

List of Tables ix

Acronyms xiii

1 Introduction 1
1.1 Desalination for industry . . . 1
1.2 Research incentives and objective . . . 3
1.3 Research questions and approach . . . 3

2 Background 4
2.1 Reverse Osmosis . . . 4
2.1.1 Parameters influencing RO process . . . 5
2.1.2 RO energy estimation . . . 6
2.2 Vacuum Membrane Distillation . . . 6
2.2.1 Heat and mass transfer in VMD . . . 7
2.2.2 Parameters influencing VMD process . . . 9
2.2.3 Factors affecting VMD concentration performance . . . 10
2.2.4 VMD energy estimation . . . 11
2.3 Electrodialysis . . . 13
2.3.1 Mass transfer in ED . . . 13
2.3.2 Parameters influencing ED performance. . . . 14
2.3.3 Factors affecting ED concentration performance . . . 15
2.3.4 ED energy estimation . . . 16

3 Experimental apparatus and methods 17
3.1 Selection of simulation and experimental test conditions . . . 17
3.2 Measuring method and equipment . . . 18
3.3 Vacuum Membrane Distillation . . . 18
3.3.1 Set-up procedure and data collection . . . 19
3.3.2 Data processing . . . 19
3.4 Electrodialysis . . . 20
3.4.1 Set-up procedure, conditions and data collection . . . 21
3.4.2 Data processing . . . 21

4 Results and discussion 22
4.1 Simulation of the effect of limiting factors for concentrating NaCl solutions by RO . . . 22
4.2 Effect of NaCl concentration on electrical conductivity . . . 23
4.3 Limiting factors of concentrating NaCl solution using VMD. . . . 24
4.3.1 Influence of NaCl feed concentration on the bulk vapour pressure. . . . 24
4.3.2 Membrane distillation coefficient . . . 25
4.3.3 Effect of feed temperature and salinity on permeate flux. . . . 25
4.3.4 Energy distribution in VMD process . . . 26
4.4 Limiting factors of concentrating NaCl solution using ED. . . . 28
4.4.1 Influence of salt concentration and cross-flow velocity on LCD . . . 28
4.4.2 Effect of partial LCD on the concentration performance by ED . . . 28
4.4.3 Effect initial volume ratio on the concentration performance of ED . . . 30
4.5 Comparison of brine concentration performance: RO, ED and VMD . . . 32

5 Conclusions an Recommendations 34
5.1 Conclusions. . . . 34
5.2 Recommendation. . . . 35

Bibliography 37

A Literature review 43
A.1 Example from practice: BRINE-MINING 43
A.2 Chemical analysis of coal-mine brine composition 44
A.3 Treatment required prior to concentration 44

B Supplementary experimental material 46
B.1 Additional WAVE simulation data 46
B.2 Hydraulic conditions of spacer filled channels 47
B.3 Determination of Limiting Current Density in an ED cell 48
B.4 Effect of volume ratio on concentration factor and energy consumption 50
B.5 Experimental configuration: laboratory set-up 51
B.6 Superheated steam 52

List of Figures

2.1 (A) Schematic of RO process and (B) cross flow operation of a RO spiral wound module. Image by **?**] 4
2.2 Concentration polarization in RO 5
2.3 Practical energy consumption analysis of single-stage and multi-stage RO, based on feed concentration 600 mM and 100% salt rejection. Images by **?**] 6
2.4 Conventional MD configurations. Image by Kiss and Readi [1]. 7
2.5 Heat and mass transfer through membrane in VMD. 8
2.6 Molecular kinetic energy distribution by Boltzmann [2] 8
2.7 Schematic diagram of the working principle of electrodialysis by Miller [3] 13
2.8 Effect of current density on voltage drop, differentiating three regions: (I) Ohmic region, (II) LCD region and (III) over-limiting region. Image by Krol et al. [4]. 15

3.1 Vacuum MD configuration at laboratory scale, Lenntech (Delfgauw). (1) Feed and concentrate bottle, (2) heating and stirring block, (3) digital precision balance, (4) MD module, (5) gas washing bottle, (6) cooling bath, (7) EC probe, (8) multimeter and (9) external logging device. 19
3.2 Conventional ED configuration at laboratory scale, Lenntech (Delfgauw).(1) ED module with membrane stack of 10 cell-pairs, (2) concentrate bottle, (3) diluate bottle, (4) electrode rinse solution bottle, (5) power supply, (6) EC probe, (7) multimeter and (8) external logging device. . 20

4.1 Effect of constant feed pressure on permeate flux, recover and rejection (a), (c) and (e) and on the SEC and concentration factor (b), (d) and (f) for different feed concentrations 23
4.2 Electrical conductivity as a function of NaCl concentration. 24
4.3 Sub figure (a) presents the effect of operating temperature on the water vapour pressure of NaCl solutions and sub figure (b) presents the detailed data between temperatures 30 and 50 ^{o}C. . . . 25
4.4 Relationship between the permeate flux and vapour pressure difference for pure water. 25
4.5 Permeate flux of the membrane under three different operating temperatures (30, 40 and 50 ^{o}C), using three different NaCl starting concentrations (20, 40 and 50 g/L) and deionized water. 26
4.6 Sub figure (a) presents the effect of operating temperature and concentration factor on the energy consumption and sub figure (b) presents the energy distribution in VMD. 27
4.7 Sub figure (a) presents the effect of COP values for thermal components on the energy consumption for achieving different concentration factors and sub figure (b) presents the COP-adjusted energy distribution in VMD. 27
4.8 Effect of cross flow velocity on limiting current density different NaCl concentrations and cross flow velocities of 0.5 and 1 cm $\cdot s^{-1}$. 28
4.9 Sub figures (a),(b) and (c) show the impact of partial LCDs and different feed solutions on the diluate and concentrate salinities over the course of reducing the diluate salinity by 50%. 29
4.10 Sub figure (a) shows the impact of applied partial LCD on the concentration factor for different feed solutions for reducing the diluate salinity by 50%. Sub figure (b) shows the impact of applied partial LCD on the energy consumption. 29
4.11 Sub figures (a),(b) and (c) show the impact of partial LCDs on the salt and water mass transport distribution and the current efficiencies for reducing the diluate salinity by 50%, for feed concentrations 20, 40 and 80 g/L, respectively. 30
4.12 Sub figures (a), (b) and (c) show the impact of partial LCDs on the salt and water mass transport distribution and the current efficiencies using an initial volume ratio of 2, while the results with initial volume ratio 4 are presented in sub figures (d), (e) and (f). 31
4.13 Sub figures (a) and (b) show the impact of volume ratios 2 and 4, respectively, on the concentration factor. Sub figure (c) shows the impact of different volume ratios on the energy consumption, based on 0.5LCD. 32
4.14 Energy consumption for different membrane technologies for concentrating different feed solutions. 32
4.15 Schematic diagram of a multistage ED using counter flow operation mode. 33

A.1 Relative speciation of CO_2, HCO_3^- and CO_3^{2-} in water as a function of pH. Image retrieved from Pedersen [**?**]. 45
A.2 Simplified brine process flow scheme 45

B.1 The progression of spatial flux variation in a pressure vessel (a) and progression of feed pressure to obtain 5, 10 and 20 NDP for different feed concentrations (b). 46
B.2 Geometrical characteristics of a spacer, top view. Da Costa et al. [5] 47
B.3 Geometrical characteristics of used feed spacer with thickness 47mil, parallel shape, top view. . 47
B.4 Vacuum MD configuration at laboratory scale, Lenntech (Delfgauw). 51
B.5 Conventional ED configuration at laboratory scale, Lenntech (Delfgauw). 51
B.6 Phase diagram of water. Source: *wikipedia.org CC BY-SA* 52
B.7 Calculation of steam properties at 1500 Pa noa [6]. 53

List of Tables

4.1 Lowering of the vapour pressure with increasing solute fraction. 24
4.2 Limiting current densities of salt concentrations using a cross-flow velocity of 1 cm $\cdot s^{-1}$. 28

A.1 Ziemowit coal-mine plant chemical sample analysis 44

Nomenclature

A_{mem}	membrane surface area
$\Delta\pi$	osmotic pressure difference over membrane
$\Delta H_{v,H_2O}$	temperature dependent latent heat of vaporization of water
Δm_f	feed solution mass difference before and after the operational run time
ΔP_{module}	pressure drop across the membrane module
Δt	operational run time
$\dot{n}$	molar flux of water across the membrane
ϵ_c	condensation efficiency of the cooling bath
$\epsilon_{p,f}$	feed pump efficiency
$\epsilon_{p,f}$	vacuum pump efficiency
η_{Na^+}	current efficiency of Na^+ transport in ED
γ	recovery
γ_l	surface tension of the liquid
λ	specific enthalpy of steam
π_c	osmotic pressure of concentrate
π_f	osmotic pressure of feed
ρ_w	density of water
θ	contact angle of a droplet on a surface
$\theta_{w,e-o}$	electro-osmotic water transport in ED
$\theta_{w,o}$	osmotic water transport in ED
$\theta_{w,o}$	osmotic water transport in ED
B	pore geometry coefficient
c_i	concentration of dissolved ion i
$C_{p,vac}$	specific heat capacity of water at a constant vacuum pressure
C_p	temperature dependent specific heat capacity of water at a constant (atmospheric) pressure
C_{VMD}	membrane distillation coefficient
CF	concentration factor
E	electrical energy
$E_{h,cond}$	energy required for condensation
$E_{h,cool}$	energy required for cooling
$E_{h,ini}$	thermal energy required for initial heating
$E_{p,f}$	energy required for recirculation pump

$E_{p,vac}$ energy required for vacuum pump

$E_{VMD,el}$ electrical energy required for VMD

$E_{VMD,h}$ thermal energy required for VMD

E_{VMD} total energy requirement for VMD

F Faraday's constant

I electrical current

LEP liquid entry pressure

m_f feed mass

M_{NaCl} NaCl mass transport in ED

M_{NaCl} amount of NaCl transported

m_p permeate mass

M_{tot} total mass transport in ED

MW_i molecular weight of dissolved ion i

MW_{NaCl} molecular weight of NaCl

MW_{NaCl} molecular weight of NaCl

MW_w molecular weight of water

N trans-membrane water flux

n_1 moles of solvent

n_2 moles of solute

N_{cp} number of cell pairs

n_{Na^+} amount of Na^+ transported in mol

n_{NaCl} amount of NaCl transported in mol

P electrical power

p vapour pressure of solution

p^0 vapour pressure of pure solvent

P_{H_2O} vapour pressure difference between feed and permeate

$p_{vac,out}$ pressure at the outlet of the vacuum pump

p_{vac} operating vacuum pressure measured at the inlet of the vacuum pump

Q useful heating or cooling production

Q_f feed flow

$Q_{h,cool}$ required cooling of steam

$Q_{h,ini}$ initial heating

q_{perm} overall heat flux through the membrane

Q_p permeate flow

$q_{vac,in}$ volume flow rate in the vacuum volume

R electrical resistance

R universal gas constant

r_{max}	membrane maximum pore size
T	temperature
T_0	initial temperature of the feed
$T_{f,b}$	desired inlet feed temperature
$T_{p,cond}$	boiling point temperature for given conditions
T_p	permeate inlet temperature
$T_{vac,in}$	temperature in vacuum pump inlet
$T_w^{Cl^+}$	hydration number for Cl^-
$T_w^{Na^+}$	hydration number for Na^+
U	electrical potential
$V_{i,d}$	initial diluate volume
W	energy input
z	charge number
z_i	valence of dissolved ion i

Acronyms

RO	Reverse Osmosis
ERD	Energy Recovery Devices
MD	Membrane Distillation
VMD	Vacuum Membrane Distillation
MSF	Multi-stage Flash Distillation
MED	Multi-effect Distillation
TDS	Total Dissolved Solids
ED	Electrodialysis
IEX	Ion Exchange
CEM	Cation Exchange Membrane
CEEM	Cation Exchange End Membrane
AEM	Anion Exchange Membranes
ERS	Electrode Rinse Solution
LCD	Limiting Current Density
CF	Concentration Factor
CP	Concentration Polarization
DCMD	Direct Contact Membrane Distillation
AGMD	Air Gap Membrane Distillation
SGMD	Sweeping Gas Membrane Distillation
TP	Temperature Polarization
LEP	Liquid Entry Pressure
COP	Coefficient of Performance
WAVE	Water Application Value Engine
PHREEQC	PH (pH), RE (redox), EQ (equilibrium), and C (program written in C)
EC	Electroconductivity
NDP	Net Driving Pressure
SEC	Specific Energy Consumption
ZLD	Zero Liquid Discharge

1 Introduction

Fresh water scarcity and the continuously increasing demand for potable water and process water for industries are major global concerns. Whilst improving water demand management reduces the disparity between water demand and supply, it must go hand in hand with better supply practices. Approaches of such practices involve developing low-cost and efficient technologies for water production and supply. One strategy that is implemented progressively in the recent years is water desalination [7]. Desalination is a purification process where high saline feed water is processed into a desalinated water stream and a concentrate stream containing salts and other dissolved chemicals [8]. Depending on the quality and the intended use for the desalinated water, post-treatment is required which may include disinfection or remineralization among other things. This strategy has become an attractive solution for water production, as it is not dependent on water sources directly affected by hydrology such as precipitation or deep percolation. Furthermore, as desalination technology advances constantly, the associated economic costs reduces, and hence, making it a competitive solution as well [9]. A growing interest in the environmental impact and economy and energy concerns related to highly concentrated stream disposal was validated through a study by Jones et al., which provides a global assessment of research and practice around desalination [10].

In general, the term desalination is used for the treatment of natural occurring water such as seawater or salty lakes. However, desalination in industries also experiences important growth. Some industries produce high saline waste streams (brine) that are in general more concentrated and complex but commonly does not produce potable water, compared to the aforementioned desalination process. These streams originate from industries such as oil and gas, textile, food and coal mining among others. Treatment of such brines generally results in effluent that can be reused within the treatment operation or safely discharged to the environment, provided that the effluent quality is according to the discharge guidelines [11, 12]. The concern with saline industry wastewaters is that the treated brine carries greater environmental consequences and thus proper discharge of the treated brine requires focus of attention, as associated greenhouse gas emissions and waste products negatively affecting marine habitat or surrounding soil must be considered [13].

1.1. Desalination for industry

In essence the desalination method is based on a separation step and often, but not always, followed by a concentration step. Industry desalination uses the same principles and thus conventional desalination technologies can be applied. These technologies can be generally categorized into two groups, thermal based and membrane based technologies. Thermal technologies work on the principle that thermal energy is supplied to water with high salinity, to evaporate water vapour. Subsequently, the water vapour is condensed to obtain product water [8, 14]. Such technology is advantageous in regions where water salinity is high and energy costs are low, for example in the Middle East. In this region fossil fuel is low-priced and water production via thermal desalination is usually co-generated with power production [15–17]. However, because of the growing concern about efficiency and energy costs involving thermal desalination and decreasing electricity costs due to constant development in renewable energy, membrane based technologies are becoming preferred systems for desalination.

Membrane based technologies can be pressure, chemical or electrical driven and use a physical barrier by means of a membrane to separate dissolved salts from the feed water. Historically, thermal technology was the referred method for water production from saline water. Presently, membrane technology is dominating the desalination sector with reverse osmosis (RO) as most commonly used in desalination process globally [8, 14, 18]. RO is a pressure driven technology, that uses high pressure to push water through a semi-

permeable membrane by overcoming the osmotic pressure and membrane resistance. The RO membrane pore size is around 1×10^{-4} μm, which means that ions and dissolved salts can be rejected. Rejection of ions by RO can be distinguished into two mechanisms, uncharged and charged membrane rejection. The former is mostly dependent on the effective radius of ions in water (size), interaction between different ions, and the diffusivity and solubility of ions. Additionally, some membranes carry charged groups. Depending on its density and charge, similar charged ions (co-ions)in the solution are rejected, while opposite charged ions (counter-ions) pass the membrane. However, a known limitation to the separation process using charged membranes is the principle of electroneutrality in ionic solutions. This means that rejection of ions by the membrane is influenced by the electrostatic interactions between the charged membrane and ions [19]. Two streams are thus produced by RO, permeate and concentrate. As RO is very susceptible to membrane fouling, pre-treatment is required. Furthermore, osmotic pressure increases linearly with increasing brine concentration and thus higher pressure is required. As the RO membrane is limited by very high pressure, highly concentrated feed streams cannot be treated directly and should pre-treated for reducing concentration and to avoid damage to the membranes [20]. High pressure translates into high energy use and decrease of the life span of membranes. Over time, new developments in the field of membrane technology allowed for lower energy consumption and overall performance efficiency of desalination systems by means of improved membrane structures, energy recovery devices (ERD) and pressure exchangers among other things [**?**].

As technology develops, conventional technologies are replaced by more simplified and more efficient configurations, such as membrane distillation (MD). MD combines distillation and membrane separation processes, where a hydrophobic micro-porous membrane separates the warm feed chamber and the permeate chamber. This process is thermally driven and works on the principle that water is volatile, however salts and other minerals are not [21]. The temperature gradient results in a vapour pressure difference across the membrane. Depending on the methods to induce the vapour pressure gradient and how the vapours are collected from the permeate side, MD modules are classified into several basic configurations [1, 22]. Particularly interesting for brine concentration is the vacuum membrane distillation (VMD) configuration, which requires a vacuum pump to extract the vapour from the permeate side. Subsequently, the vapours condense in an external condenser [18]. Compared to other thermal desalination processes such as multi-stage flash distillation (MSF) and multi-effect distillation (MED), MD can be operated at much lower temperatures and is much more compact, thus can be applied at smaller scale. Furthermore, high rejections for non-volatile components can achieved and is less sensitive to feed variations (e.g., pH and TDS), unlike RO. However, energy savings regarding comparison of MD configurations to competing brine concentration processes are not yet extensively researched in literature. For industrial application of MD, this means a limitation due to uncertainty in energy and economic costs [23, 24].

Electrodialysis (ED) is a membrane technology driven by electric current. ED is a more advanced separation process, that has been widely used in applications for separating and concentrating purposes. The ED membrane sequence consists of alternating cation and anion exchange membranes, CEM and AEM respectively. The CEM contains negatively charged groups in the polymer matrix and the AEM contains positively charged groups. Spacers are placed in between the CEM and AEM to form a cell pair. In turn, multiple cell pairs create a stack that is situated in between an anode and a cathode. Provided that electrical potential is created in between the electrodes, circulating electrolyte through the ED module allows ions to move through membranes towards the electrodes. Ions in an electrolyte will be excluded from the membrane that has the same charged group. In essence, this is the exclusion mechanism in ED that allows for ion transport through CEM and AEM [25]. Cations are transported through CEMs towards the cathode, but this transport is interfered at the surface of the subsequent AEMs and the cations are retained in this compartment. Likewise, the transport of anions towards the anode is similar. Thus, in one cell pair a concentrate and a diluate compartment is realized. The rate of desalination in an ED system is determined by the feed concentration and composition, applied current density and the duration of the solution in a stack among other things. As ED is driven by electric current, a major benefit regarding energy consumption is that electrical energy is directly used. Possible energy losses in energy conversion are thus minimized, when comparing ED to mechanically or thermally driven membrane technologies such as RO and VMD. Many studies validated the great potential of extracting and concentrating salts and high quality water recovery from saline streams using ED [26–30].

About 77% of the current global desalination capacity (115 Mm^3/d) uses RO technology, [31]. Practices of RO mostly involves desalination of various water sources. Almost half of the current RO desalinated water originates from seawater, while the second largest water source is brackish water and accounts for about a third of the global RO desalination capacity. Besides drinking or industrial water production, RO is also used for wastewater treatment in industries for reducing their water footprint [32]. VMD competes with RO in desalination when waste heat is available and the water source has elevated osmotic pressures, among other

things. For example, VMD has been applied to desalinate hyper saline groundwater with salinities > 6.3% and temperatures of > 45°C, because the high salinity and elevated temperature makes RO impractical for this application [33]. In 2017, ED accounted for approximately 6% of the total brackish water desalination capacity and is still a relevant membrane technique for this application [31, 34]. ED is also commonly used in hybrid systems, in which ED is placed after RO or MD to reduce the brine volume and brine concentration costs among other things [35].

Improved membrane separation technologies allow for better performance and reduced energy consumption whilst minimizing the production of waste. Treatment of high saline and more complex waste streams can be actualised and could provide solutions for proper treatment of brine from highly polluting industries. The performance of a desalination plant is defined by numerous factors, such as the quality of feed, desalination techniques, recovery ratio, and production and disposal of waste products among other things. Further treatment of the concentrated stream creates the possibility for salt and mineral recovery. Thus, apart from recovering water, industry desalination has the potential to minimize waste production by converting high saline waste streams into valuable resources and subsequently allows for business opportunities and can make contribution towards a circular economy. In any case, a sustainable assessment of a brine treatment plant is required to ensure its feasibility and to consider the most optimal solution on a case-by-case basis.

1.2. Research incentives and objective

Limited practical research on brine concentration comparison between desalination techniques with regards to performance and energy requirements is the main motive in this research. The aim of this research is to broaden the current knowledge on brine concentration with an assessment on different membrane techniques in combination with concentrated NaCl stream recovery and analysis of energy consumption. The membrane techniques that are considered for the comparison are RO, ED and VMD, due to their relevance and potential in current industry water treatment practices. The considered concentration techniques have different driving forces and thus performance parameter normalization by shared properties is required for fair comparison. The footing of concentration processes is the achieved concentration factor, which is irrespective of driving force. Concentration processes involve three streams: the saline feed water, highly saline concentrate stream and low-salinity dilute stream or product water. The concentration factor (CF) is defined as the concentration of dissolved substances in the concentrate stream divided by that of the feed water. To achieve the research goal, a main research objective was formulated.

Main research objective

Determine limiting factors of ED, RO and VMD for concentrating a wide range of NaCl solutions for the recovery of concentrated streams and evaluate the energy performance by a comparative study.

1.3. Research questions and approach

The research objective was fulfilled by firstly addressing the performances of RO, ED and VMD separately. Secondly, the concentration performance of the techniques were assessed as a whole and compared. Finally, a preliminary evaluation for energy requirement of the considered techniques was performed. Data for ED and VMD were experimentally collected, whilst design software was used to obtain RO data. Synthetic NaCl solutions with concentrations 20, 40 and 80 g/L were used in experiments, to emulate different brine streams.

1. How do RO limiting factors affect concentrating brine and how does it relate to its energy consumption?
2. How do ED limiting factors affect concentrating brine and how does it relate to its energy consumption?
3. How do VMD limiting factors affect concentrating brine and how does it relate to its energy consumption?
4. How do RO, VMD and ED compare in terms of concentration performance and energy consumption?

2

Background

This chapter provides theoretical basis for the experimental design and work, including governing equations. Basic principles are described for each technique and the influence of operating conditions, materials and other possible limitations on its performance are discussed. Finally, this information is used to select test conditions for the experimental research.

2.1. Reverse Osmosis

RO is the dominating pressure-driven desalination technology, in which water molecules are pushed across a semi-permeable salt-rejecting membrane by applied pressure. A schematic of the RO process is depicted in Figure 2.1. Pore sizes of less than 1 nm are characteristic to RO membranes, which means that most dissolved salts and micro-contaminants are rejected. The product is a purified stream, whilst the rejected stream is concentrated brine. Logically, osmotic water transport is expected from low (permeate) to high (reject compartment) solute concentration across the membrane. To counter this osmotic water transport, the applied pressure must at all times be greater than the osmotic pressure difference between the concentrated brine and the purified stream. In other words, the applied pressure increases the chemical potential of the water molecules in the brine stream such that it drives the molecules across the membrane.

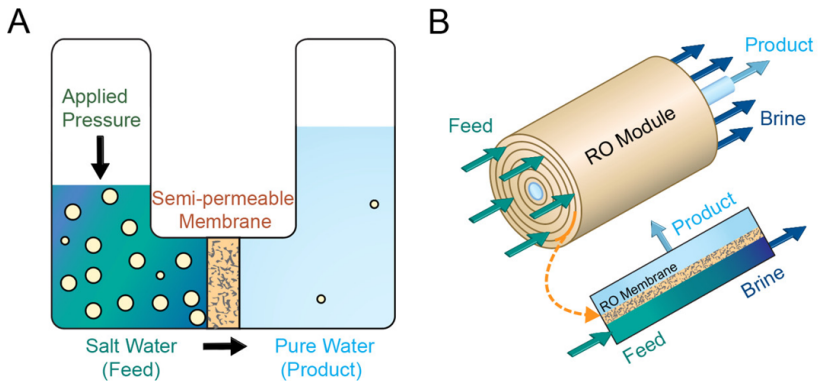

Figure 2.1: (A) Schematic of RO process and (B) cross flow operation of a RO spiral wound module. Image by **?**]

A widely accepted approximation of the osmotic pressure of a solution is described by the Van 't Hoff equation as follows,

$$\pi = \sum \frac{RT \cdot c_i \cdot z_i}{MW_i} \tag{2.1}$$

where:

R = universal gas constant
T = temperature
c_i = concentration of dissolved ion i
z_i = valence of dissolved ion i
MW_i = molecular weight of dissolved ion i

In this research it is thus assumed that the substances in the solution obey the ideal gas law and that the osmotic pressure of a solution is proportional to its salt concentration. For a solution with multiple dissolved ions it is sufficient to consider most important ions, which are HCO_3^-, SO_4^{2-}, Cl^-, Na^+, Ca^{2+} and Mg^{2+}. Usually the RO permeate osmotic pressure is neglected in the osmotic pressure difference calculation, as the permeate concentration is very low compared to the feed concentration.

$$\Delta\pi = \frac{\pi_f + \pi_c}{2} \tag{2.2}$$

where $\Delta\pi$ is the osmotic pressure difference over a membrane, π_f and π_c are the osmotic pressure of the feed and concentrate, respectively. By introduction of the overall production of the system (i.e. recovery), whilst considering that all salt is retained in the feed compartment, Equation 2.2 can be rewritten like so,

$$\gamma = \frac{Q_p}{Q_f} \cdot 100\% \tag{2.3}$$

$$\Delta\pi = \pi_f \cdot \frac{2-\gamma}{2\cdot(1-\gamma)} \tag{2.4}$$

where γ is the recovery. The minimum applied pressure is thus proportional to the concentration of dissolved ions in the feed. The higher the feed concentration, the higher the required applied pressure. The applied pressure on the membrane is finite, of which exceeding can cause (permanent) membrane damage. This is a great limitation when using RO to concentrate brines. Other limitations are side-effects due to changes in the solution's properties during operation. The higher the salt concentration, the more susceptible the membrane surface is to accumulation of retained salt. The increased concentration in the boundary layer of the membrane induces concentration polarization (CP), see Figure 2.2. This results in rapid decline of flux and gives rise to possible salt leakage and scaling. This effect could be minimized by enhancing turbulence in the boundary layer, i.e. high cross-flow velocity.

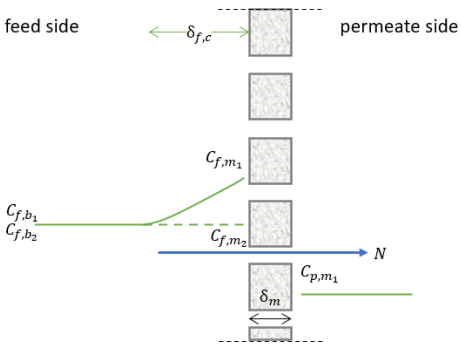

Figure 2.2: Concentration polarization in RO

2.1.1. Parameters influencing RO process

In terms of concentrating brine, the recovery of an RO module is directly related to the concentration factor.

$$CF = \frac{1}{1-\gamma} \tag{2.5}$$

where CF is the concentration factor. As the goal is to increase concentration factor, finding a proper balance between maintaining high membrane performance and reduced the energy consumption is crucial. In practice, recovery ratio of brackish water desalination using RO can reach up to 80% , whilst for seawater the optimum recovery rate is in the range of 50% - 60% [**?**]. The limitation on aforementioned values are based on the salt concentration of the feed stream and the mechanical limitation of the membrane, as the highest practical applied pressure on conventional seawater RO membranes is about 40 bar. Higher recoveries might result in exceeding solubility limits of certain salts, thus higher membrane fouling rates that result in scaling. Scaling fouls the membrane by blocking water passage through the membranes. Higher feed pressure is then required to maintain satisfactory permeate flow and overall resulting in reduced energy efficiency. To improve recovery, RO modules can be placed in series what is known as staging. The principle of staging is to increase overall system recovery by feeding the concentrate to subsequent modules while the permeate streams are collected. As such, the osmotic pressure increases at subsequent stages. It is common to use two stages for desalination of highly concentrated brines, such as seawater. Prevention of permeate flux decrease

can be achieved by several treatment additions, such as dosing of anti-scalants, chemical cleaning and increasing cross-flow velocity. Concerning the last option, recirculation of the concentrate stream can reduce energy consumption.

2.1.2. RO energy estimation

Consider a batch RO system in which water is recovered using applied pressure that closely approaches the concentrated brine throughout the process. On the presumption that, as discussed in Section 2.1, (i) osmotic pressure is proportional to its salt concentration and (ii) salt is fully retained in the feed compartment, the aforementioned system can approach the minimum theoretical energy consumption of desalination (i.e, thermodynamically reversible process). However, this way of operating an RO system with ever-changing applied pressure throughout the process is impractical when minimal variance in permeate flux is desired. Not to mention neglecting the performance limitation caused by possible membrane scaling, salt precipitation at high salinities and membrane operating limits.In practice, a constant applied pressure above the osmotic pressure of the brine is used to operate RO. The derivation of practical minimum energy consumption for RO desalination using single-stage and multi-stage is well presented in **?**]. The analyses make use of the same presumptions as discussed in Section 2.1. In Figure 2.3, the blue area represents the minimum theoretical energy for RO desalination for a thermodynamically reversible process. The yellow area bordered by the red striped lines represents the excess pressure during the time that a constant pressure is applied to the system, up until equilibrium pressure is achieved. Thus, total area bordered by the red striped lines represents the practical minimum energy consumption. When considering multi-stage RO, the desired water recovery is achieved incrementally by feeding the concentrate stream to subsequent modules. Each stage will operate at increased constant applied pressure that equals the osmotic pressure of the brine and hence, the practical minimum energy to achieve the same water recovery (i.e., concentration factor) is reduced. However with increased stages, the capital costs of such system increases and thus a trade-off between energy consumption and investment costs must be applied that suits the objective.

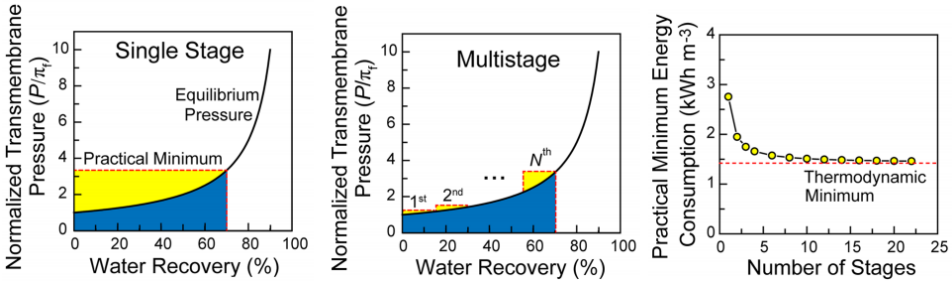

Figure 2.3: Practical energy consumption analysis of single-stage and multi-stage RO, based on feed concentration 600 mM and 100% salt rejection. Images by **?**]

The above-discussed energy consumption presumes ideal pumps and energy recovery devices, whereas in reality the efficiencies of such devices influences the overall energy consumption. Modeling software programs for simulating and design the operation of membrane filtration are available, that provides analyses of the system such as the overall energy consumption taking the additional devices in consideration. Such software programs are provided by membrane filtration suppliers and continuously evolve to meet newer system design needs. The simulation results comply largely to practical results and are therefore widely used in practice to design full systems.

2.2. Vacuum Membrane Distillation

MD is a thermally driven separation process combined with membrane technology. MD modules carry a warm feed chamber and a permeate chamber that are separated by a hydrophobic micro-porous ($\leq 1\mu$m) membrane. Distillation works on the principle that volatile compounds, such as water vapour molecules, transfer from the warm aqueous solution through the membrane as a result from partial pressure difference (Δp) induced by the temperature gradient between the chambers. Depending on the methods to induce the vapour pressure gradient and how the vapours are collected from the permeate side, MD modules are classified into four basic configurations (see Figure 2.4): direct contact membrane distillation (DCMD), air gap membrane distillation (AGMD), sweeping gas membrane distillation (SGMD) and VMD. In all configurations, the membrane is in contact with aqueous solution on the feed side. When considering a salt solution, a transmembrane water flux N [$kg\,m^{-2}h^{-1}$] exists as water is the only volatile compound in salt solutions. The flux

can be expressed as

$$N = \frac{\Delta m_f}{A_{mem} \cdot \Delta t} \tag{2.6}$$

where:

Δm_f = feed solution mass difference before and after the operational run time
Δt = operational run time
A_{mem} = membrane surface

The molar water flux can be calculated using the molar mass of H_2O [18 $g\ mol^{-1}$]. The dissimilarity in MD configuration is on the permeate side. For DCMD, condensation of vapor occurs in the cold permeate stream. It is easy-to-operate, widely employed in industrial application and multiple module forms can be used, such as flat sheet, spiral wound and hollow fibre. The major drawback of this configuration is the high heat loss by conduction, as the hot feed is separated from the cold permeate by only a membrane. High heat loss means low energy efficiency and depending on the purpose of the distillate, the permeate stream might not be desirably if solely the distillate is preferred. The AGMD is similar to the DCMD, but still air and a condensation plate are introduced. The permeate is collected as distillate on the condensation plate, whilst the cooling is introduced by a coolant. Still air is a natural insulator, and therefore heat loss by conduction and convection is reduced. The trade-off is the additional mass transfer resistance, as the effective temperature difference (i.e., driving force) is reduced by such insulation layer and thus the fluxes of AGMD are typically low. As opposed to DCMD, direct collection of distillate is possible, since the coolant is not in contact with the permeate. AGMD is suitable for removing volatile compounds from aqueous solution. SGMD is similar to the DCMD, but uses an inert sweeping gas that captures the vapour at the membrane surface of the permeate side. The seized vapors in the gas is then led to an external condenser. Heat loss is reduced similar to the AGMD configuration, but mass transfer of vapor is increased due to the sweeping gas. Condensation does not take place inside the module and the condenser should be large, as only a small volume of permeate as vapor diffuses in a large sweep gas volume. Overall, the SGMD might be an undesirable choice if a compact design is preferred. This configuration is also suitable for removing volatile compounds from aqueous solutions. VMD is very similar to SGMD. Instead of using an inert sweeping gas, the atmospheric pressure in the permeate is continuously reduced to partial vacuum pressures to enhance the vapour pressure difference across the membrane. Higher driving forces can be achieved even at relatively low operating temperatures and thus higher fluxes are achieved compared to the aforementioned configurations. Though, risk of membrane pore wetting is highest compared to the other configurations. VMD is suitable for concentrating and removing volatile compounds from aqueous solutions. The configuration of interest in this research is VMD. For this configuration, a vacuum pump is essential to extract the vapours from the MD module and lead them to an external condenser.

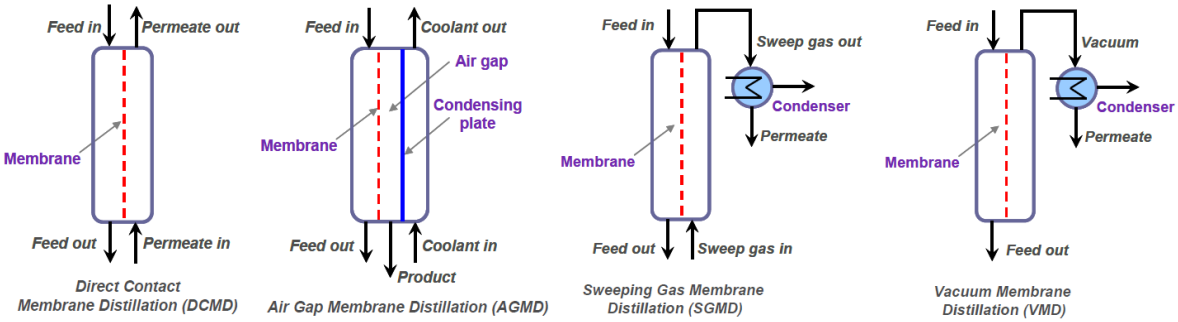

Figure 2.4: Conventional MD configurations. Image by Kiss and Readi [1].

2.2.1. Heat and mass transfer in VMD

The heat and mass transfer through a membrane in VMD can be adequately visualized in Figure 2.5 [36]. A thermal boundary layer ($\delta_{f,t}$) is formed during VMD operation, which presents a resistance to heat transfer. Consider a salt solution at elevated temperature ($T_{f,b}$) on the feed side of the membrane. The temperature of the bulk decreases as it reaches the liquid-vapour interface temperature ($T_{f,m}$), after which the rate of heat loss increases due to vaporization and finally reaching the permeate membrane temperature ($T_{p,m}$). This phenomenon is termed as temperature polarization (TP) and negatively influences the driving force in MD, and thus mass transfer. Vaporization also causes a higher salt concentration (C_{m_1}) near the interface compared to the bulk concentration (C_{b_1}) and gives rise to concentration polarization. This phenomenon

reduces the vapour pressure difference across the membrane, which also negatively affects the mass transfer. However the occurrence of vacuum in the permeate side of VMD allows for higher partial pressure difference, thus higher driving force compared to other MD configurations. Additionally, conductive heat losses in VMD is minimized due to the vacuum gap and thus T_p can be approximated to $T_{p,m}$ [22, 37]. Hence, the heat flux through the liquid boundary layer in VMD can be defined as

$$q_{perm} = N\Delta H_{v,H_2O} \tag{2.7}$$

where:

q_{perm} = overall heat flux through the membrane
$\Delta H_{v,H_2O}$ = temperature dependent latent heat of vaporization of water

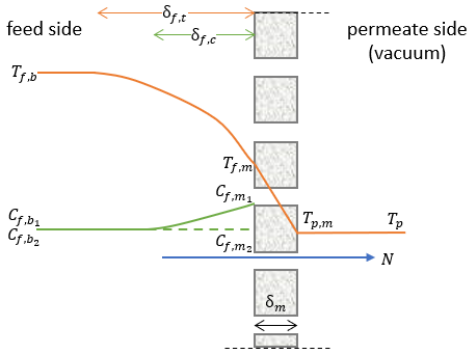

Figure 2.5: Heat and mass transfer through membrane in VMD.

The mass transfer in MD is induced by the partial pressure difference across the membrane ΔP_{H_2O} [*Pa*]. In essence, the mass transfer across the membrane is complicated and includes coupled processes. A general approach to overall modeling for predicting permeate fluxes at given operation conditions is the linear relationship between the permeate flux and the water vapour pressure difference across the membrane ΔP_{H_2O}. A membrane distillation coefficient C_{VMD} is obtained from this relationship, which is subsequently a function of the membrane properties (i.e., membrane geometric characteristics), temperature and vapour properties. The membrane distillation coefficient can be appropriately expressed as,

$$C_{VMD} = \frac{N}{\Delta P_{H_2O}} \tag{2.8}$$

where:

N = permeate flux
ΔP_{H_2O} = vapour pressure difference between feed and permeate

The vapour pressure on the feed side is dependent on the temperature and composition of the solution and is assumed as vapour pressure in the bulk.

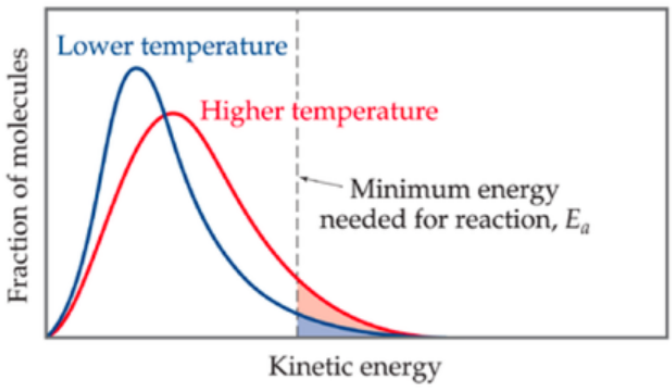

Figure 2.6: Molecular kinetic energy distribution by Boltzmann [2]

Consider a liquid, such as water or alcohol in an open container. Molecules carry a certain kinetic energy even in liquid form. The kinetic energy of the molecules follow the Boltzmann energy distribution, see Figure

2.6, which shows that there is always a small fraction of molecules that have high kinetic energy. If this fraction of molecules in the liquid has sufficient kinetic energy to exceed the intermolecular forces in the liquid phase, they enter the gas phase even at temperatures below the liquid's regular boiling point. While this fraction of molecules escape into the gas phase the average temperature of the liquid falls, but heat from the surrounding can be absorbed by the liquid to maintain its average molecular speed (i.e., enthalpy of vaporization). This means that all liquid can vaporize when given enough time and that there is always vapour above the liquid's surface, which is carried away in the open air considering the open container. Now consider a liquid in a closed container and like any gas, the vapour above the liquid will exert a pressure. In this situation the vapours are trapped and the liquid will not fully vaporize as some vapours condense back into liquid form. The amount of liquid in the container will remain constant if the rate of condensation equals to the rate of vaporization and so a certain partial pressure is attained above the liquids' surface inside the closed container. This pressure is known as the vapour pressure of the liquid and imparts dynamic equilibrium in a system. Mathematical expressions like Antoine equation, see Equation 2.9, exists to calculate the temperature related vapour pressure for pure substance using component specific coefficients.

$$\log_{10} P = A - \frac{B}{C+T} \tag{2.9}$$

Water is a pure substance, because it only contains one type of molecule and therefore the Antoine equation applies to this substance. The Antoine equation coefficients A, B and C for water are 5.11, 1687 and 230.17, respectively. When a non-volatile compound like NaCl is added to a solvent, the mixture becomes a solution and the behaviour of the solvent changes. The surface of the solution is covered with solvent and solute molecules, thus the fraction of surface area that is covered by the solvent is reduced and therefore also the chance of these molecules escaping into the gas phase. This explains that with increasing solute concentration in the solution, the vapour pressure becomes lower. Mathematically, the vapour pressure lowering of a liquid-solid solution is described as Raoult's Law and is applicable for only ideal solutions. This means that in a solution, a solvent molecule uses the same amount of energy to break away from the surface as it were in a pure solvent. This is unlikely as it disregards the solvent-solute attraction, which could be stronger than the solvent-solvent attraction and therefore an increased energy is required for a solvent molecules to break free in a real solution. However for uncomplicated solutions such as NaCl solution, it is acceptable to use Raoult's law to estimate the vapour pressure of the liquid-solute mixture, see Equation 2.10.

$$\frac{p^0 - p}{p^0} = \frac{n_2}{n_1 + n_2} \tag{2.10}$$

where:

p^0 = vapour pressure of pure solvent
p = vapour pressure of solution
n_1 = moles of solvent
n_2 = moles of solute

In VMD the pressure of the permeate side is vacuum pump dependent. Overall, it can be concluded that the performance of MD relies heavily on the intricate relationship between the simultaneous thermal and mass transfers.

2.2.2. Parameters influencing VMD process

The following sections provides information on the influence of membrane characteristics and operating parameters on VMD performance, to select proper membrane and operating conditions to achieve high driving force.

Keeping the pores free of liquid is essential in MD process, for which liquid entry pressure (LEP) is an important characteristic to consider. LEP signifies the minimum pressure required for the liquid to penetrate membrane pores and thus should not be exceeded. A method to investigate a membrane LEP is described by Franken et al. [38]

$$LEP = \frac{-2B\gamma_l cos\theta}{r_{max}} \tag{2.11}$$

where:

B = pore geometry coefficient
γ_l = surface tension of the liquid
θ = contact angle of a droplet on a surface
r_{max} = membrane maximum pore size

We can derive from Equation 2.11 that a small maximum pore size is preferred to achieve high LEP. Water or solutions that contain inorganic compounds in water show high γ_l, whereas surface active agents (i.e. organic compounds) dissolved in water decreases the liquids γ_l. Hydrophobicity of a membrane increases the LEP, as the contact angle of a droplet on such surfaces is larger than 90°. This holds true for commonly fabricated polymer MD membranes such as PTFE, PVDF and PP [39, 40]. Regarding LEP, the smaller the maximum pore size the higher the LEP. However, permeate flux increases with bigger pore size. Thus, a good consideration could be choosing a membrane with a small enough maximum pore size to avoid wetting. In general membrane processes, the permeability is affected by the membrane thickness. With thicker membranes the mass transfer resistance increases, whereas the the conductive heat loss decreases [41]. As heat loss through conduction in VMD is poor due to the vacuum volume in the permeate side, a thin membrane is preferred. Enhanced permeability can also be achieved with high porosity, as this increases the effective surface area for evaporation. Usually, high porosity goes hand in hand with large pore size, which decreases the LEP. Therefore an additional compromise must be settled between pore size and porosity to limit the risk of membrane wetting [1, 40].

2.2.3. Factors affecting VMD concentration performance

Theoretically, MD allows for fully rejection non-volatile compounds as volatile compounds evaporate at the warm interface of the membrane. In turn, only vapours pass through the membrane. For feed solutions with high surface tension, such as water and solutions of inorganic compounds in water, non-wetting is most probably [38]. Furthermore, the degree of vapour pressure of a liquid depends on intermolecular forces present in the solution amongst others. Weaker intermolecular forces (i.e., volatile compounds) allow molecules to escape with less effort, thus the vaporization rate will be high and a higher partial pressure can be reached before an equal rate of condensation is attained. Consequently, the vapour pressure is high and a higher driving force can be achieved. Alternatively, if the liquid contains molecules with strong intermolecular forces (i.e., non-volatile compounds), the vapor pressure is low. As the concentration of non-volatile compounds in the solution increases, the vapour pressure of the solvent decreases.

Besides the feed composition, temperature greatly controls the magnitude of the solution's vapour pressure. If the temperature increases, the average molecular kinetic energy increases and consequently the fraction of liquid molecules that overcome the intermolecular forces to escape as vapours. This fraction increases exponentially with temperature. Gas molecules will travel with higher speed and result in more frequent and heavier collision, thus overall creating a higher partial pressure.

Higher effective velocities are achieved due to the presence of spacers in membrane modules, as they reduce the void volume compared to flat channel configurations. Increased effective velocities induces higher feed flow mixing, which minimizes TP and CP among other things. The temperature and concentration at the membrane surfaces approaches those in the bulk and in turn, mass transfer through the membrane is improved. This general effect in MD configurations was observed by El-Bourawi et al. [36]. Reynolds numbers are used to describe boundaries of fluid flow regimes in channels ranging from laminar, unsteady to turbulent conditions and is determined by the combined effect of fluid properties, flow velocity and the hydraulic diameter of the channel. The hydraulic conditions in flat spacer-filled channels can be described in the same sense as for channel flow, by appropriating the hydraulic diameter to a flat spacer-filled channel using derivations by Schock and Miquel [42] and Da Costa et al. [5]. These derivations are based on net-like spacer structures in any combination of the geometric characteristics voidage, mesh size, angle, thickness and filament diameter. As such, the Reynolds number of spacer filled channels is defined as the combined effect of the fluid properties, interstitial (seepage) velocity and spacer geometry. Several studies were conducted to investigate the influence of spacer geometry on the fluid flow in channels [5, 42, 43]. Mojab et al. investigated the fluid flow behaviour in typical spacer filled channels for different flow velocities and found that fully unstable flow was achieved with Re > 350 and that Re = 1000 gives rise to the turbulent flow regime.

The vacuum pressure in the permeate side of the MD module benefits the separation process in multiple ways. Firstly, the permeate pressure is reduced greatly below the equilibrium vapour pressure and hence permits higher permeate flux compared to other MD configurations [39]. Secondly, heat conduction through the membrane in a VMD system can be assumed negligible due to the absence of thermal conductivity by vacuum [36, 44]. The thermal efficiency by VMD is thus higher compared to other MD configurations, which could translate in better overall energy efficiency. However, it can be expected that with increasing vacuum pressure (i.e. lowering downstream pressure) the hydrostatic pressure across the membrane increases and reaching towards LEP. This is a major disadvantage of VMD, as this effect poses a risk to pore wetting. Furthermore, lowering the vapour pressure in the permeate side also lowers the boiling point of water vapour. Therefore a cooling and condensation component is required to ensure condensation of water vapour.

2.2.4. VMD energy estimation

For VMD the following components are considered for the energy calculations: pump for feed circulation, vacuum pump and thermal energy for heating. The following section breaks down the main energy components of VMD and summarizes its principal theories to create a basis for the experimental study to quantify energy demand. Subsequent energy calculations can be normalized by unit volume of produced concentrate to have fair comparison between techniques. A continuous batch process was considered for all concentration experiments.

In general, two types of energy can be considered: electrical energy E_{el} and thermal energy E_h. Pumps are considered components of E_{el} type and components that involves heating or cooling contribute to E_h. The overall energy requirement for VMD can thus be defined as the summation of the aforementioned,

$$E_{VMD} = E_{VMD,el} + E_{VMD,h} \tag{2.12}$$

$$E_{VMD,el} = E_{p,f} + E_{p,vac} \tag{2.13}$$

$$E_{VMD,h} = E_{h,ini} + E_{h,cool} + E_{h,cond} \tag{2.14}$$

Electrical energy requirement

Recirculation of feed stream through the membrane module is induced by a feed pump of which the electrical energy [kWh] can be calculated by,

$$E_{p,f} = \frac{\Delta P_{module} Q_f}{\epsilon_{p,f}} \Delta t \tag{2.15}$$

where:

ΔP_{module} = pressure drop across the membrane module
Q_f = volumetric flow rate of the feed
$\epsilon_{p,f}$ = feed pump efficiency
Δt = experimental duration

At the permeate side of the module a vacuum pump operates at a pressure lower than atmospheric pressure to continuously evacuate gas molecules from the permeate volume. A study by Huttunen et al. [45] provides calculations to estimate the required energy to maintain partial vacuum in the permeate side

$$E_{p,vac} = q_{vac,in} p_{vac} \ln \frac{p_{vac,out}}{p_{vac}} \frac{\Delta t}{\epsilon_{p,vac}} \tag{2.16}$$

where:

$q_{vac,in}$ = volume flow rate in the vacuum volume
p_{vac} = operating vacuum pressure measured at the inlet of the vacuum pump
$p_{vac,out}$ = pressure at the outlet of the vacuum pump
$\epsilon_{p,f}$ = vacuum pump efficiency

It can be assumed that the gas mixture is discharged at atmospheric pressure, thus $p_{vac,out} = p_{atm}$. The volume in the permeate side is a mixture of gas molecules, consisting of air (non-condensable) and water vapour (condensable), that is displaced with a temperature and pressure dependent volumetric flow rate. An important assumption for the estimation of the vacuum volume flow rate is that the non-condensable gas is saturated with the condensable vapour. The air-water vapour mixture is thus assumed to be an ideal gas and the volumetric flow rate can be calculated using the ideal gas equation [46],

$$q_{vac,in} = \frac{(\dot{n}\epsilon_c) R T_{vac,in}}{p_{vac}} \tag{2.17}$$

where:

$\dot{n}$ = molar flux of water across the membrane
ϵ_c = condensation efficiency of the cooling bath
$T_{vac,in}$ = temperature in vacuum pump inlet

Using Equation 2.17, $q_{vac,in}$ can be calculated for Equation 2.16. The prior sequence is assumed without a cooler in between the permeate volume and vacuum pump. However, a cooling bath is required to collect the water vapour. The ϵ_c of the cooling bath is expected to be lower than one, thus the gas mixture discharged at the outlet of the vacuum pump includes part of the non-condensed water vapour. Hence, $q_{vac,in}$ is being accounted for the loss of a small part of $\dot{n}$ by the condensation efficiency.

Thermal energy requirement

Feed side

Energy for heating can be classified into initial heating $Q_{h,ini}$ *[J]* of the feed and additional heating to make up for the heat loss in the MD module by e.g., recirculation. This additional heating is assumed negligible in the considered test set-up due to its scale. In practice if the feed stream is already at elevated temperature and a continuous mode of configuration is considered, these expressions are negligible. Assuming that waste heat is not present in the system, the energy required to heat up the feed to a desired inlet temperature can be calculated using the following equation,

$$Q_{h,ini} = m_f \int_{T_0}^{T_{f,b}} C_p dT \tag{2.18}$$

where:

m_f = feed mass
C_p = temperature dependent specific heat capacity of water at a constant (atmospheric) pressure
$T_{f,b}$ = desired inlet feed temperature
T_0 = initial temperature of the feed

The initial heating of the feed is once-only at the start of operation, if the feed's original temperature is not equal to the desired operating temperature.

Permeate side

In the module at the feed side, heat is extracted from the bulk for evaporation by a heat flux across the membrane. After the water vapour passes through the membrane, the water vapour in the steam can be collected by condensation. The heat required for vaporization is equal to that for condensation, but has the opposite sign. Since the permeate side is in vacuum condition at 1500Pa, the boiling point of water vapour is decreased to approximately 13°C (see Appendix B.3 for the steam table). The temperature of the water vapour at the permeate membrane surface T_p is approximated to $T_{f,b}$, meaning that the steam is at a temperature higher than its boiling point. Therefore, cooling is required for removing sensible heat to lower the temperature of the steam below the corresponding boiling point temperature at vacuum condition, $Q_{h,cool}$ *[J]*.

$$Q_{h,cool} = m_p \int_{T_p}^{T_{p,cond}} C_{p,vac} dT \tag{2.19}$$

where:

m_p = permeate mass
$C_{p,vac}$ = specific heat capacity of water at a constant vacuum pressure
T_p = permeate inlet temperature
$T_{p,cond}$ = boiling point temperature for given conditions

Finally, thermal heat needs to be removed to condensate the water vapour using the specific enthalpy of steam λ at vacuum condition.

$$Q_{h,cond} = m_p \lambda \tag{2.20}$$

COP and heat recovery

Thermal energy in form of heat or cooling is induced by a heat pump that is driven by power. The efficiency of such heat pumps is expressed as Coefficient of performance (COP) and has different definitions for a chiller or heater. In principle, the COP is the ratio of useful heat or cooling production, Q, with given energy input, W.

$$COP = \frac{|Q|}{W} \tag{2.21}$$

A study by Hepbasli et al. [47] presents a review of wastewater source heat pump systems in terms of application and performance assessments and refers to COP value ranges of 1.77 - 10.63 for heating and 2.23 - 5.35 for cooling. The large spread is due to numerous factors that affect the efficiency of a heat pump, such as heat pump type, climate and auxiliary equipment among other things. The aforementioned thermal energy components are based on thermodynamic laws and therefore energetically assessed. The thermal efficiencies of such components could not be precisely quantified and therefore exergetic assessment of the VMD system could not be performed accurately. When conceptualizing a VMD system, COP can thus be considered for the thermal components. Furthermore, recycling of waste heat can also be considered to improve the overall energy efficiency of the VMD system.

2.3. Electrodialysis

The principle of ED is illustrated in Figure 2.7 of which the key elements lie in the membrane stack. The ED membrane sequence consists of alternating cation and anion exchange membranes, CEM and AEM respectively. The CEM contains negatively charged groups in the polymer matrix and the AEM contains positively charged groups. Spacers are placed in between the CEM and AEM to form a cell pair. In turn, multiple cell pairs create a stack that is situated in between electrodes. Provided that electrical potential is created in between the electrodes, circulating electrolyte through the ED module allows ions to move through membranes towards the electrodes. Ions in an electrolyte will be excluded from the membrane that has the same charged group. In essence, this is the exclusion mechanism in ED that allows for ion transport through CEM and AEM [25]. Cations are transported through CEMs towards the cathode, but this transport is interfered at the surface of the subsequent AEMs and the cations are retained in this compartment. Likewise, the transport of anions towards the anode is similar. The result is an increase in ion concentration in alternate chambers, whereas the other chambers become depleted. The concentrated solution can be referred to as concentrate or brine and the depleted solution is referred to as the diluate.

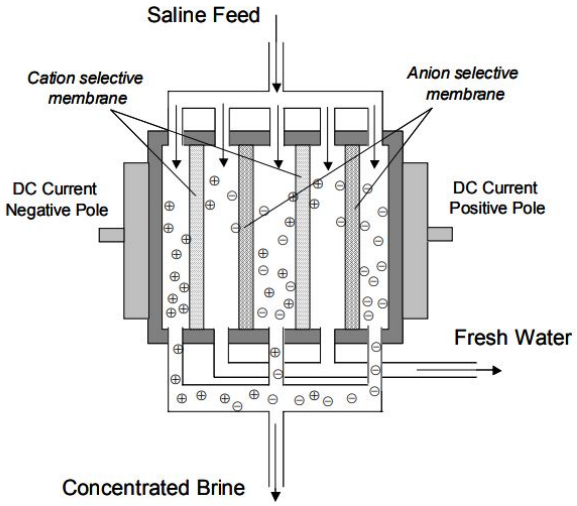

Figure 2.7: Schematic diagram of the working principle of electrodialysis by Miller [3]

2.3.1. Mass transfer in ED

A key part that contributes to the efficiency of ED process is mass transport through the IEX membranes, which is transport of ions as result of an electro-chemical potential gradient.

$$M_{NaCl} = \frac{\Delta n_{NaCl} \cdot MW_{NaCl}}{V_{i,d} \cdot \rho_w} \cdot 100\% \tag{2.22}$$

where:

Δn_{NaCl} = amount of NaCl transported in mol
MW_{NaCl} = molecular weight of NaCl
$V_{i,d}$ = initial diluate volume
ρ_w = density of water

The salt transport M_{NaCl} is expressed relative to the initial diluate mass. Besides ion transport, solvent transport through membranes also occur as a result of chemical potential differences of solvents in adjacent compartments. Previous studies show that water transport in ED limits the concentration purpose as it dilutes the concentrate compartment [48–50]. It is therefore also important to assess the water transport from the diluate to the concentrate compartment. By attraction of cations towards the cathode and anions towards the anode, a concentration gradient between the AEM and CEM compartments is created. This concentration gradient gives rise to osmotic water transport. Furthermore, there exists strong interactions between dissolved ions and water molecules called ion-dipole force. Due to this force, water molecules cluster with their negative side around positive ions (Na^+). Similarly, negative ions (Cl^-) attract the positive side of water molecules. The water molecules around the ions are arranged in concentric shells with decreasing ion to water molecule bond strength further away from the ion [51]. Thus, it can be assumed that at least the water molecules in the first hydration shell migrates with the ion. This phenomenon is called hydration and gives

rise to electro-osmotic water transport. Since electro-osmotic water transport is directly linked to salt transfer, by knowing the hydration numbers of migrating species enables prediction of this type of water transport. Following the law of electroneutrality, it is assumed that for each transported mole Na^+, one mole of Cl^- is transported too.

$$\theta_{w,e-o} = \frac{n_{Na^+} \cdot (T_w^{Na^+} + T_w^{Cl^-}) \cdot MW_w}{V_{i,d} \cdot \rho_w} \cdot 100\% \tag{2.23}$$

where:

n_{Na^+} = amount of Na^+ transported in mol
$T_w^{Na^+}$ = hydration number for Na^+ (3.5)
$T_w^{Cl^1}$ = hydration number for Cl^- (2)
MW_w = molecular weight of water

The electro-osmotic water transport $\theta_{w,e-o}$ can be predicted using Equation 2.23 and similarly to the salt transport, it is expressed as mass transport relative to the initial diluate mass. The total mass transport M_{tot}, is the sum of M_{NaCl}, $\theta_{w,e-o}$ and the osmotic water transport, $\theta_{w,o}$. The latter can be determined by subtraction of the former two from the total mass transport.

$$M_{tot} = M_{NaCl} + \theta_{w,e-o} + \theta_{w,o} \tag{2.24}$$

Water transport through the CEEM, to the electrode compartment, is neglected. These membranes form obstructions for water transport as they are relatively thicker compared to inner membranes. The end membranes are more chemically and mechanically resistant compared to inner membranes, as they should be stable against oxidative attack and make sure that the transmembrane pressure in the inner membrane stack is close to zero.

2.3.2. Parameters influencing ED performance

The following sections provides information on the influence of module and membrane characteristics and operating parameters on ED performance, to select proper membrane and operating conditions.

The driving force of ED is the electrical potential U created between the electrodes. The electrical current I (i.e. flux of electrical charges) is directly proportional to U as described by Ohm's law,

$$U = I \cdot R \tag{2.25}$$

where R is the electrical resistance. Considering a general electro-chemical cell, R is dependent on various characteristics, such as the distance between the electrodes, the material's specific resistance and the size of the effective electrode surface area. When considering ED systems, additional components add to the overall resistance R_{tot} of the system, such as the IEX membranes, spacers and resistance of the different streams: diluate, concentrate and electrode rinse solution (ERS). From this we can conclude that certain components indicate fixed attributes of R_{tot}, whereas during ED operation side-effects may occur that increases the R_{tot} contribution of electro-chemical changes in streams within the stack [52]. Since applied current is proportional to the electrode surface, current density is used in practice as this fundamental quantity is independent of electrode surface.

With operating time at a certain current density, ion depletion in the diluate compartments causes the membrane surface concentration to reach zero. In other words, the rate of supply of ions from the bulk towards the membrane surface is similar to that of the diffusion rate through the membranes and concentration polarization occurs. The current density at which this phenomenon appears is called the limiting current density (LCD). If the LCD is exceeded, the linear relationship of U-I according to Ohm's law no longer applies, see Figure 2.8. The electrical resistance in the diluate increases and possible water dissociation can occur. This leads to pH changes in the solutions and overall negatively affects current utilization, thus LCD is a critical design parameter as it determines the direct efficiency of ED process. Previous studies have demonstrated that LCD is mostly dependent on the ion concentration and flow velocity of the diluate compartment. The higher the flow and concentration of the diluate compartment, the higher the LCD [53, 54]. Cowan and Brown (1959) propose a practical method to determine the LCD for salt solutions [55].

Another important ED performance indicator is current utilization, which can be defined as how effective ions are transported across the IEX membranes for a certain applied current. While ion migration occurs from the diluate to the concentrate compartment, diffusion is also present in the ED process. Diffusion is a process of ion transport in the opposite direction in which ED attempts to achieve. If diffusion occurs the ED system requires extra current to move back the ions towards the desired direction, which means that diffusion reduces the overall current efficiency of the ED process. In basic electro-chemical terms, current

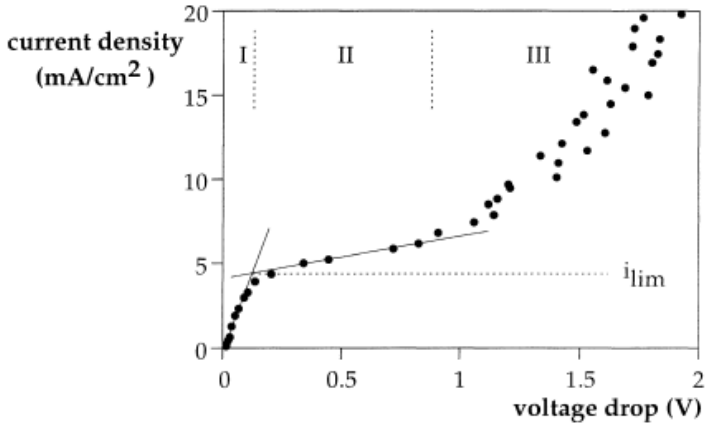

Figure 2.8: Effect of current density on voltage drop, differentiating three regions: (I) Ohmic region, (II) LCD region and (III) over-limiting region. Image by Krol et al. [4].

is rate and charge is amount. Similar to Equation 2.23, in which electroneutrality is taken into account, the current efficiency of Na^+ can be calculated using the amount of transported Na^+ from the diluate as electrical charge and the total electrical energy required for this transport [50].

$$\eta_{Na^+} = \frac{z \cdot F \cdot n_{Na^+ d}}{N_{cp} \cdot I \cdot \Delta t} \tag{2.26}$$

where:

F = Faraday's constant
N_{cp} = number of cell pairs

To elaborate further on the exclusion mechanism of IEX membranes mentioned in Section 2.3, ions that move through the membranes are referred to as counter ions and ions that carry similar electrical charge as the membrane are co-ions. To what amount the co-ions are rejected by an IEX membrane depends on the membrane and solution properties. In essence, the properties of an IEX membrane is determined by two specifications: the basic material of which the backbone is made of, usually polymers, and the moieties used as fixed charges in membranes. The former determines the mechanical, chemical and thermal stability of the membrane, while the latter determines its perm-selectivity and electrical resistance [56]. Monovalent ion-perm selective membranes exists to allow permeation of monovalent ions, while preventing passage of multivalent ions. These membranes are beneficial for removal of specific ions from waste streams, such as selective salt removal from saline streams.

It is widely accepted that when the current density exceeds LCD, the ED process exhibits higher electrical resistance and thus lower current utilization. This critical side-effect during ED operation needs to be taken into account for design and optimization. Furthermore, the selection of ion-exchange membranes should be based on high perm-selectivity, low electrical resistance and good mechanical and chemical stability.

2.3.3. Factors affecting ED concentration performance

Feed concentration affects the degree of desalination to an extent. As mentioned previously, current density should not exceed LCD due to ion depletion in the diluate solution-membrane interface. The more ions are present in the solution, the more electricity the solution can conduct. High conductivity also means more current flow is produced, thus higher current densities can be applied. In other words, a low diluate concentration specification means low operating current density. Such specification and high initial brine concentration usually means longer treatment duration. The reverse is also true, a high diluate concentration specification using high applied current means faster treatment duration. In some cases it can be energetically favourable to design an ED systems using decreasing applied current density after each pass, whether in continuous flow or batch operation [50].

Similar to VMD, the interstitial flow velocity can be calculated for ED spacers. The calculation for achieving fully unstable flow conditions using ED spacers compared to VMD, show higher required interstitial flow velocities. This is due to the difference in spacer geometry. The ED spacer has an effective cross flow area that is almost three times less compared to that of the VMD spacer. Furthermore, the hydraulic diameter of the ED spacer is about eight times smaller compared to the VMD spacer. This means that the mesh of the ED spacer is finer compared to that of the VMD, and thus significantly higher interstitial flow velocities are

required in ED spacers to achieve the same flow conditions as in the VMD spacer. Instead of deciding the operational solution velocity based on flow regime, it is more reasonable to relate the velocity in the ED stack to LCD whilst considering a final diluate concentration. Besides high solution concentration, as mentioned before, the LCD also increases greatly with increasing cross flow velocity as commonly reported in literature [50, 53–55]. No optimal cross flow velocity has been reported in literature, which indicates that tuning of operational conditions for an ED cell determines the desired objective and can be optimized for most economical operation.

The degree of desalination achieved is mainly determined by feed and target diluate concentration, applied current density and cross flow velocity. Low current density increases capital costs, but decreases overall energy (operational) costs. High current density influences the costs in opposite direction, thus ED design usually involves a trade-off between operational conditions and material requirements for the determination of optimal current density.

2.3.4. ED energy estimation

The minimum electrical energy required to operate ED derived from the electric power equation,

$$E = P \cdot \Delta t \tag{2.27}$$

$$P = U \cdot I \tag{2.28}$$

where P is the electrical power provided by a power supply. By substitution of Equation 2.25 and 2.28 in Equation 2.27 the following expression is obtained.

$$E = I^2 \cdot R \cdot \Delta t \tag{2.29}$$

Thus, the minimum required electrical energy for ED can be directly linked to the applied current and resistance of the system. In practice, the following expression for the consumed electrical energy for ED process is assumed.

$$E_{ED,PS} = \sum_{i=0}^{i} (U_i \cdot I_i \cdot \Delta t) \tag{2.30}$$

where:

U_i = electric potential difference at data point i
I_i = applied current at data point i

The product of the aforementioned is the consumed power at each data point, P_i $[W]$. The electrical energy can be obtained by multiplication of P_i with the time interval Δt $[s]$. The total electrical energy supplied can be calculated by its summation. Finally, the electrical energy for the feed recirculation pump is based on Equation 2.15. The total energy required for ED can be expressed as,

$$E_{ED} = E_{ED,PS} + E_{p,f} \tag{2.31}$$

3

Experimental apparatus and methods

The following sections describe the selected experimental conditions, methods and apparatus that were used to conduct experiments and simulations. Furthermore, explanation is given about experimental and simulation data processing. The RO simulations were performed using WAVE software that was made available at Lenntech. All experiments were carried out in the Lenntech laboratory in Delfgauw, the Netherlands. Experiments using ED and VMD with test conditions presented in the following sections were performed at laboratory scale to assess NaCl solution concentration performance and its corresponding energy consumption.

3.1. Selection of simulation and experimental test conditions

The following section discusses experimental conditions from literature findings to substantiate the selection of experimental test conditions for the considered research. The main objective of this thesis was to determine limiting factors of RO, VMD and ED for concentrating a wide range of NaCl solutions. Therefore, NaCl feed concentrations 20, 40 and 80 g/L were used as starting points for the simulations and experiments. All laboratory experiments were conducted in batch mode.

RO

The following factors affecting the RO concentration performance were examined using the WAVE software [57]: applied pressure, recovery ratio and permeate flux. Moreover, the design parameters were explored to minimize energy consumption while maximizing salt rejection. The selected membrane for these simulations was XLE-4040, a conventional seawater RO membrane that can handle the highest applied pressure (120 bar) from the software library. To make a fair comparison for small-scale systems and considering that testing different concentrations emulates a multi-stage RO system, a one-stage RO system is assumed in this study. The design will be limited to one pressure vessel per stage and the number of elements per pressure vessel is set to six, which is a standard number. The goal is to achieve highest concentration factor, while considering RO system limitations for concentrating brine (i.e., prioritize concentrate quality over permeate quality). The effect of applying different net driving pressures will be investigated for different starting concentrations. The simulations will be performed using concentrations of 20, 40 and 70 g/L, as the software does not allow feed concentrations higher than 70 g/L.

VMD

Theoretically, distillation of a NaCl solution can be performed until its solubility is reached. For a temperature range of 0 to 100 ^{o}C, this salt has an average solubility of 38 g per 100 g of water. However, fouling of the membrane by precipitation of the salt must be avoided as this was not the objective of the research. The purpose of this research is to investigate different operational parameters on the produced water flux by MD, which is directly linked to the CF. To this end, the MD experiments at different test conditions were performed until a CF of 1.1 was reached.

- ***Feed concentration:*** As mentioned in Section 2.2.3, the vapour pressure in the feed decreases with increasing solute concentration. The effect of feed concentrations 20, 40 and 80 g/L on the permeate water flux was investigated. In order to do so, PHREECQ simulations were made to investigate the effect of NaCl concentration on the vapour pressure of the solution.
- ***Operating temperature:*** High vapour pressures can be achieved by increasing the temperature of the

solution. The effect of operating temperatures 30, 40 and 50 °C on the permeate water flux was investigated.
- ***Unsteady flow condition:*** For the considered experimental set-up and operating conditions, the operational settings were selected based on the required interstitial velocity to achieve fully unsteady flow (Re = 350). These calculations are presented in B.2.

ED

Equal feed concentration and volume was fed to the diluate and concentrate chambers of the ED module. In this study, the operating principle for the ED experiments to operate ED until 50% of the salt from the diluate was removed.

- ***LCD and operational CD:*** The effect of 90%, 75% and 50% partial LCD on current efficiency, concentration factor and possible side-effects were investigated and quantified.
- ***Feed and final diluate concentrations:*** The effect of feed concentrations 20, 40 and 80 g/L and 50% salt removal from the diluate stream on the concentration factor and possible side-effects were investigated.
- ***Diluate to concentrate volume ratio:*** When considering a fixed 50% salt removal from the diluate stream, higher concentration factors could be achieved if the salt is transported to a smaller volume. The effect of volume ratio's 1, 2 and 4 on the concentration factor and possible side-effects were investigated.

3.2. Measuring method and equipment

A continuous batch mode was considered for the operation of ED and VMD experiments, meaning that the solution was recirculated back to the feed bottle(s) after passing the ED or VMD module using a Watson Marlow 530S peristaltic pump. Different NaCl solutions were prepared by dissolving the desired amount of salt in demineralized water. Electrical conductivity was used as an indicator for concentration of NaCl in solution, as NaCl solution is a strong electrolyte. A calibration curve was realized to put in place the relationship between the NaCl concentration of the solution and its EC. During the experiments, the EC of the target solution was continuously measured. Subsequently, the corresponding NaCl concentration was determined using the relationship between NaCl concentration and the EC. The following measuring methods were identical for each experiment.

- *EC and temperature*: During the ED and VMD experiments, the EC and temperature of the NaCl solution in the feed bottle were continuously monitored for each experiment using a WTW TetraCon conductivity probe along with a WTW Multi-parameter portable meter IDS3630.

- *Changes in feed solution mass*: The change in feed mass was measured using a digital precision balance KERN PCB 10000-1. For ED experiments, the diluate and concentrate masses were manually measured before and after each experiments. For VMD experiments, the feed solution mass was measured continuously and digitally logged via an interface cable RS-232 that connects the balance to a laptop.

- *Concentration factor*: The achieved CF value for each experiment was determined by the NaCl concentration of the initial stream and that of the final product stream.

3.3. Vacuum Membrane Distillation

The laboratory set up and a schematic flow diagram of the VMD experiments are shown in Appendix B.5 and Figure 3.1, respectively. The specific apparatus used for VMD experiments consisted of the following:

- KERN PCB 10000-1 precision balance
- IKA RH digital magnetic stirrer with heating
- IKA ETS-D5 electric contact thermometer
- 500mL laboratory bottle DURAN®
- Digital pressure sensors FESTO SPAN in ranges 0...2 bar and 0...-1 bar
- Sterlitech CF042 Clear Cast Acrylic forward osmosis (FO) membrane cell
- Sterlitech flat-sheet laminated (PP neting) PTFE membrane with pore size 0.1μm and active membrane area of 33.5cm^2
- Sterlitech CF042 Low Foulant Diamond spacers 47mil (feed) and 31mil (permeate)

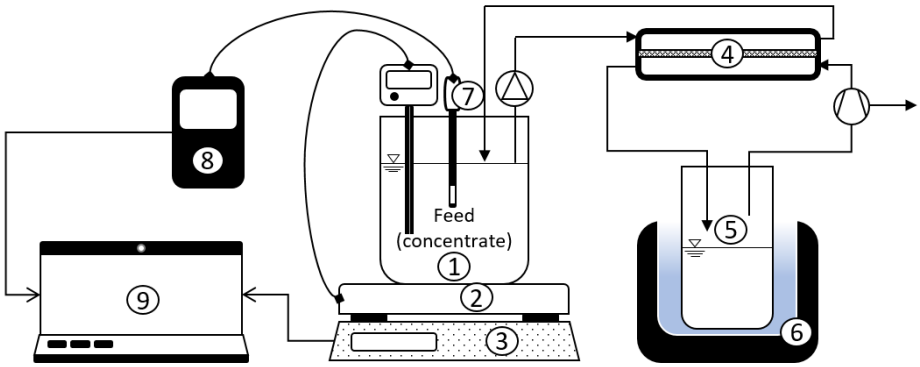

Figure 3.1: Vacuum MD configuration at laboratory scale, Lenntech (Delfgauw). (1) Feed and concentrate bottle, (2) heating and stirring block, (3) digital precision balance, (4) MD module, (5) gas washing bottle, (6) cooling bath, (7) EC probe, (8) multimeter and (9) external logging device.

- Gas washing bottles Drechsel head form DURAN®
- Diaphragm vacuum pump N816.3 KT.18 (ultimate vacuum 15 mbar abs.), control valve and vacuum gauge LABOPORT®
- Cooling baths (ice packs in plastic boxes)

3.3.1. Set-up procedure and data collection

Prior to the experiments, simulations using PHREEQC were performed for different concentrations of NaCl in aqueous solution to estimate the vapour pressure in the feed side. In order to verify whether the PHREEQC simulation produces reliable outputs, its pure water simulation output was compared to Antoine's mathematical expression of the temperature dependent vapour pressure for pure substances using Equation 2.9. Concentrations of 0, 5, 20, 40, 80 and 160 g/L and temperatures between 0 and 80 ^{o}C were used for the simulations. During the experiments the bottled solution was heated to, and continuously kept at the desired temperature using the thermostat and heating plate. Subsequently, the heating plate was placed onto the digital balance, which was connected to an external device (laptop). The mass data was transferred and logged continuously. The mass change over time of the feed solution was continuously recorded, while the initial and final feed solution masses were manually weighted. The solution was recirculated from the feed bottle to the feed side of the MD module and back to the feed bottle by a peristaltic pump. The EC in the feed bottle was continuously logged. The feed and permeate sides of the MD module were separated by a flat-sheet laminated membrane, in between two spacers. The 47mil spacer promoted turbulent flow in the feed side, while the permeate spacer prevented the membrane to be stuck unto the permeate outlet by vacuum. Partial vacuum of 1500 Pa in the permeate side of the system was realized by the vacuum pump. The permeate outlet was connected to three gas washing bottles in series, which were placed in cooling baths. The gas washing bottles served as vapour traps, minimizing vapour condensation (and thus contamination) in the vacuum pump such that the pump could achieve its ultimate specified pressure level rapidly. The cooling bath ensured cold air in the gas washing bottles, stimulating water vapour condensation. The masses of the gas washing bottles were manually weighted before and after each experiment. Digital pressure sensors were placed before the feed inlet and after the permeate outlet of the MD module.

3.3.2. Data processing

The determination of mass transfer through the membrane was assessed by the different feed and permeate weight measuring procedures. The presumption is that the manually weighted masses of the feed solution is most accurate compared to the permeate side, as the cold bath trap did not fully condense the vapour. A permeability test using demineralized water as feed solution was performed before and after the experiments for blank-comparison.

1. The water flux through the MD membrane was calculated using Equation 2.6. The feed bottle was measure before and after the experiments. The mass change rate was obtained using the continuous logging data from the precision balance.
2. The mass transfer coefficient was calculated using Equation 2.8 and the vapour pressure difference across the membrane. The vacuum pump operated at partial vacuum pressure of 1500Pa, whilst the vapour pressure of the feed solution were obtained from the PHREEQC simulations.
3. The heat flux through the liquid boundary layer was calculated using Equation 2.7 and the temperature dependent latent heat of vaporization of water.

4. The volume flow rate of saturated air that is displaced by the vacuum pump was calculated using Equation 2.17. The molar flux of water across the membrane was calculated using the water flux, Equation 2.6.
5. The temperature of the feed solution was room temperature (20^oC) and requires once-only heat to achieve the desired initial temperature of the feed solution. This amount of heat was calculated using Equation 2.18.
6. Cooling at the permeate side of the membrane is required to lower the steam temperature to below boiling point temperature at vacuum conditions. This heat was calculated using Equation 2.19. Additionally, after lowering the temperature of the steam, heat is required to condensate the water vapour. This heat was calculated using Equation 2.20. A steam table was used to select the proper parameters at vacuum conditions, see Appendix B.6.
7. Thermal energy in form of cooling or heating is induced by a heat pump, which has an efficiency expressed as COP. Common values for chillers and heater was found in literature. The useful heat or cooling production were calculated using values of 6 and 4, respectively, and Equation 2.21.
8. Recirculation of the feed stream is induced by a feed pump of which the electrical energy was calculated using Equation 2.15.
9. The vacuum pump operated at a pressure lower than atmospheric pressure to continuously evacuate gas molecules from the permeate volume for maintaining partial vacuum pressure. The electrical energy required to operate the vacuum pump was calculated using Equation 2.16.

3.4. Electrodialysis

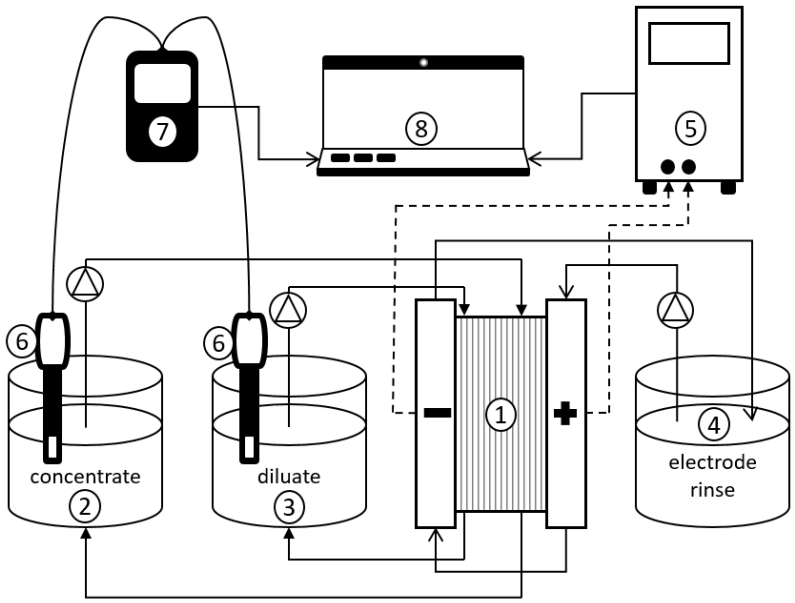

Figure 3.2: Conventional ED configuration at laboratory scale, Lenntech (Delfgauw).(1) ED module with membrane stack of 10 cell-pairs, (2) concentrate bottle, (3) diluate bottle, (4) electrode rinse solution bottle, (5) power supply, (6) EC probe, (7) multimeter and (8) external logging device.

The laboratory set up and a schematic flow diagram for the ED experiments are shown in Appendix B.5 and Figure 3.2, respectively. The specific apparatus used for ED experiments consisted of the following:

- 500mL laboratory bottle DURAN®
- Digital pressure sensors FESTO SPAN in ranges 0...2 bar
- Power supply
- Magnetic stirring plates
- PCcell GmH ED 64002, electrode surface $6.4{\cdot}10^{-3} m^2$
- PCcell GmH ED stack MVP, 10 cell pairs (10 AEM, 9 CEM and 2 CEEM). Total anion exchange membrane surface $6.4{\cdot}10^{-2} m^{-2}$ and total cation exchange membrane surface $5.8{\cdot}10^{-3} m^2$.
- TENMNA power supply
- Stirring plate

3.4.1. Set-up procedure, conditions and data collection

Whilst VMD and RO concentrate the brine by decreasing the water content in the feed, ED concentrates the brine by transportation of ions from the diluate to the feed compartment. A feed stream is fed to the ED as initial diluate and concentrate streams, thus both starting with identical ion concentration. The feed stream can be fed to the diluate compartment only, while the concentrate stream starts with clean water. The former way of operation is preferred as it eliminates the need for clean water and was thus used during the experiments. In the ED experiments, the module was fed equal starting concentration solution in the diluate and concentrate chambers, while the ERS was a 1M $NaNO_3$ solution. The three streams were recirculated through the ED module by means of a peristaltic feed pump. The ED stack consisted of 10 cell pairs with alternating monovalent AEM and CEM membranes with in-between spacers. The EC in the diluate and concentrate beakers were continuously monitored. The module was provided with a set current by the power supply, according to the calculated LCD for each test condition. The current and the electric potential data during the experiment were continuously logged using the laptop. Pressure sensors were placed before the feed inlets to determine the pressure drop across the module.

3.4.2. Data processing

Processing data to obtain the concentration factors included conversion of the obtained EC measurements to concentration in NaCl g/L using the calibration curve.

1. The change in solution mass was measured by weighing the solutions before and after each experiment. The volume was approximated using an average density of NaCl solution at 293,15 K for wt% between 1 and 19, $\rho_{avg,NaCl}$ = 1061 kg/m^3. The final concentrations were corrected for the volume change during that experiment. The CF was then calculated by dividing the final concentrate concentration by its initial concentration.
2. The mass transfer in ED is the sum of the salt, osmotic water transport and electro-osmotic water transport as explained in Section 2.3.1. The change in solution mass was assumed to be the total mass change. The salt transport was calculated using Equation 2.22 and the electro-osmotic water transport was approximated using Equation 2.23. The osmotic water transport was calculated by subtracting the mass transport contribution of salt and electro-osmosis from the measured change in total mass.
3. For each experiment, the current efficiency was calculated as high current efficiencies are desirable to minimize operating costs. Current efficiency was calculated using Equation 2.25.
4. The electrical energy consumption for ion transport in ED was calculated using Equation 2.30 and the energy for recirculating the feed was calculated using 2.15. The energy consumption can be expressed as normalization by feed volume or by transported salt.

4

Results and discussion

4.1. Simulation of the effect of limiting factors for concentrating NaCl solutions by RO

Figures 4.1 (a), (c) and (e) shows the effect of constant net driving pressure (NDP) on the recovery, rejection and average permeate flux per element at a single stage RO system design at different feed concentrations. Figures 4.1 (b), (d) and (f) shows the effect of constant NDP on the specific energy consumption (SEC) normalized by the produced concentrate and the concentration factor at different feed concentrations. The recovery of the system increases with increasing NDP, which was observed for each feed concentration. The highest trend in recovery with NDP was observed at the lowest feed concentration, while the lowest trend was observed at the highest feed concentration. this can be explained by the actual applied pressure, which is increases with increasing feed concentration until it reaches the membrane's pressure limit.

The achieved NDP also translates to concentration factors, which is lowest at 5 bar and highest at 20 bar. Results show that the rejection has a slightly decreasing trend with increasing NDP, which indicates that the permeate quality decays at higher feed pressures. However, the overall rejection was higher than 97% in each simulation and thus the permeate quality did not decay significantly. While this rejection trend could lead to lower concentration factors, the increase in recovery with NDP is greater than the rejection trend and thus results in overall increase of concentration factor. Considering that the trend in recovery flattens and decreases with feed concentration, the highest concentration factor trend with NDP was observed at low concentrations. This relates to the ability to achieve higher recoveries at low feed concentration, as the related applied pressure is well below the membrane's maximum pressure limit. The difference between applied pressure and the maximum pressure diminishes with increasing feed concentrations.

The difference in flux per element is presented in Figure 4.1 (a) as error bars, which is highest in the first element and decreases exponentially with each element (see Appendix B.1). Results show that spatial variation in permeate flux amplifies with increasing NDP. A system with low spatial variation in permeate flux is preferred in general, which is observed at the lowest NDP for each concentration. However, a high cross flow velocity on the feed side of the membrane is also important to consider to counter polarization effects among other things. A permeate flux of 15 to 18 LMH is recommended for sea water RO systems. Considering that the importance of applying high cross flow velocities becomes more significant with concentrations higher than sea water (i.e., 3.5% salinity), it can be conclude that the application of RO for concentrating brine with concentrations higher than 40 g/L seems unfeasible due to low flux. It was expected that the average fluxes per applied NDP should result in same value at different feed concentrations, however it shows a decreasing trend. The reason could be that the WAVE software considers unwanted side-effects, such as concentration polarization, which becomes more significant at increasing concentrations. Finally, the energy consumption has a positive correlation with NDP. The energy consumption for feed concentration 20 g/L was 4, 13 and 38 kWh/m^3 corresponding with concentration factors 1.8, 2.9 and 4.7 (35, 57 and 91 g/L), respectively.

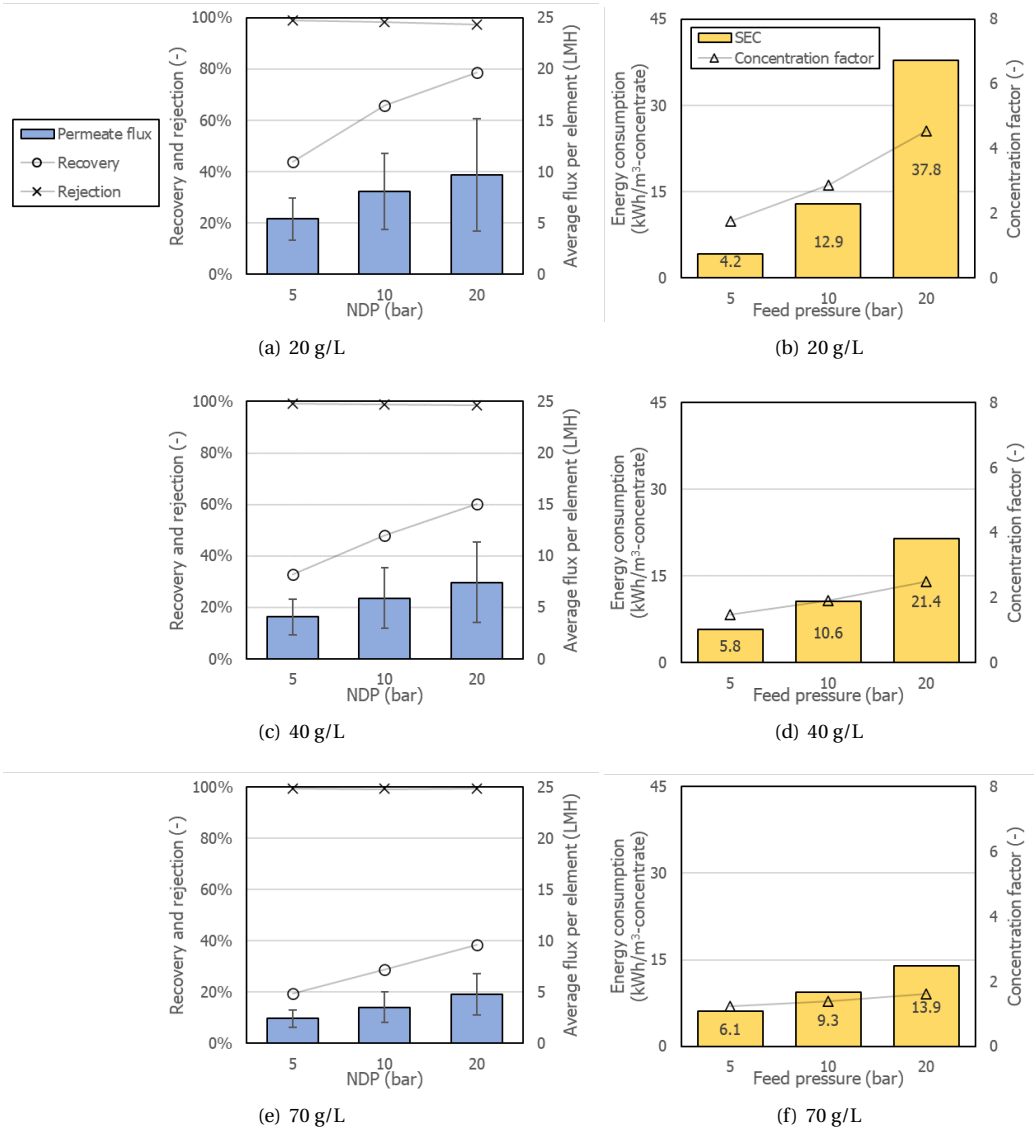

(a) 20 g/L (b) 20 g/L

(c) 40 g/L (d) 40 g/L

(e) 70 g/L (f) 70 g/L

Figure 4.1: Effect of constant feed pressure on permeate flux, recover and rejection (a), (c) and (e) and on the SEC and concentration factor (b), (d) and (f) for different feed concentrations

4.2. Effect of NaCl concentration on electrical conductivity

Electrical conductivity (EC) can be used as an indicator for salt concentrations, like NaCl, in solution. NaCl solution is a strong electrolyte, which means that in aqueous solution the ions are charged and can move when external voltage is applied, allowing the solution to conduct electricity. The more ions are present in the solution, the more electricity the solution can conduct and therefore the higher the conductivity. A calibration curve was realized to put in place the relationship between the NaCl concentration of the solution and its EC, as shown in Figure 4.2. Theoretically, the conductivity should increase in direct proportion to the ion concentration. In practice, this does not hold true. The conductivity does not only depend on the charge carriers, the ions, it also depends on its mobility. As the concentration of the ion increases in a solution, the mobility of these charge carriers decreases and appropriately the conductivity represents a quadratic effect. The measured values were extrapolated and at higher salt concentrations this phenomena occurs, as presented in Figure 4.2. During the experiments, the EC of the target solution is continuously measured. Subsequently, the corresponding NaCl concentration is determined using the relationship between NaCl concentration and the EC presented in Figure 4.2.

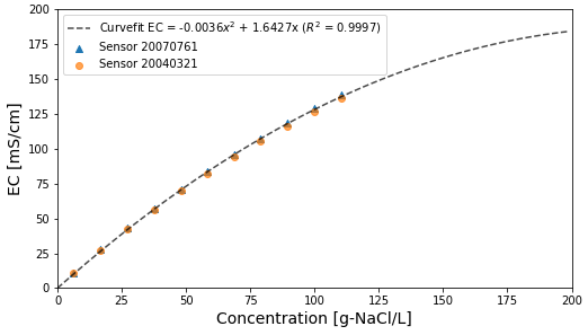

Figure 4.2: Electrical conductivity as a function of NaCl concentration.

4.3. Limiting factors of concentrating NaCl solution using VMD

The VMD experiments were conducted to study the effect of different NaCl feed concentrations and operating temperatures on the concentration performance on the water flux. This permeate flux has a direct relationship with the achieved concentration factor, as water is the only volatile compound in the considered solutions. In this work, two VMD parameters were assessed: feed operating temperature and NaCl feed concentration. The feed flow rate was adjusted accordingly to the operating temperature and spacer geometric parameters for regulating a constant Reynolds number of 350, while the pressure in the permeate side was held constant at a partial vacuum pressure of 1500 Pa by the vacuum pump. The detailed calculations of feed flow rate for the experimental conditions is presented in Appendix B.1. The maximum solubility limit for NaCl in water at 25 ^{o}C is 357 mg/mL (i.e., 26.3 wt%) and does not change significantly with temperature. In theory, distillation can be applied until the treated solution has reached its maximum solubility level. Considering that the objective is to test different experimental conditions rather than crystallizing NaCl, the VMD experiments were performed until a CF of 1.1 was achieved. As such, it is presumed sufficient data was obtained to assess the technology on concentration limiting factors and energy consumption. The NaCl feed solutions were prepared using deionized water with EC values between 18 and 250 μS/cm. The EC of the collected permeate of each experiment was measured and the values were repeatedly under 250 μS/cm and thus it was proven that the membrane fully rejected the salt. All test conditions were repeated twice to evaluate the spread of the data and improve the reliability of the investigation.

4.3.1. Influence of NaCl feed concentration on the bulk vapour pressure

The effect of operating temperature on the water vapour pressure of different NaCl solutions are presented in Figure 4.3 (a). The figure show that the PHREEQC simulation output and Antoine's vapour pressure calculation for pure water are in agreement, and therefore it is assumed that the PHREEQC model produces reliable outputs for this assessment. The simulations show an exponential trend for the vapour pressure of the different solutions with increasing temperature. This can be explained by the liquid-vapour equilibrium concept, discussed in Section 2.2.1. With increasing temperature, the fraction of molecules with high kinetic energy increases and thus higher rates of vaporization is achieved. The observation agrees with the kinetic theory, previously discussed in 2.2.1.

Though the values of increasing vapour pressure seems similar for different solution simulation at first, differences in results appear if we take aim at a portion of the graph. Figure 4.3 (b) shows the simulated vapour pressures for different NaCl solutions in a temperature range of 30 to 50 ^{o}C. With increasing NaCl concentration in the solution, the vapour pressure is lower at identical temperatures. This is because the solute mole fraction increases strongly with higher solute concentrations, and therefore the vapour pressure reduces accordingly.

		NaCl concentration [g·L^{-1}]		
		20	40	80
Temperature [^{o}C]	30	1.19 %	2.41%	5.05%
	40	1.19%	2.43%	4.90%
	50	1.19%	2.41%	5.05%

Table 4.1: Lowering of the vapour pressure with increasing solute fraction.

Table 4.1 presents the lowering of the vapour pressure due to increased solute fraction in the considered NaCl solutions compared to pure water. It is observed that the change in water vapour pressure of NaCl so-

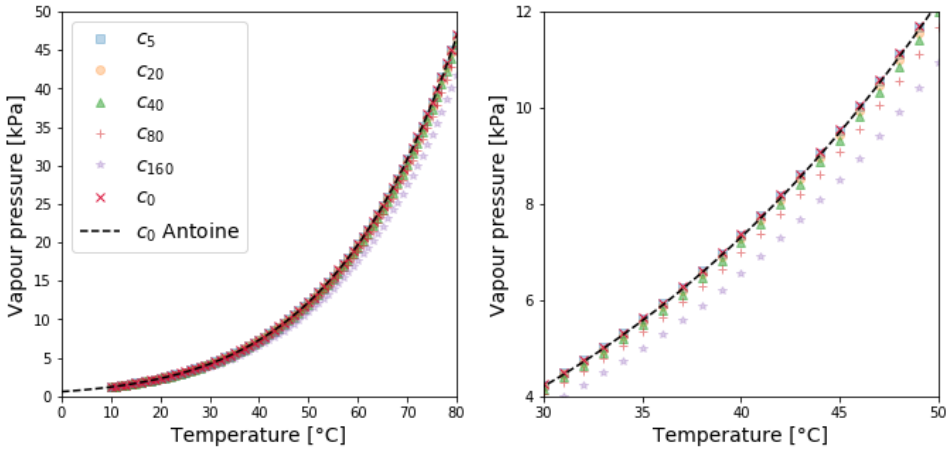

(a) (b)

Figure 4.3: Sub figure (a) presents the effect of operating temperature on the water vapour pressure of NaCl solutions and sub figure (b) presents the detailed data between temperatures 30 and 50 ^{o}C.

lutions is of a similar value for each concentration at the considered temperatures, i.e., the vapour pressure lowering for a 20 g/L solution is 1.2% at each temperature. The vapour pressure lowering at 20 g/L compared to 40 g/L is by a factor of 2 (i.e., 1.2% versus 2.4%), which is similar to its concentration factor. However the vapour pressure lowering at 20 g/L compared to 80 g/L is by a factor of 4.2, which is higher than its concentration factor of 4. This indicates that the lowering of vapour pressure intensifies at higher solute concentrations. Though, the overall effect of vapour pressure lowering due to increasing operating temperature and NaCl concentration is not striking.

4.3.2. Membrane distillation coefficient

The permeate flux of deionized water was measured at different temperatures. The simulated vapour pressure differences at these temperatures were then plotted against the permeate fluxes, see Figure 4.4. The result shows a linear relationship between the pure water flux and the vapour pressure difference of which the slope represents the overall membrane distillation coefficient, C_{VMD} = 0,003 kg/m^2/h/Pa. This coefficient enables prediction of the permeate flux at different operating temperatures, but is membrane and vapour specific.

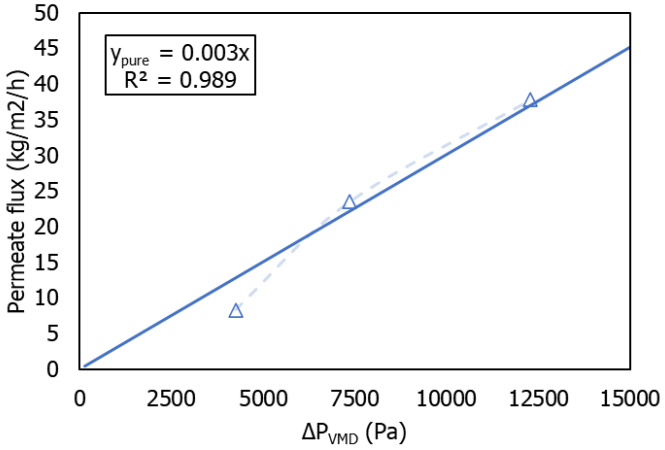

Figure 4.4: Relationship between the permeate flux and vapour pressure difference for pure water.

4.3.3. Effect of feed temperature and salinity on permeate flux

At the lowest considered operating temperature of 30 ^{o}C, the results do not show the phenomena clearly. Moreover, the permeate flux for deionized water is lower than permeate fluxes for the different NaCl feed concentrations. A decreasing trend in water flux should be observed for increasing concentrations due to lowering of the vapour pressure, but this is not the case. The imprecision of data could be due to the sample

size (i.e., concentration factor of 1.1), which might have been small to obtain reliable results at low operating temperature. The lab-scale set-up was not insulated and the sample volume was small, thus loss of heat to the environment and improper temperature regulation by the thermostat at low operating temperatures could have influence the results negatively.

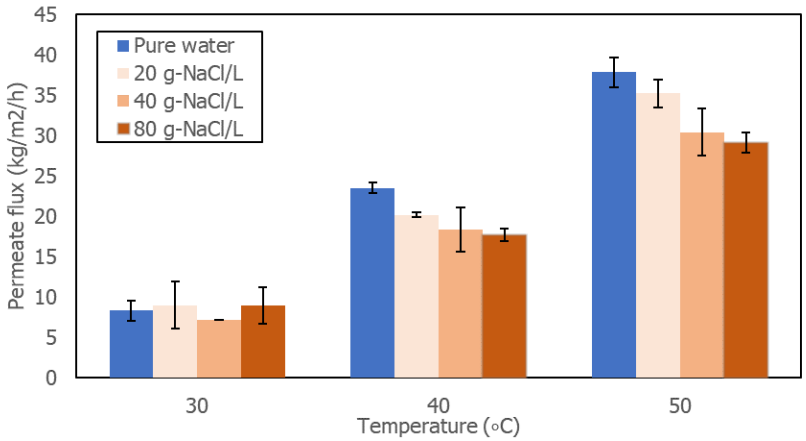

Figure 4.5: Permeate flux of the membrane under three different operating temperatures (30, 40 and 50 ^{o}C), using three different NaCl starting concentrations (20, 40 and 50 g/L) and deionized water.

4.3.4. Energy distribution in VMD process

In the previous section it was discussed that operating temperature has a greater effect on the permeate flux compared to the feed concentration. The average flux of the feed concentrations per operating temperature was thus assumed to calculate the energy consumption. The average fluxes for 30, 40 and 50 ^{o}C used for the calculations are 7, 19 and 32 kg/m^2/h, respectively. Figure 4.6 (a) and (b) present the effect of operating temperature and concentration factor on the energy consumption and its distribution. Figure 4.6 (a) shows clearly that the energy consumption to concentrate a solution to the same concentration factor at different temperatures is very similar. This is reasonable, because the same amount of water is needed to evaporate to achieve the same concentration factor. However, the increase in energy consumption with concentration factor is not proportional. Results prove that an exponential relation exists between the concentration and the energy consumption. This means that VMD proves to be most efficient when applied to high feed concentrations. There is a slight increase in energy consumption with higher temperatures, which is related to the energy contributed by the cooling step. More energy is consumed to cool down higher temperatures, however the increase in energy is insignificant. Figure 4.6 (b) presents the energy distribution of different components used for VMD, which is consistent with increasing operating temperature. The results show that condensation contributes to the highest energy consumption, which accounts for 81% of the total energy consumption. The second-highest energy consumer in the system is the vacuum pump, which accounts for 18.9%. The remaining 0.1% is contributed by the other components, which is insignificant compared to the condenser and vacuum pump. It is worthy to mention that most of the energy consumed is on the permeate side of the of such systems and therefore it is clear that in VMD the operating temperature does not contribute to a significant change in overall energy consumption. A high operating temperature merely dictates how fast the concentration happens (i.e., high operating flux).

COP values can be considered for the thermal components when conceptualizing a VMD system, which was discussed in Section 2.2.4. For heating elements a COP value of 6.2 was considered, while a COP value of 3.8 was considered for cooling elements. Figure 4.7 presents the effect of COP values on the overall energy consumption by VMD. Results show that the overall energy consumption decreased by a factor of 2.4, which is significant. Furthermore, the energy distribution changed to rather equal parts. With improved COP values, the energy contribution by thermal components decreases and results in a significant decrease in overall energy consumption. From these results it is clear that the energy consumption by VMD is greatly limited by the efficiency of the vacuum pump.

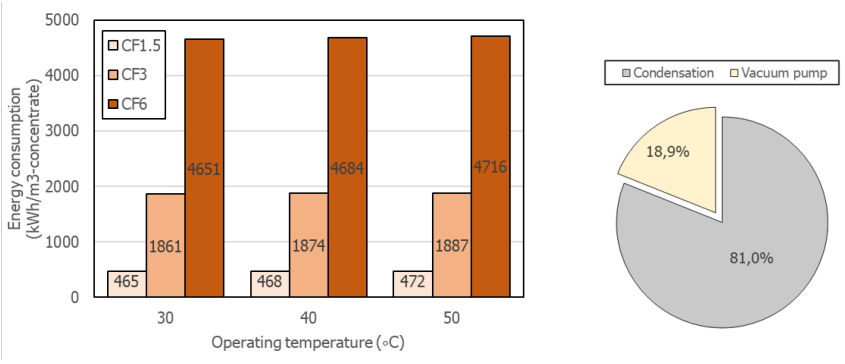

(a) (b)

Figure 4.6: Sub figure (a) presents the effect of operating temperature and concentration factor on the energy consumption and sub figure (b) presents the energy distribution in VMD.

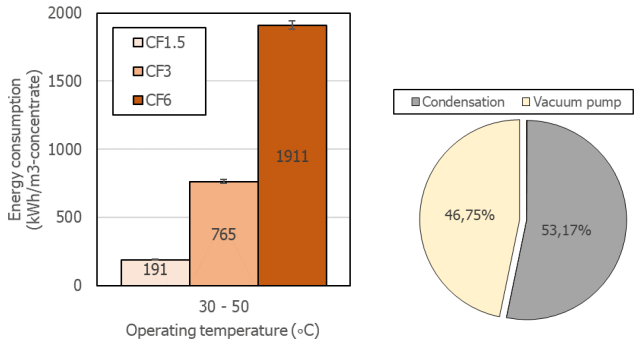

(a) (b)

Figure 4.7: Sub figure (a) presents the effect of COP values for thermal components on the energy consumption for achieving different concentration factors and sub figure (b) presents the COP-adjusted energy distribution in VMD.

4.4. Limiting factors of concentrating NaCl solution using ED

The ED experiments were conducted to study the concentration performance in terms of operating principle, feed concentration and achieved concentration factors. As ED can be operated under different settings, based on the approach, the chosen operating principle of ED in this study is to reduce the salt concentration by 50% from the diluate applying different current densities. Initial concentrations of 20, 40 and 80 g/L were used as feed solution. Furthermore, the effect of different initial diluate to concentrate volume ratios was studied.

4.4.1. Influence of salt concentration and cross-flow velocity on LCD

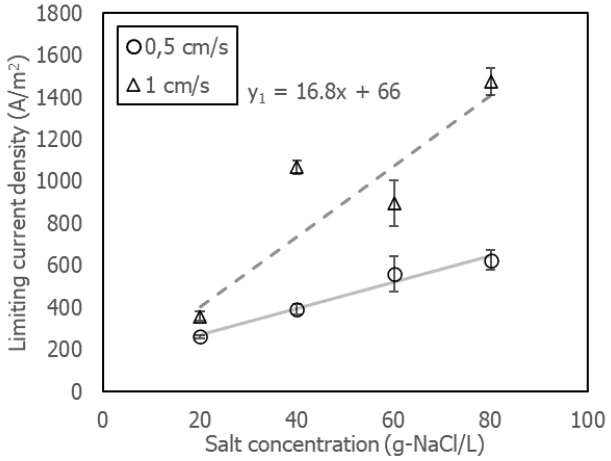

Figure 4.8: Effect of cross flow velocity on limiting current density different NaCl concentrations and cross flow velocities of 0.5 and 1 cm $\cdot s^{-1}$.

		Salt concentration		
		10	20	40
	LCD	234	402	738
	0.50	117	201	369
Partial LCD	0.75	175	301	554
	0.90	210	362	665

Table 4.2: Limiting current densities of salt concentrations using a cross-flow velocity of 1 cm $\cdot s^{-1}$.

Following the operating principle using the final diluate concentration as the restriction, the effect of salt concentration and cross-flow velocity on the LCD was studied. The LCDs were experimentally determined using the method by Cowan and Brown (1959) for salt concentrations 20, 40, 60 and 80 g/L and cross flow velocities of 0.5 and 1 cm/s. The elaborate findings of this experiment can be found in Appendix B.3. The obtained LCDs were plotted against the salt concentrations for each cross flow velocity, as presented in Figure 4.6. The results show that with increasing salt concentration, the LCD increases and that the LCD increases with cross flow velocity, but is not proportional. Usually, the lowering of the slope occurs in solutions with multiple compounds. This behaviour is the effect of hindrance on ionic removal by other compounds (i.e., organic molecules). Though the prepared feed solution does not contain other compounds and such retarding effect was not expected, the obtained results does correspond to the general findings from literature. As mentioned in Section 2.3.2, no optimal cross flow velocity has been reported in literature. In principle higher LCDs can still be achieved when applying higher cross flow velocities, but operational-wise it might not be economically feasible due to the related high power supply and possible negative side-effects (i.e., cooling required). In the continuation of this study, all ED experiments were performed using the highest determined cross-flow velocity of 1 cm/s.

4.4.2. Effect of partial LCD on the concentration performance by ED

Effect of partial LCD on energy consumption

To prevent negative effects, such as water dissociation on the IEX membranes, it is important to operate ED under the LCD as previously discussed in Section 2.3.2. However, it is also interesting to investigate the effect of partial LCDs on the concentration performance and energy consumption. The ED experiments were conducted using constant current densities presented in Table 4.2, using the linear relationship in Figure 4.6 corresponding to a cross flow velocity of 1 cm/s. Figure 4.9 (a), (b) and (c) presents the evolution of concentration in the diluate and concentrate streams over time. Salt migration from the diluate to concentrate channels were clearly observed as the concentrations in the diluate stream reduced while the salt concentration increases in the concentrate stream. A 50% concentration reduction was achieved for each diluate stream, as intended. A constant CD was applied throughout each experiment, which suggests that with lower applied partial LCD (i.e., lower CD) the operational time to achieve the goal is prolonged compared to higher partial LCD, provided that other parameters remain constant. Increasing the partial LCD from 0.50 to 0.90 reduces the operational time from 21 to 11 minutes for feed concentration 20 g/L. Increasing the partial LCD

from 0.50 to 0.75 for the same feed concentration reduced the operational time from 21 to 13 minutes. The results suggest that the operational time is not proportional to the applied CD between partial LCDs of 0.50 and 0.90. Similar trends were observed for feed concentrations 40 and 80 g/L. This can be explained by the non-proportional relationship between the experimentally determined LCDs and the salt concentration, which also directly translates to the energy consumption.

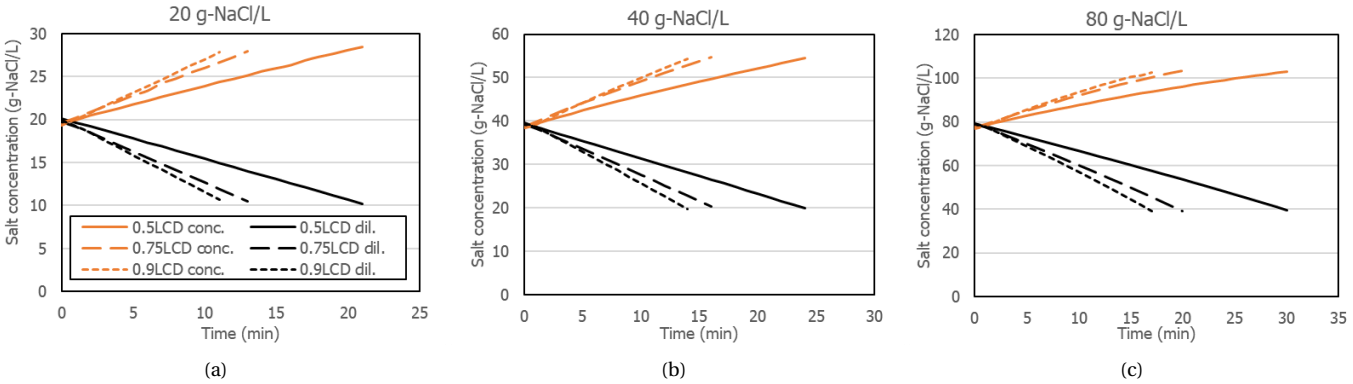

(a) (b) (c)

Figure 4.9: Sub figures (a),(b) and (c) show the impact of partial LCDs and different feed solutions on the diluate and concentrate salinities over the course of reducing the diluate salinity by 50%.

Effect of partial LCD on concentration factor

Figures 4.10 (a) and (b) present the achieved concentration factors and energy consumption normalized to m^3 produced concentrate. Though a dilution factor of 2 was achieved in the diluate stream, the results show that the concentration factor in the concentrate stream was not equal. The average concentration factors achieved were 1.5, 1.4 and 1.3 for initial feed concentrations 20, 40 and 80 g/L, respectively. Furthermore, energy consumption increases with higher applied CDs for each feed concentration, while similar concentration factors were achieved. This means that it is more advantageous to apply lower CDs to achieve the same desalination of the diluate, because the concentration factor is limited to the amount of salt transported from the diluate. The reason why the energy consumption is higher for high feed concentrations is because the absolute salt transport is larger at higher concentration.

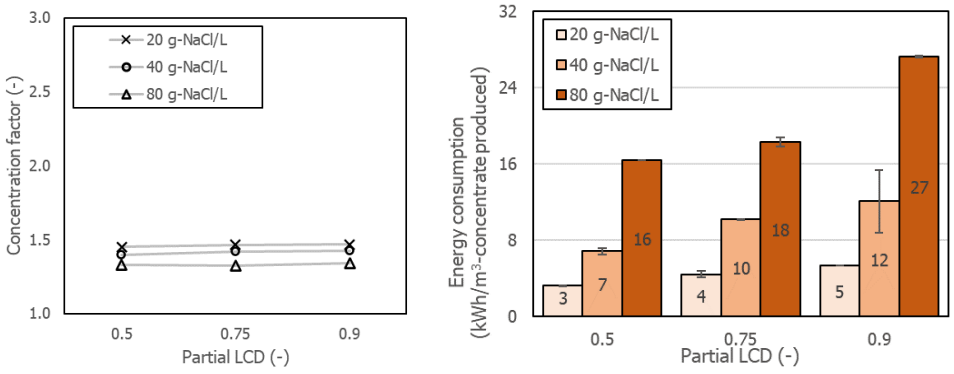

(a) (b)

Figure 4.10: Sub figure (a) shows the impact of applied partial LCD on the concentration factor for different feed solutions for reducing the diluate salinity by 50%. Sub figure (b) shows the impact of applied partial LCD on the energy consumption.

Figure 4.10 (a) shows that lower concentration factors are achieved with higher feed concentrations, which can be explained by the presence of osmosis, electro-osmosis and diffusion. The mass transport of salt and water were measured and calculated based on the initial diluate mass, which are presented in Figures 4.11 (a), (b) and (c). The total mass transport to achieve a dilution factor of 2 in the diluate for feed concentrations 20, 40 and 80 g/L are 6%, 11% and 21% on average. Figure 4.11 (b) shows that the osmotic water transport consistently contributes to half of the total mass transport with partial applied LCDs, whereas Figure 4.11 (c) show that the osmotic water transport contributes to less than half of the total mass transport. Figure 4.11 (a) shows a decreasing trend in osmotic water transport with increasing current density. A study by Doorn-

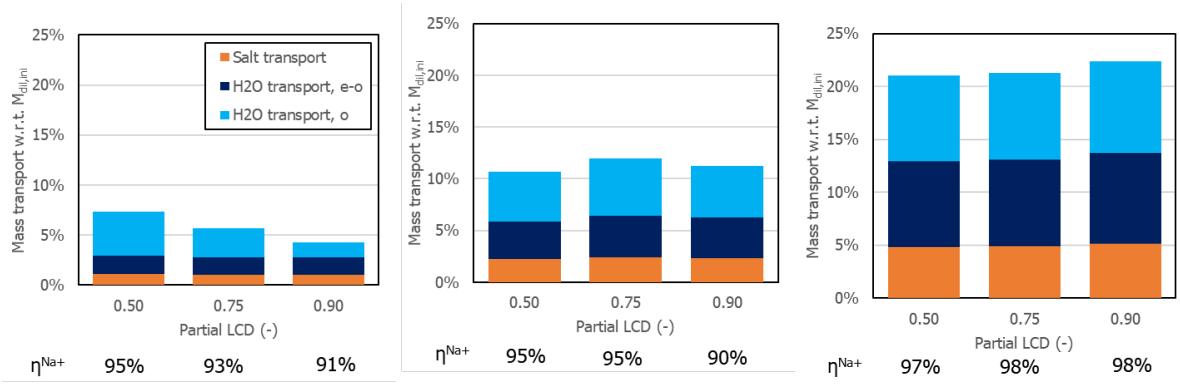

Figure 4.11: Sub figures (a),(b) and (c) show the impact of partial LCDs on the salt and water mass transport distribution and the current efficiencies for reducing the diluate salinity by 50%, for feed concentrations 20, 40 and 80 g/L, respectively.

busch et al. [58] investigated the effect of uniform current densities on water flux, among other things, using a synthetic brine (30 gNaCl/L) and showed that higher current densities resulted in increased electro-osmotic water fluxes, which is opposite what is observed in Figure 4.11 (a). A possible explanation for a decreasing contribution of osmotic water transport at the lowest feed concentration could be that the operating time is dominant over the mass transfer coefficient contribution by osmosis, while at higher feed concentrations effect is reversed. Figure 4.11 (c) shows a slight increasing osmotic water transport trend with higher applied CD, which is a similar observation made by Doornbusch et al. [58]. However, not enough data was collected to prove this behaviour to be consistent. Furthermore, the results show that the osmotic water transport contribution to the overall mass transport decreases with increasing feed concentrations provided that same operational settings are applied i.e., determine partial LCDs accordingly. It is important to mention that the absolute water transport increases with higher feed concentrations. Meaning that the concentrate stream becomes more diluted and thus lower concentration factors will be achieved with higher feed concentrations based on these operational settings, which was previously observed in Figure 4.10 (a). Figures 4.11 (a) and (b) show that current efficiency decreases with higher applied CD, which could mean that diffusion is more dominant at CDs close to LCD. Figure 4.11 (c) does not show the same trend, but proves that high current efficiencies are achieved with higher feed concentrations. This means that current utilization is affected less by diffusion with high feed concentrations. In theory, the rate of diffusion increases with greater concentration gradient across the membrane among other things. It was thus expected that for higher feed concentrations, lower current efficiencies should be observed. This was not observed in this study, but the overall current efficiencies are higher than 90%. This proves that the selected ED operating process is rather efficient.

4.4.3. Effect initial volume ratio on the concentration performance of ED

In the previous subsection it was discussed that concentration factors are limited by amount of salt transport from the diluate. The incentive to investigate different initial volume ratios was to make an effort to achieve higher concentration factors in the concentrate stream. The initial volume ratio is defined as $\Phi = V_{dil} : V_{conc}$. Initial volume ratio 2 (Φ_2) and 4 (Φ_4) were investigated additional to the base case, in which the volume ratio was 1 (Φ_1). Other operating parameters were kept the same. The effect of different initial volume ratio on the salt and water mass transport are presented in Figure 4.12. The total mass transport to reduce the salt concentration in the diluate by half for feed concentrations 20, 40 and 80 g/L are 5%, 11% and 22% on average for the evaluated volume ratios. These values correspond to the values of Φ_1, as previously observed. It is very remarkable that the total mass transport and its salt and water contribution at each feed concentration is fairly equal for a different initial volume ratio. Furthermore, the previous observation in which the operating time is dominant over the mass transfer coefficient contribution by osmosis at lower feed concentrations at Φ_1, was not observed at Φ_2 and Φ_4. The achieved concentration factors for volume ratios 2 and 4 are presented in Figures 4.13 (a) and (b), respectively. Average concentration factors of 1.5, 1.8 and 2.5 were achieved for feed concentration 20 g/L at Φ_1, Φ_2 and Φ_4, respectively, while average concentration factors of 1.3, 1.5 and 1.8 were achieved for feed concentration 80 g/L. The results show that the effect of higher volume ratios results in higher overall concentration factors. This is because the same amount of salt is transported into smaller volumes, while the osmotic water transport and current efficiencies are comparative at different initial volume ratios. Hence, more concentrated salt solutions can be obtained when increasing the initial volume ratio. A study by Jiang et al. [59] investigated the effect of volume ratio on the TDS of the concen-

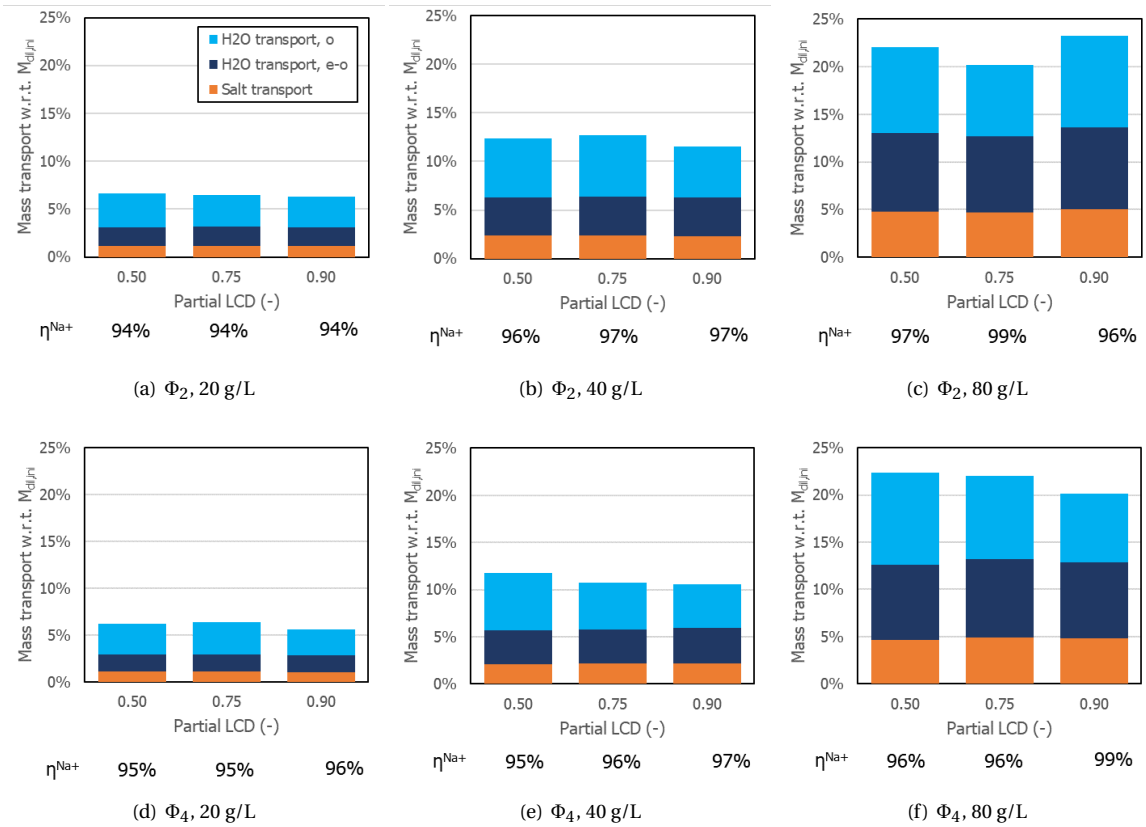

(a) Φ_2, 20 g/L (b) Φ_2, 40 g/L (c) Φ_2, 80 g/L

(d) Φ_4, 20 g/L (e) Φ_4, 40 g/L (f) Φ_4, 80 g/L

Figure 4.12: Sub figures (a), (b) and (c) show the impact of partial LCDs on the salt and water mass transport distribution and the current efficiencies using an initial volume ratio of 2, while the results with initial volume ratio 4 are presented in sub figures (d), (e) and (f).

trate compartment and shares the same observation. This research observed a factor 1.4 increase in TDS concentration by applying a volume ratio of 3, using RO brine and current density 50 A/m^2.

Figure 4.13 (c) presents the energy consumption required to obtain the aforementioned concentration factors for different feed solutions. These results concerns the experiments performed at 0.5LCD, because it was previously observed that it is more advantageous to apply lower CD whilst the same CF are achieved. The energy consumption seems to increase proportionally when comparing the data sets of Φ_1 and Φ_2 with regards to 50% salt reduction in the diluate stream. For feed concentration 20 g/L using Φ_1 required 3 kWh/m^3, whilst using Φ_2 required 7 kWh/m^3. The required energy increased by a factor of two, which also corresponds to the volume ratio increase. This is reasonable, because the amount of salt to be transported using Φ_2 is twice as much compared to Φ_1 and thus requires twice the amount of energy. Comparison of the energy consumption of data sets Φ_1 and Φ_4 show that transporting four times the amount of salt does not result in an energy consumption increase by the same factor, but less. The results prove that the energy required to reduce 50% of the diluate concentration is proportional to the volume ratio when assuming Φ_2, but does not hold true for larger volume ratios. The concentration factors achieved using Φ_1, Φ_2 and Φ_4 are presented in Figure 4.10 (a), Figure 4.13 (a) and Figure 4.13 (b). The results show that with increasing volume ratio, higher concentration factors were achieved. The highest increase in concentration factor was achieved using feed concentration 20 g/L (1.5, 1.8 and 2.5), whilst the lowest increase in concentration factor was achieved using feed concentration 80 g/L (1.3, 1.6 and 1.8). These comparisons also prove that the increase in concentration factor is not proportional to the increase in volume ratio. Appendix B.3 presents the full data set of the effect of volume ratio on concentration factor and energy consumption, including the results of partial LCDs 0.75 and 0.90.

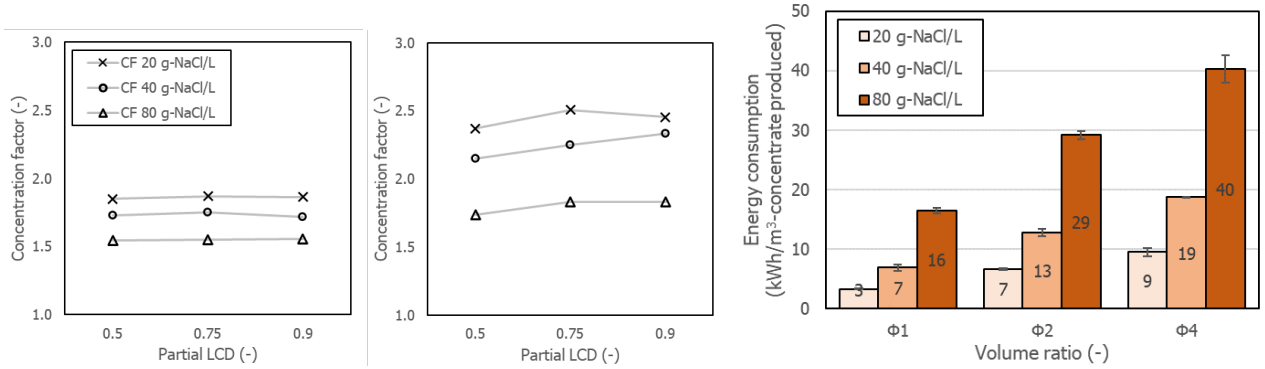

(a) Φ_2 (b) Φ_4 (c)

Figure 4.13: Sub figures (a) and (b) show the impact of volume ratios 2 and 4, respectively, on the concentration factor. Sub figure (c) shows the impact of different volume ratios on the energy consumption, based on 0.5LCD.

4.5. Comparison of brine concentration performance: RO, ED and VMD

The energy consumption to concentrate different feed solutions using RO, ED and VMD are presented in Figure 4.14 (a), (b) and (c), respectively.

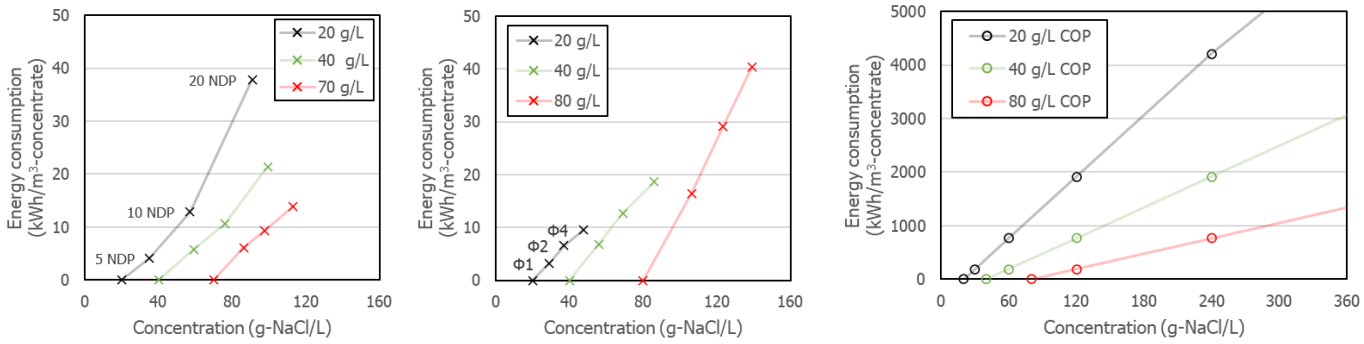

(a) RO (b) ED (c) VMD

Figure 4.14: Energy consumption for different membrane technologies for concentrating different feed solutions.

The RO results show that it is possible to concentrate a wide range of feed concentration and that energy consumption can be reduced by staging. To concentrate 20 g/L to 80 g/L could be performed by two stages, for example. The first concentration step can be performed to achieve CF = 2 by applying an NDP slightly higher than 5 for which the energy consumption is about 5 kWh/m^3. When achieving 40 g/L after the first stage, a second stage with higher applied pressure can be used to achieve another CF = 2 by applying a NDP of 10 for which the energy consumption is about 10 kWh/m^3. In total 15 kWh/m^3 is used to achieve a final concentration of 80 g/L using two stages, compared to 38 kWh/m^3 if the concentration step is performed using one stage. An energy reduction by factor 2.5 can be achieved when using a two-stage RO system compared to a single-stage RO system. However, as discussed in the previous section, the application of RO for concentrating feed solutions higher than 40 g/L seems unfeasible due to low flux production. Low flux production is correlated to low cross flow velocities, which leads to negative side-effects such as increased boundary layer on the feed side of the membrane. Furthermore, conventional seawater RO systems are limited to about 50 bar. High pressure reverse osmosis (HPRO) systems can go up to 120 bar, based on the mechanical limitation of the membrane. However, the components for HPRO systems are usually more expensive as they require higher mechanical strength to ensure consistent performance. This results in higher initial costs, which does not out-weight the choice to use a different membrane technology after the concentration limitation has been achieved with RO. The maximum achievable concentration related to a feed pressure of 50 bar using RO is 57 g/L, for feed concentration 20 g/L and 10 NDP (see Figure 4.1 (b)). The energy consumption that is associated to this concentration step is 38 kWh/m^3.

The ED results show that it is also possible to concentrate a wide range of feed concentration and that

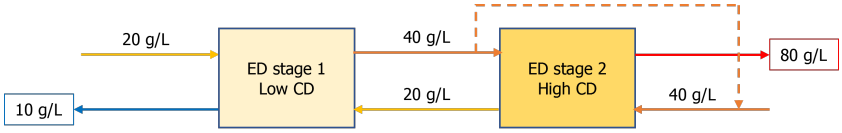

Figure 4.15: Schematic diagram of a multistage ED using counter flow operation mode.

higher concentration factors can be achieved using high initial volume ratios, while minimizing the effect of osmotic water transport and diffusion on the final concentrate concentration. High concentration factors can also be achieved by ED staging and using a counter flow operation mode. Multistage ED is beneficial becaus higher CD can be applied after each subsequent concentration stage, due to increasing LCDs with higher concentration. This effectively decreases the energy consumption compared to constant applied CD. Moreover, previous results prove that there is a concentration factor limitation caused by the amount of salt transport when applying a constant CD. As such, an overal larger amount of salt transport can be achieved using multistage ED. Counter flow operation mode is beneficial because it decreases the concentration gradient across the membranes, which further decreases the effect of osmotic water transport and diffusion. This means that higher concentration factors per stage can be achieved. A possible schematic of such multistage ED with counter flow operation mode is presented in Figure 4.15. To concentrate 20 g/L to 140 g/L could be performed by multistage as follows. Figure 4.14 (b) shows that CF = 2 can be achieved when applying a volume ratio of 4, for which the energy consumption is about 8 kWh/m^3. So far, the energy consumption by ED is slightly higher compared to the energy required to achieve the same concentration using RO with a multi-stage design but is very comparable. At 40 g/L a higher CD can be applied, which can achieve a concentration of 80 g/L for which the energy consumption is about 17 kWh/m^3. At 80 g/L a higher CD can be applied, which can achieve a concentration of 140 g/L for which the energy consumption is 40 kWh/m^3. The total energy required to concentrate 20 g/L to 140 g/L is 65 kWh/m^3. As indicated earlier, the RO system becomes unfeasible when achieving concentrations higher than 57 g/L and thus ED is preferred over RO due to its ability to concentrate further.

The VMD results show that the average energy consumption to concentrate brine is much higher compared to ED and RO. As a comparison to concentrate 20 g/L to 60 g/L using RO and ED requires 13 and 18 kWh/m^3, respectively. Using VMD for this step requires 765 kWh/m^3, while considering COP values for heating elements. The VMD energy consumption for a similar concentration factor increases by a factor of 61, which is significant. As the VMD energy consumption is governed by the amount of water to be evaporated, it is more feasible to apply VMD at higher feed concentrations. This also means that the increase in energy consumption of VMD, compared to RO and ED, increases significantly with lower feed concentrations. While for RO and ED the trend is opposite i.e., the energy consumption of RO and ED decreases with lower feed concentrations. In theory VMD is able to concentrate a salt solution to its solubility limit, whereas RO and ED cannot. Thus, this technology has added value in case zero liquid discharge (ZLD) is needed. This means that VMD is a suitable choice as a final concentration step, but not for concentrating brines within the considered range.

Although the energy consumption to concentrate lower feed concentrations for RO were not simulated, it can be assumed that RO is the optimal choice to produce high quality permeate compared to VMD. This is because the energy consumption for VMD is a factor 100 higher compared to RO to produce the same or better permeate quality, while prioritizing concentration. Lower feed concentrations were not tested using ED, but it is expected that RO will outperform ED in this range, in terms of energy consumption. Although lower feed concentrations were not tested using VMD, the VMD energy consumption increases significantly with lower feed concentrations as mentioned before.

5

Conclusions an Recommendations

5.1. Conclusions

The goal of this research was to broaden current knowledge on brine concentration using RO, ED and VMD by assessing its limitations for concentration and energy consumption. To achieve this goal, research questions were posed in Section 1.3 to provide an approach for this study assessment. The answers to the research questions and conclusion are presented in this section.

How do RO limiting factors affect concentrating brine and how does it relate to its energy consumption?

Concentration performance by RO is limited by the osmotic pressure exerted by the feed concentration. A higher NDP resulted in increased concentration, but is limited to the maximum allowable applied pressure on the membrane. A higher applied NDP also resulted in more spatial variation in flux for each element, which is undesirable as it results in performance distribution imbalances in a pressure vessel. The average fluxes declined greatly with higher concentrations for which negative side effects, such as increase in boundary layer, are more likely to occur. NaCl concentrations of 57 g/L and lower were proven to be feasible using RO, which can be performed by conventional sea water RO membranes with maximum applied pressure of 50 bar. All in all, RO systems are sensitive to feed quality and operating conditions. Although the WAVE software simulations provide good indication of the performance, it lacks information with regards to practical limitations. The impact of fouling that leads to reduced performance in the long-term, is overlooked. In reality, the energy consumption will be significantly higher than estimated by the WAVE software.

How do ED limiting factors affect concentrating brine and how does it relate to its energy consumption?

Concentration performance by ED is limited by the amount of transported salt, effects of osmotic water transport and diffusion. Experimental results showed that LCD is positively correlated to salt concentration and higher cross flow velocities. Increasing the LCD by applying high cross flow velocities is not necessarily desired, as it might increase operational costs due to required cooling. The effect of increasing partial LCDs on energy consumption was found to be disadvantageous. Higher energy consumption was observed using higher partial LCDs, whilst the concentration quality remains constant. This effect intensifies at higher feed concentrations, whilst considering a constant dilution factor of 2 for the diluate stream. Furthermore, it was observed that the dilution and concentration factors in the diluate and concentrate stream, respectively, was not inversely proportional. This is due to the effect of osmotic water transport and diffusion which is present in the ED process and increases with greater concentration gradients i.e., increasing feed concentrations. Higher initial volume ratios were found to be advantageous for achieving higher concentration factors, whilst the effect of osmotic water transport and diffusion on the concentrate quality did not change. The concentration range between 10 g/L and 140 g/L was proven to be feasible using ED, which was experimentally proven considering a set dilution factor of 2 for the diluate stream, applying 0.5 LCD based on the final diluate quality and using an initial volume ratio of 4.

How do VMD limiting factors affect concentrating brine and how does it relate to its energy consumption?

Increasing feed concentration resulted in lower vapour pressures and thus lower driving force. The permeate fluxes decreased with increasing feed concentration and were always lower compared to a pure water

flux. This effect intensifies with increasing operating temperatures. Increasing operating temperatures resulted in overall higher permeate fluxes. The effect of feed concentration on the permeate flux proved to be insignificant compared to the effect of operating temperature. The average flux obtained using operating temperature 30°C was 7 kg/m^2/h and increased to 19 and 32 kg/m^2/h at operating temperatures 40°C and 50°C, respectively. Main energy components in VMD are thermal energy required for initial heating, cooling and condensation, while electrical energy is required for the recirculation pump and vacuum pump. The energy distribution in VMD is governed by condensation and the vacuum pump, which corresponds to 81% and 18.9%, respectively. The energy required for cooling the steam, initial heating of the feed from 20 degC and recirculating the solution accounted for less than 0.1%. The energy consumption for VMD can be lowered significantly when considering COP values. Assuming practical COP values of 6.2 and 3.8 for heating and cooling, respectively, decreased the energy consumption by a factor of 2.4. In principle, concentration of brines using VMD can be performed until the solution's solubility limit and therefore the application of VMD is suitable for any feed concentration. However, concentration performance by VMD is limited by its energy consumption as it is controlled by the amount of water to be evaporated. Therefore it is more feasible to apply VMD at higher feed concentrations, which is suitable as a final concentration step to achieve ZLD for example. RO and ED are preferred choices for concentrations lower than 140 and 10 g/L, respectively.

How do VMD and ED compare against RO in terms of concentration performance and energy consumption?

The energy consumption to concentrate 20 g/L to 57 g/L using a one-stage RO system at 10 NDP was 13 kWh/m^3. The same concentration step could be performed using a two-stage ED, which required 18 kWh/m^3. Using VMD for this step increased energy consumption by a factor of 61. RO and ED prove to be similar in energy consumption in a concentration range between 20 g/L to 57 g/L. However ED is able to concentrate further and thus becomes the more preferred technology in the range of 10 g/L to 140 g/L. For concentrations higher than 140 g/L, VMD becomes the preferred choice. In terms of producing high quality permeate, RO was found to be the optimal choice compared to VMD for the following reason. The energy consumption of VMD increases with lower feed concentrations, while for RO and ED the energy consumption decreases.

5.2. Recommendation

This research intended to serve as a foundation to broaden the knowledge of brine treatment using RO, ED and VMD. Naturally, further research needs to be performed to have a better understanding of the opportunities of using the aforementioned membrane technologies in practice. Topics and general remarks for further research are summarized below.

- The simulations and experiments were performed using (synthetic) NaCl solutions. Repeating the experiments using actual brine is recommended, because the water matrix is more complex and includes components that might alter the concentration performance evaluated in this study. By doing so, the effect of actual brine to synthetic NaCl solution on the concentration performance and energy consumption can be compared. Furthermore, it is recommended to perform RO concentration experiments for comparison with the simulation results.

- In this study, considerable assumptions were made for energy calculations of the VMD process. In particular the heat calculations neglected actual heat loss of the system and temperature fluctuations due to practical limitations of the experimental set-up. Furthermore, the VMD experiments were performed using a flat sheet membrane with a surface area of 34 cm^2. It is recommended to repeat the VMD experiments in a more controlled environment (i.e., temperature controlled cooling and heating) and using a larger membrane surface area to obtain more reliable and accurate results.

- Besides VMD, other thermal (membrane) technologies could also be relevant for brine concentrating application. Especially for application in leading industries or areas where residual heat is available, thermal (membrane) technologies are expected to be the viable option compared to pressure or electrically driven separation technologies. Therefore, it is recommended to compare the results of this study with other methods of evaporation using residual heat.

- The focus of this study was on concentration performance and associated energy consumption only. For a continuation of this study, it is recommended to review the expenditures associated to the investment and operational expenses. Exploring this topic provides extra weighting factors to the decision tree when choosing a technique or a hybrid system for a case-by-case study and will provide more accurate practical solutions.

- The simulation and experiments were designed based on limited sample sizes (i.e., small and lab-scale production). Several non-conventional operation modes were suggested in this research, such as a multi-stage ED using counter flow. Such operation modes are recommended to investigate at larger scale, to see the effect of operation mode on the concentration performance and energy consumption for brine treatment. This step is recommended to understand the actual technology performance in practice, while optimizing the design.
- The acquired data in this study is insufficient to optimize parameters in existing models. Expanding the current research data by performing experiments using more elaborate parameter ranges is recommended to acquire a complete understanding of the concentration performance and energy consumption for brine treatment. As such, mathematical models can be used and optimized using an extended database.

Bibliography

[1] Anton A. Kiss and Olga M. Kattan Readi. An industrial perspective on membrane distillation processes. *Journal of Chemical Technology & Biotechnology*, 93(8):2047–2055, 2018. ISSN 1097-4660. doi: 10.1002/jctb.5674. URL https://onlinelibrary.wiley.com/doi/abs/10.1002/jctb.5674. _eprint: https://onlinelibrary.wiley.com/doi/pdf/10.1002/jctb.5674 tex.ids: kissIndustrialPerspectiveMembrane2018, kissIndustrialPerspectiveMembrane2018a.

[2] 6.2 Collision Theory. URL http://ibchemninja.weebly.com/62-collision-theory.html. accessed on 2022-08-18.

[3] James Miller. Review of Water Resources and Desalination Technologies. Technical Report SAND2003-0800, 809106, March 2003. URL https://www.osti.gov/servlets/purl/809106/.

[4] J. J. Krol, M. Wessling, and H. Strathmann. Concentration polarization with monopolar ion exchange membranes: current–voltage curves and water dissociation. *Journal of Membrane Science*, 162(1):145–154, September 1999. ISSN 0376-7388. doi: 10.1016/S0376-7388(99)00133-7. URL https://www.sciencedirect.com/science/article/pii/S0376738899001337.

[5] A. R. Da Costa, A. G. Fane, and D. E. Wiley. Spacer characterization and pressure drop modelling in spacer-filled channels for ultrafiltration. *Journal of Membrane Science*, 87(1):79–98, February 1994. ISSN 0376-7388. doi: 10.1016/0376-7388(93)E0076-P. URL http://www.sciencedirect.com/science/article/pii/0376738893E0076P. tex.ids: dacostaSpacerCharacterizationPressure1994.

[6] Online calculation of properties of water and steam. URL https://www.peacesoftware.de/einigewerte/wasser_dampf_e.html. accessed on 2021-05-21.

[7] Musthafa O. Mavukkandy, Chahd M. Chabib, Ibrahim Mustafa, Amal Al Ghaferi, and Faisal AlMarzooqi. Brine management in desalination industry: From waste to resources generation. *Desalination*, 472:114187, December 2019. ISSN 0011-9164. doi: 10.1016/j.desal.2019.114187. URL http://www.sciencedirect.com/science/article/pii/S0011916419317278.

[8] Natasha C. Darre and Gurpal S. Toor. Desalination of Water: a Review. *Current Pollution Reports*, 4(2):104–111, June 2018. ISSN 2198-6592. doi: 10.1007/s40726-018-0085-9. URL https://doi.org/10.1007/s40726-018-0085-9.

[9] Savvina Loutatidou, Musthafa O. Mavukkandy, Sudip Chakraborty, and Hassan A. Arafat. Chapter 1 - Introduction: What is Sustainable Desalination? In Hassan A. Arafat, editor, *Desalination Sustainability*, pages 1–30. Elsevier, January 2017. ISBN 978-0-12-809791-5. doi: 10.1016/B978-0-12-809791-5.00001-8. URL http://www.sciencedirect.com/science/article/pii/B9780128097915000018.

[10] Edward Jones, Manzoor Qadir, Michelle T. H. van Vliet, Vladimir Smakhtin, and Seong-mu Kang. The state of desalination and brine production: A global outlook. *Science of The Total Environment*, 657:1343–1356, March 2019. ISSN 0048-9697. doi: 10.1016/j.scitotenv.2018.12.076. URL http://www.sciencedirect.com/science/article/pii/S0048969718349167.

[11] Industrial Uses of Water | Essential Guide | Aquatech, . URL https://www.aquatechtrade.com/news/industrial-water/industrial-water-essential-guide/. Library Catalog: www.aquatechtrade.com.

[12] Brine (Zero Liquid Discharge) FAQ, . URL https://www.lenntech.com/processes/desalination/general/brine-faq.htm. accessed on 2020-03-11.

[13] Bernt Ericsson and Bengt Hallmans. Treatment of saline wastewater for zero discharge at the Debiensko coal mines in Poland. *Desalination*, 105(1-2):115–123, June 1996. ISSN 00119164. doi: 10.1016/0011-9164(96)00065-3. URL https://linkinghub.elsevier.com/retrieve/pii/0011916496000653.

[14] Veera Gnaneswar Gude. Desalination and sustainability – An appraisal and current perspective. *Water Research*, 89:87–106, February 2016. ISSN 0043-1354. doi: 10.1016/j.watres.2015.11.012. URL http://www.sciencedirect.com/science/article/pii/S0043135415303390.

[15] Desalinated water affects the energy equation in the Middle East – Analysis. URL https://www.iea.org/commentaries/desalinated-water-affects-the-energy-equation-in-the-middle-east. accessed on 2020-02-10.

[16] Dynamic growth for desalination and water reuse in 2019, February 2019. URL https://idadesal.org/dynamic-growth-for-desalination-and-water-reuse-in-2019/. accessed on 2020-02-10.

[17] Toufic Mezher, Hassan Fath, Zeina Abbas, and Arslan Khaled. Techno-economic assessment and environmental impacts of desalination technologies. *Desalination*, 266(1):263–273, January 2011. ISSN 0011-9164. doi: 10.1016/j.desal.2010.08.035. URL http://www.sciencedirect.com/science/article/pii/S0011916410006296.

[18] Enrico Drioli, Aamer Ali, and Francesca Macedonio. Membrane distillation: Recent developments and perspectives. *Desalination*, 356:56–84, January 2015. ISSN 0011-9164. doi: 10.1016/j.desal.2014.10.028. URL http://www.sciencedirect.com/science/article/pii/S0011916414005517. tex.ids: drioliMembraneDistillationRecent2015.

[19] Arne Verliefde, Emile Cornelissen, Sebastiaan Heijman, J.Q.J.C. Verberk, Gary Amy, Bart Van der Bruggen, and J. Dijk. The role of electrostatic interactions on the rejection of organic solutes in aqueous solutions with nanofiltration. *Journal of Membrane Science*, 322:52–66, September 2008. doi: 10.1016/j.memsci.2008.05.022.

[20] Particles, scaling and biofouling. URL https://www.lenntech.com/particles-scaling-biofouling.htm. accessed on 2020-04-06.

[21] Fawzi A. Banat and Jana Simandl. Desalination by Membrane Distillation: A Parametric Study. *Separation Science and Technology*, 33(2):201–226, January 1998. ISSN 0149-6395. doi: 10.1080/01496399808544764. URL https://doi.org/10.1080/01496399808544764. Publisher: Taylor & Francis _eprint: https://doi.org/10.1080/01496399808544764.

[22] Yonggang Zhang, Yuelian Peng, Shulan Ji, Zhehao Li, and Ping Chen. Review of thermal efficiency and heat recycling in membrane distillation processes. *Desalination*, 367:223–239, July 2015. ISSN 0011-9164. doi: 10.1016/j.desal.2015.04.013. URL https://www.sciencedirect.com/science/article/pii/S0011916415002581.

[23] Heru Susanto. Towards practical implementations of membrane distillation. *Chemical Engineering and Processing: Process Intensification*, 50:139–150, February 2011. doi: 10.1016/j.cep.2010.12.008.

[24] Navya Thomas, Musthafa O. Mavukkandy, Savvina Loutatidou, and Hassan A. Arafat. Membrane distillation research & implementation: Lessons from the past five decades. *Separation and Purification Technology*, 189:108–127, December 2017. ISSN 1383-5866. doi: 10.1016/j.seppur.2017.07.069. URL http://www.sciencedirect.com/science/article/pii/S1383586617319469.

[25] H. Strathmann. Electrodialysis, a mature technology with a multitude of new applications. *Desalination*, 264(3):268–288, December 2010. ISSN 0011-9164. doi: 10.1016/j.desal.2010.04.069. URL http://www.sciencedirect.com/science/article/pii/S0011916410002985.

[26] Jie Liu, Junsheng Yuan, Zhiyong Ji, Bingjun Wang, Yachao Hao, and Xiaofu Guo. Concentrating brine from seawater desalination process by nanofiltration–electrodialysis integrated membrane technology. *Desalination*, 390:53–61, July 2016. ISSN 0011-9164. doi: 10.1016/j.desal.2016.03.012. URL http://www.sciencedirect.com/science/article/pii/S0011916416301266.

[27] Hong-Joo Lee, F. Sarfert, H. Strathmann, and Seung-Hyeon Moon. Designing of an electrodialysis desalination plant. *Desalination*, 142(3):267–286, March 2002. ISSN 0011-9164. doi: 10.1016/S0011-9164(02)00208-4. URL http://www.sciencedirect.com/science/article/pii/S0011916402002084.

[28] A.H. Galama, M. Saakes, H. Bruning, H.H.M. Rijnaarts, and J.W. Post. Seawater predesalination with electrodialysis. *Desalination*, 342:61–69, 2014. doi: 10.1016/j.desal.2013.07.012.

[29] Karim M. Chehayeb, Daniel M. Farhat, Kishor G. Nayar, and John H. Lienhard. Optimal design and operation of electrodialysis for brackish-water desalination and for high-salinity brine concentration. *Desalination*, 420:167–182, October 2017. ISSN 0011-9164. doi: 10.1016/j.desal.2017.07.003. URL http://www.sciencedirect.com/science/article/pii/S0011916417305763.

[30] Marian Turek. Electrodialytic desalination and concentration of coal-mine brine. *Desalination*, 162:355–359, March 2004. ISSN 00119164. doi: 10.1016/S0011-9164(04)00069-4. URL https://linkinghub.elsevier.com/retrieve/pii/S0011916404000694.

[31] Nirajan Dhakal, Sergio G. Salinas-Rodriguez, Jamal Hamdani, Almotasembellah Abushaban, Hassan Sawalha, Jan C. Schippers, and Maria D. Kennedy. Is Desalination a Solution to Freshwater Scarcity in Developing Countries? *Membranes*, 12(4):381, March 2022. ISSN 2077-0375. doi: 10.3390/membranes12040381. URL https://www.mdpi.com/2077-0375/12/4/381.

[32] Valentina Colla, Teresa Annunziata Branca, Felice Rosito, Carmelo Lucca, Beatriz Padilla Vivas, and Vanesa Menéndez Delmiro. Sustainable Reverse Osmosis application for wastewater treatment in the steel industry. *Journal of Cleaner Production*, 130:103–115, September 2016. ISSN 0959-6526. doi: 10.1016/j.jclepro.2015.09.025. URL https://www.sciencedirect.com/science/article/pii/S0959652615012469.

[33] Joel Minier-Matar, Ramesh Sharma, Altaf Hussain, Arnold Janson, and Samer Adham. Field evaluation of membrane distillation followed by humidification/dehumidification crystallizer for inland desalination of saline groundwater. *Desalination*, 398:12–21, November 2016. ISSN 0011-9164. doi: 10.1016/j.desal.2016.07.006. URL https://www.sciencedirect.com/science/article/pii/S0011916416307962.

[34] Natasha C. Wright, Sahil R. Shah, Susan E. Amrose, and Amos G. Winter. A robust model of brackish water electrodialysis desalination with experimental comparison at different size scales. *Desalination*, 443:27–43, October 2018. ISSN 0011-9164. doi: 10.1016/j.desal.2018.04.018. URL https://www.sciencedirect.com/science/article/pii/S0011916417325262.

[35] Kishor G. Nayar, Jenifer Fernandes, Ronan K. McGovern, Kyle P. Dominguez, Adriene McCance, Bader S. Al-Anzi, and John H. Lienhard. Cost and energy requirements of hybrid RO and ED brine concentration systems for salt production. *Desalination*, 456:97–120, April 2019. ISSN 0011-9164. doi: 10.1016/j.desal.2018.11.018. URL https://www.sciencedirect.com/science/article/pii/S0011916418312761.

[36] M. S. El-Bourawi, Z. Ding, R. Ma, and M. Khayet. A framework for better understanding membrane distillation separation process. *Journal of Membrane Science*, 285(1):4–29, November 2006. ISSN 0376-7388. doi: 10.1016/j.memsci.2006.08.002. URL https://www.sciencedirect.com/science/article/pii/S0376738806005230.

[37] S. Bandini, C. Gostoli, and G. C. Sarti. Separation efficiency in vacuum membrane distillation. *Journal of Membrane Science*, 73(2):217–229, October 1992. ISSN 0376-7388. doi: 10.1016/0376-7388(92)80131-3. URL http://www.sciencedirect.com/science/article/pii/0376738892801313.

[38] A. C. M. Franken, J. A. M. Nolten, M. H. V. Mulder, D. Bargeman, and C. A. Smolders. Wetting criteria for the applicability of membrane distillation. *Journal of Membrane Science*, 33(3):315–328, October 1987. ISSN 0376-7388. doi: 10.1016/S0376-7388(00)80288-4. URL http://www.sciencedirect.com/science/article/pii/S0376738800802884.

[39] Mostafa Abu-Zeid, Yaqin Zhang, Hang Dong, Lin Zhang, Huan-Lin Chen, and Lian Hou. A comprehensive review of vacuum membrane distillation technique. *Desalination*, 356, January 2015. doi: 10.1016/j.desal.2014.10.033.

[40] L. Martínez-Díez, F.J. Florido-Díaz, and M.I. Vázquez-González. Study of evaporation efficiency in membrane distillation. *Desalination*, 126(1-3):193–198, November 1999. ISSN 00119164. doi: 10.1016/S0011-9164(99)00174-5. URL https://linkinghub.elsevier.com/retrieve/pii/S0011916499001745.

[41] Jianhua Zhang, Noel Dow, Mikel Duke, Eddy Ostarcevic, Jun-De Li, and Stephen Gray. Identification of material and physical features of membrane distillation membranes for high performance desalination. *Journal of Membrane Science*, 349(1):295–303, March 2010. ISSN 0376-7388. doi: 10.1016/j.memsci.2009.11.056. URL https://www.sciencedirect.com/science/article/pii/S0376738809008709. tex.ids= zhangIdentificationMaterialPhysical2010a.

[42] G. Schock and A. Miquel. Mass transfer and pressure loss in spiral wound modules. *Desalination*, 64:339–352, January 1987. ISSN 0011-9164. doi: 10.1016/0011-9164(87)90107-X. URL https://www.sciencedirect.com/science/article/pii/001191648790107X.

[43] S. M. Mojab, A. Pollard, J. G. Pharoah, S. B. Beale, and E. S. Hanff. Unsteady Laminar to Turbulent Flow in a Spacer-Filled Channel. *Flow, Turbulence and Combustion*, 92(1-2):563–577, January 2014. ISSN 1386-6184, 1573-1987. doi: 10.1007/s10494-013-9514-4. URL http://link.springer.com/10.1007/s10494-013-9514-4.

[44] Gayathri Naidu, Yongjun Choi, Sanghyun Jeong, Tae Mun Hwang, and Saravanamuthu Vigneswaran. Experiments and modeling of a vacuum membrane distillation for high saline water. *Journal of Industrial and Engineering Chemistry*, 20(4):2174–2183, July 2014. ISSN 1226-086X. doi: 10.1016/j.jiec.2013.09.048. URL http://www.sciencedirect.com/science/article/pii/S1226086X13004681.

[45] Manu Huttunen, Lauri Nygren, Teemu Kinnarinen, Antti Häkkinen, Tuomo Lindh, Jero Ahola, and Vesa Karvonen. Specific energy consumption of cake dewatering with vacuum filters. *Minerals Engineering*, 100:144–154, January 2017. ISSN 0892-6875. doi: 10.1016/j.mineng.2016.10.025. URL https://www.sciencedirect.com/science/article/pii/S0892687516303727.

[46] David R Lide, Grace Baysinger, Swain Chemistry, Lev I Berger, Robert N Goldberg, and Henry V Kehiaian. CRC Handbook of Chemistry and Physics. page 2660.

[47] Arif Hepbasli, Emrah Biyik, Orhan Ekren, Huseyin Gunerhan, and Mustafa Araz. A key review of wastewater source heat pump (WWSHP) systems. *Energy Conversion and Management*, 88:700–722, December 2014. ISSN 0196-8904. doi: 10.1016/j.enconman.2014.08.065. URL https://www.sciencedirect.com/science/article/pii/S0196890414007900.

[48] Wouter Pronk, Martin Biebow, and Markus Boller. Electrodialysis for Recovering Salts from a Urine Solution Containing Micropollutants. *Environmental Science & Technology*, 40(7):2414–2420, April 2006. ISSN 0013-936X. doi: 10.1021/es051921i. URL https://doi.org/10.1021/es051921i. Publisher: American Chemical Society.

[49] T. Rottiers, K. Ghyselbrecht, B. Meesschaert, B. Van der Bruggen, and L. Pinoy. Influence of the type of anion membrane on solvent flux and back diffusion in electrodialysis of concentrated NaCl solutions. *Chemical Engineering Science*, 113:95–100, July 2014. ISSN 0009-2509. doi: 10.1016/j.ces.2014.04.008. URL http://www.sciencedirect.com/science/article/pii/S0009250914001560.

[50] Niels van Linden, Henri Spanjers, and Jules B. van Lier. Application of dynamic current density for increased concentration factors and reduced energy consumption for concentrating ammonium by electrodialysis. *Water Research*, 163:114856, October 2019. ISSN 0043-1354. doi: 10.1016/j.watres.2019.114856. URL http://www.sciencedirect.com/science/article/pii/S0043135419306220.

[51] Yizhak Marcus. *Ions in Water and Biophysical Implications*. Springer Netherlands, Dordrecht, 2012. ISBN 978-94-007-4646-6 978-94-007-4647-3. doi: 10.1007/978-94-007-4647-3. URL http://link.springer.com/10.1007/978-94-007-4647-3. tex.ids: marcusIonsWaterBiophysical2012.

[52] Giacomo Bandinu. Electrodialysis with bipolar membranes for ammonia recovery in wastewater: An innovative concept for the treatment of ammonia residual streams. 2019. URL https://repository.tudelft.nl/islandora/object/uuid%3Ac40b8437-898f-424c-a6d4-045d5998cb30.

[53] Mariagiorgia La Cerva, Luigi Gurreri, Michele Tedesco, Andrea Cipollina, Michele Ciofalo, Alessandro Tamburini, and Giorgio Micale. Determination of limiting current density and current efficiency in electrodialysis units. *Desalination*, 445:138–148, November 2018. ISSN 0011-9164. doi: 10.1016/j.desal.2018.07.028. URL http://www.sciencedirect.com/science/article/pii/S0011916418305502.

[54] Hong-Joo Lee, Heiner Strathmann, and Seung-Hyeon Moon. Determination of the limiting current density in electrodialysis desalination as an empirical function of linear velocity. *Desalination*, 190(1):43–50, April 2006. ISSN 0011-9164. doi: 10.1016/j.desal.2005.08.004. URL http://www.sciencedirect.com/science/article/pii/S0011916406001226.

[55] Donald A. Cowan and Jerry H. Brown. Effect of Turbulence on Limiting Current in Electrodialysis Cells. *Industrial & Engineering Chemistry*, 51(12):1445–1448, December 1959. ISSN 0019-7866. doi: 10.1021/ie50600a026. URL https://doi.org/10.1021/ie50600a026.

[56] H. Strathmann. 2.14 - Electromembrane Processes: Basic Aspects and Applications. In Enrico Drioli and Lidietta Giorno, editors, *Comprehensive Membrane Science and Engineering*, pages 391–429. Elsevier, Oxford, January 2010. ISBN 978-0-08-093250-7. doi: 10.1016/B978-0-08-093250-7.00048-7. URL http://www.sciencedirect.com/science/article/pii/B9780080932507000487.

[57] WAVE Water Treatment Design Software, 2021.

[58] G. J. Doornbusch, M. Tedesco, J. W. Post, Z. Borneman, and K. Nijmeijer. Experimental investigation of multistage electrodialysis for seawater desalination. *Desalination*, 464:105–114, August 2019. ISSN 0011-9164. doi: 10.1016/j.desal.2019.04.025. URL https://www.sciencedirect.com/science/article/pii/S001191641930222X.

[59] Chenxiao Jiang, Yaoming Wang, Zenghui Zhang, and Tongwen Xu. Electrodialysis of concentrated brine from RO plant to produce coarse salt and freshwater. *Journal of Membrane Science*, 450:323–330, January 2014. doi: 10.1016/j.memsci.2013.09.020.

[60] EU annual hard coal consumption declines further, . URL https://ec.europa.eu/info/news/eu-annual-coal-consumption-declines-further-2019-aug-23_en. accessed on 2020-02-11.

[61] Coal Mining Effluent Guidelines | Effluent Guidelines | US EPA, . URL https://www.epa.gov/eg/coal-mining-effluent-guidelines. accessed on 2020-04-01.

[62] European Union . Water Framework Directive, December 2000. URL https://eur-lex.europa.eu/legal-content/NL/TXT/?uri=OJ:L:2000:327:TOC. accessed on 2020-02-11.

[63] Hagare B Dharmappa. Wastewater Characteristics, Management and Reuse in Mining and Mineral Processing Industries. page 10.

[64] Marian Turek and Maciej Gonet. Nanofiltration in the utilization of coal-mine brines. *Desalination*, 108(1-3):171–177, February 1997. ISSN 00119164. doi: 10.1016/S0011-9164(97)00024-6. URL https://linkinghub.elsevier.com/retrieve/pii/S0011916497000246.

[65] Marian Turek, Piotr Dydo, and Romuald Klimek. Salt production from coal-mine brine in ED–evaporation–crystallization system. *Desalination*, 184(1-3):439–446, November 2005. ISSN 00119164. doi: 10.1016/j.desal.2005.03.047. URL https://linkinghub.elsevier.com/retrieve/pii/S0011916405005898.

[66] Bill Forsyth, Alan Cameron, and Scott Miller. Explosives and Water quality.

[67] Tim Mclaughlin. Clean coal's dirty secret: More pollution, not less. URL https://www.reuters.com/investigates/special-report/usa-coal-pollution/. Library Catalog: www.reuters.com.

[68] Mandar Gadgil and Steven Feeney. Mercury Emissions Control Technology Selection – Let Installed Air Quality Control System (AQCS) Equipment Guide Technology Choice. page 16, 2015.

[69] Fracking in the Coalfields - How coal & gas affect our waters. URL https://www.fractracker.org/projects/water-monitor/fracking-coalfields/. accessed on 2020-03-19.

[70] D. Craw, C. G. Rufaut, L. Haffert, and A. Todd. Mobilisation and attenuation of boron during coal mine rehabilitation, Wangaloa, New Zealand. *Science of The Total Environment*, 368(2):444–455, September 2006. ISSN 0048-9697. doi: 10.1016/j.scitotenv.2006.04.020. URL http://www.sciencedirect.com/science/article/pii/S0048969706003111.

[71] Farshid Vejahati, Zhenghe Xu, and Rajender Gupta. Trace elements in coal: Associations with coal and minerals and their behavior during coal utilization – A review. *Fuel*, 89(4):904–911, April 2010. ISSN 0016-2361. doi: 10.1016/j.fuel.2009.06.013. URL http://www.sciencedirect.com/science/article/pii/S0016236109002890.

[72] Silicon (Si) and water. URL https://www.lenntech.com/periodic/water/silicon/silicon-and-water.htm. accessed on 2020-03-19.

[73] Ting Li and Jingfeng Li. Concentrated Brine Treatment using New Energy in Coal Mine Evaporation Ponds. *IOP Conference Series: Earth and Environmental Science*, 100:012013, December 2017. doi: 10.1088/1755-1315/100/1/012013.

[74] Stanislaw Chałupnik and Małgorzata Wysocka. Changes of radium concentration in discharge waters from coal mines in Poland as a result of mitigation. In Broder J. Merkel and Andrea Hasche-Berger, editors, *Uranium, Mining and Hydrogeology*, pages 839–850. Springer, Berlin, Heidelberg, 2008. ISBN 978-3-540-87746-2. doi: 10.1007/978-3-540-87746-2_110. URL https://doi.org/10.1007/978-3-540-87746-2_110.

[75] Eugeniusz J. Sobczyk, Jerzy Kicki, and Piotr Sauga. *Deep Mining Challenges : International Mining Forum 2009*. Krakow, February 2009.

[76] Heiner Strathmann. 2.12 Electromembrane Processes: Basic Aspects and Applications. In *Comprehensive Membrane Science and Engineering*, pages 355–392. Elsevier, 2017. ISBN 978-0-444-63796-3. doi: 10.1016/B978-0-12-409547-2.12257-7. URL https://linkinghub.elsevier.com/retrieve/pii/B9780124095472122577.

[77] Chapter 5 - Removal of suspended solids. In Nelson Leonard Nemerow, editor, *Industrial Waste Treatment*, pages 53–77. Butterworth-Heinemann, Burlington, January 2007. ISBN 978-0-12-372493-9. doi: 10.1016/B978-012372493-9/50040-5. URL http://www.sciencedirect.com/science/article/pii/B9780123724939500405.

[78] Xavier Cordova and Jhonny Valverde. Application of the bipolar electrodialysis technique for the production of hydrochloric acid from wastewater regeneration of ion exchange resins. *Journal of Sciences and Engineering*, 1, December 2017. doi: 10.32829/sej.v1i1.26.

[79] Dionysia Diamantidou. Ionic separation of the IEX spent regenerant using Nanofiltration. 2018. URL https://repository.tudelft.nl/islandora/object/uuid%3A78d8f8e4-ceb4-4d85-b2d7-e5662b49b35f.

[80] A. Pérez-González, R. Ibáñez, P. Gómez, A.M. Urtiaga, I. Ortiz, and J.A. Irabien. Nanofiltration separation of polyvalent and monovalent anions in desalination brines. *Journal of Membrane Science*, 473: 16–27, January 2015. ISSN 03767388. doi: 10.1016/j.memsci.2014.08.045. URL https://linkinghub.elsevier.com/retrieve/pii/S0376738814006693.

A

Literature review

A.1. Example from practice: BRINE-MINING

According to EUROSTAT (2019), the production of hard coal in the European Union (EU-28) shows a steady decreasing trend since 1990. The production of hard coal in EU-28 is dominated by Poland, which accounts for approximately 86% of the total share in 2018. Several other EU-28 countries contributing to hard coal and brown coal production are the United Kingdom, Czech Republic, Greece, Bulgaria among others. Whilst coal extraction for power production is progressively being replaced by renewable energy sources and natural gas, import of coal for oil and gas production still reigns over the use of alternative energy sources. Furthermore, coking coal is a vital component in metallurgy as carbon source and has been identified as a critical raw material by the European Commission. Australia and China are the largest coking coal exporters, thus the supply risk for the metallurgy sector is high. Due to its economic importance, the coal production in EU-28 will continue to remain an important sector [13, 60, 61].

Coal-mines have long been known to produce excessive amounts of brine, which is harmful to ecosystems and aquatic life if discharged directly in open waters and restrains the measures against chemical pollution of surface water according to the Water Framework Directive (WFD 2000) [62]. The source of coal-mine brine is generally from seepage of excavated areas of the mine, underground dust suppression and equipment cooling during mine operation. Wastewater is also produced during the coal preparation process, such as coal washing to increase its energy efficiency, and from contaminated storm-water at the coal storage facilities [61, 63]. Coal-mine brine is characterized by high concentration of salts and minerals, of which sodium Na^+ and chloride Cl^- are most abundant. Furthermore, high concentrations of calcium Ca^{2+} and sulphate SO_4^{2-} in coal-mine brine are also considered obstacles in the determination of treatment processes [64]. Additionally, the salinity of the discharged brine limits water supply for the direct environment and communities. Whilst coal delivers high value to the EU-28, the countries responsible for coal production are also accountable for the environmental cost at national level. This alarming impact enlarges in view of countries with limited water resources, making it complicated for these countries to manage their water resources well for industrial and municipal purposes. For this reason, the EU-28 LIFE programme financially supports the implementation of the WFD and its Circular Economy package by commissioning the coal-mining industry to improve its wastewater management performance. The aim of LIFE BRINE-MINING will be achieved through development and the application of an economically viable and innovative system and full recovery of resources from coal-mining wastewater. The project will work towards treatment and direct recovery of end-products (salts and water) of high quality and purity. For the duration of this project, consumers that are interested in the resources are involved to ensure market specification satisfaction and exploitation of the recovered materials.

In spite of the aforementioned environmental problems characterizing the mining sector, the treatment of coal mine brine has not yet been extensively studied. In particular, high energy consumption associated with conventional technologies for separating and concentrating coal-mine brine streams is still an issue [65]. Furthermore coal-mine brine contains a considerable large amount of minerals and salts, of which some are becoming scarce and expensive. A possible recovery of such salts and minerals may mitigate its scarcity to an extent and reduce the overall desalination treatment process costs. As an example of many brine producing industries, coal-mining is referred to as guiding principle for general brine treatment in this research (see Appendix A.2 and A.3 for background information). The focus of this research is on the concentration step and more specifically treatment of the NF permeate with high concentrations of Na^+ and Cl^-.

Table A.1: Ziemowit coal-mine plant chemical sample analysis

Constituent	Units	Ziemowit-500 AVG ± STD	Ziemowit-650 AVG ± STD	Threshold pollution value
Chloride (Cl^-)	[mg/L]	4201.7 ± 210.3	50775 ± 478.7	1000
Bromide (Br^-)	[mg/L]	< 50	161 ± 1.4	n.a.
Bicarbonate (HCO_3^-)	[mg/L]	535 ± 9	195 ± 0	n.a.
Nitrate (NO_3^-)	[mg/L]	< 50	< 50	n.a.
Sulphate (SO_4^{2-})	[mg/L]	453.3 ± 13.7	2762.5 ± 29.9	n.a.
Sodium (Na^+)	[mg/L]	2628.3 ± 121.2	25950 ± 264.6	800
Potassium (K^+)	[mg/L]	50.8 ± 1.3	434 ± 4.1	n.a.
Magnesium (Mg^{2+})	[mg/L]	102.2 ± 7.3	1981 ± 14.3	n.a.
Calcium (Ca^{2+})	[mg/L]	94.7 ± 7.6	1747.5 ± 12.6	n.a.
Boron (B)	[mg/L]	5.7 ± 0.2	12.2 ± 0.2	n.a.
Manganese (Mn)	[mg/L]	< 0.1	3.6 ± 0.1	n.a.
Silicon (Si)	[mg/L]	9.3 ± 0.7	6.7 ± 0.4	n.a.
Strontium (Sr)	[mg/L]	2.6 ± 0.1	23.3 ± 0.4	n.a.

A.2. Chemical analysis of coal-mine brine composition

In literature the coal-mine brine is characterized with large amounts of sulphates, bicarbonate and chloride salts of sodium, magnesium, calcium and potassium, originating from geogenic salt accumulation. The water samples confirm this, as high concentrations of these substances are found in coal-mine brine. Nitrate is also found in the brine and requires removal as it will induce eutrophication if left untreated. A possible explanation could be the explosive used in the mining operation, as primary source of NO_3^-. The explosives contain significant amounts of ammonium nitrate (NH_4NO_3), sometimes $Ca(NO_3)_2$ or $NaNO_3$ [66]. The chemical $CaBr_2$ is often used in the mining process for coal refining, which is a possible explanation of Bromide present in the brine[67, 68]. Higher concentration of Br^- is found in brine originating from lower depths. Discharging bromide in surface water can be of harm to aquatic life and if the surface water is used for drinking water production, there is a risk of trihalomethanes formation as drinking water treatment plants often use chlorine to remove microorganisms [69]. Though trace elements (TEs) are found in smaller concentrations, they have great environmental significance because of potential toxicity issues for ecosystems [70]. Furthermore, the toxicity potential for drinking water causes great concern for public health [71]. Low amounts of Silicon found in the brine could originate from weathering of underground surfaces during coal-mining processes [72]. Another important parameter is the pH of the coal-mine wastewater, as it has significant effect on the solubility of metals in the water[63]. The concentration of suspended solids (SS) is also important to consider when proposing a pre-treatment step. Unfortunately the pH and TSS concentration, as well as the temperature of the water samples, were not available. It is assumed that the pH and temperature of the brine is around 7 and 25°C. It is also assumed that coal dust from the mining activity contributes to high SS concentration [73]. Past studies also indicate that natural radioactive isotopes may occur in coal-mine brine [74]. Threshold values for Cl^- and Na^+ were found for waste waters set out in the Order by the Minister of Environment (Poland, 2006) [75].

A.3. Treatment required prior to concentration

Based on the coal-mine brine composition and generalized brine process flow scheme (see Figure A.2), pre-treatment steps are presumed. Pre-treatment is required to ensure efficient treatment in downstream processes. It is possible for SS to carry electrical charges, which can deposit on the membrane surface and thus increase the resistance of the membrane [76]. The SS concentration can be reduced by mechanical filtration units with different pore sizes. Sedimentation could also be an option, assuming that the coal-washery is settleable [77]. To remove any remaining colloids and suspended solids, Ultrafiltration (UF) can be installed after the aforementioned processes. The HCO_3^- concentration should be reduced as well, to avoid $CaCO_3$ and $MgCO_3$ formation which can foul the membranes. A solution for decarbonization is acid dosing (HCl) and degassing columns in sequence. The H^+ is released in the solution (see figure A.1), the pH of the solution drops and allows decarbonization process to happen in the subsequent degassing column. As such, CO_2 is removed from the solution. The cost of chemical additives must be considered, which can be reduced if downstream processes allows for HCl recovery, such as the application of bipolar membrane electrodialysis (BPMED) [78**?**]. To separate monovalent and multivalent ions, NF can be applied. Antiscalant dosing must be considered, as scaling of sulphate salts on the membranes are expected. It can be assumed that the

NF is able to reject multivalent ions (Mg^{2+}, Ca^{2+}, SO_4^{2-}), producing a permeate with mostly monovalent ions [79, 80]. Subsequent concentration steps can be applied to both the concentrate and permeate stream of the NF. The permeate stream has high potential for the recovery of NaCl by crystallization if concentrated further.

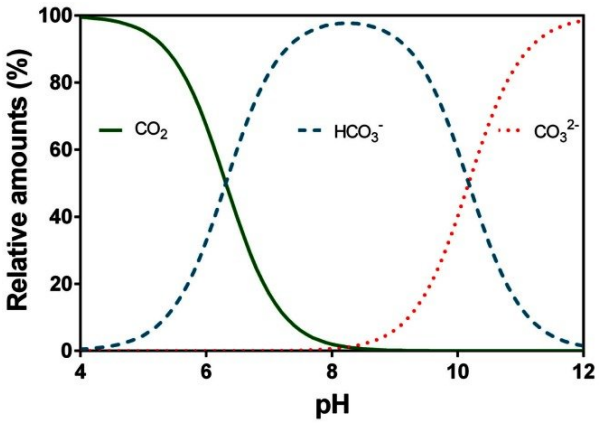

Figure A.1: Relative speciation of CO_2, HCO_3^- and CO_3^{2-} in water as a function of pH. Image retrieved from Pedersen [**?**].

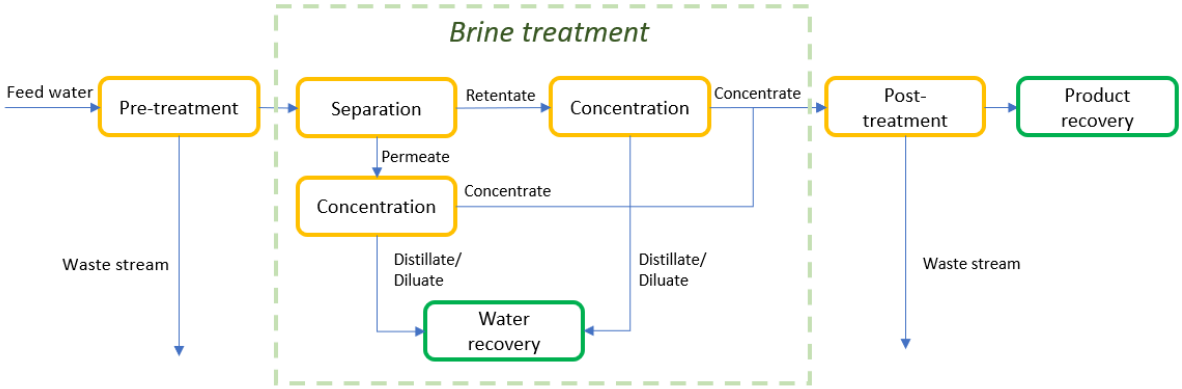

Figure A.2: Simplified brine process flow scheme

B

Supplementary experimental material

B.1. Additional WAVE simulation data

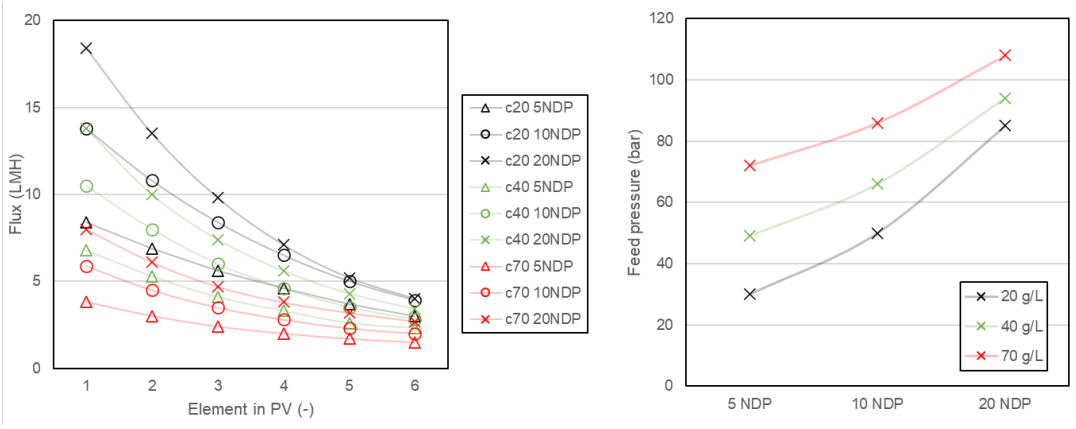

(a) (b)

Figure B.1: The progression of spatial flux variation in a pressure vessel (a) and progression of feed pressure to obtain 5, 10 and 20 NDP for different feed concentrations (b).

B.2. Hydraulic conditions of spacer filled channels

The appropriate hydraulic conditions in flat spacer-filled channels was determined for each set of VMD conditions, using derivations by Da Costa et al. [5] and Schock and Miquel [42], summarized by **?**]. The selected feed spacer for the VMD experiments was a parallel shaped spacer with 47mil thickness. The geometrical characteristics of this spacer is shown in Figure B.3. Fully unstable flow in spacer-filled channels is achieved at Reynolds numbers starting from 350. Accordingly, the required flow was calculated for different operating temperatures.

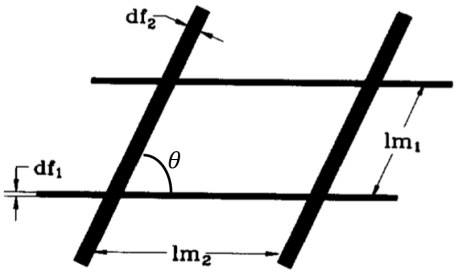

Figure B.2: Geometrical characteristics of a spacer, top view. Da Costa et al. [5]

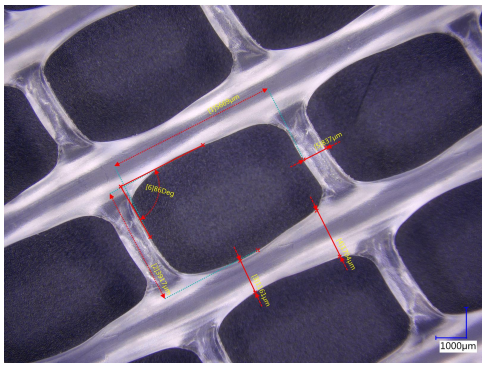

Figure B.3: Geometrical characteristics of used feed spacer with thickness 47mil, parallel shape, top view.

[CF042A-FO] Spacer type: 47mil, Parallel

Input			Output			T	v,w	u	Qreq	Qreq	RPM
Definition	Unit	Value	Definition	Unit	Value	℃	-	*m/s*	*ml/min*	*L/h*	-
Spacer geometry			Hydraulic conditions in feed			20	1.01E-06	0.178	748.5	44.91	412.4
$l_{m,1}$	*m*	5.67E-03	V_{tot}	m^3	5.10E-08	30	8.05E-07	0.142	599.1	35.95	330.1
$l_{m,2}$	*m*	3.92E-03	V_{sp}	m^3	1.13E-08	40	6.63E-07	0.117	493.5	29.61	271.9
$d_{f,1}$	*m*	1.43E-03	$A_{w,fc}$	m^2	4.43E-05	50	5.59E-07	0.099	415.7	24.94	229.0
$d_{f,2}$	*m*	8.37E-04	$A_{w,s}$	m^2	3.58E-05	60	4.79E-07	0.085	356.4	21.38	196.4
θ	°	86	d_h	*m*	1.98E-03	70	4.17E-07	0.074	309.9	18.60	170.8
t_{sp}	*m*	1.19E-03	ε	-	0.78	80	3.67E-07	0.065	272.8	16.37	150.3
			A_{cs}	m^2	9.02E-05	90	3.26E-07	0.058	242.5	14.55	133.6
Flow test cell geometry			$A_{cf,eff}$	m^2	7.02E-05						
h_c	*m*	2.30E-03									
w_c	*m*	3.92E-02									
Operational settings											
Re	-	350									
ρ_w	kg/m^3	1074.17									
T	℃	[20,90]									

B.3. Determination of Limiting Current Density in an ED cell

The method by Cowan and Brown [55] was applied to each operational setting. For each set of condition, the current-voltage curve was measured and the limiting current of each was found on the current at which the derivative of the curve equals zero. To convert the value into current density, the current is divided by the electrode area. The electrode area of the ED cell is $6.4 \cdot 10^{-3} m^2$.

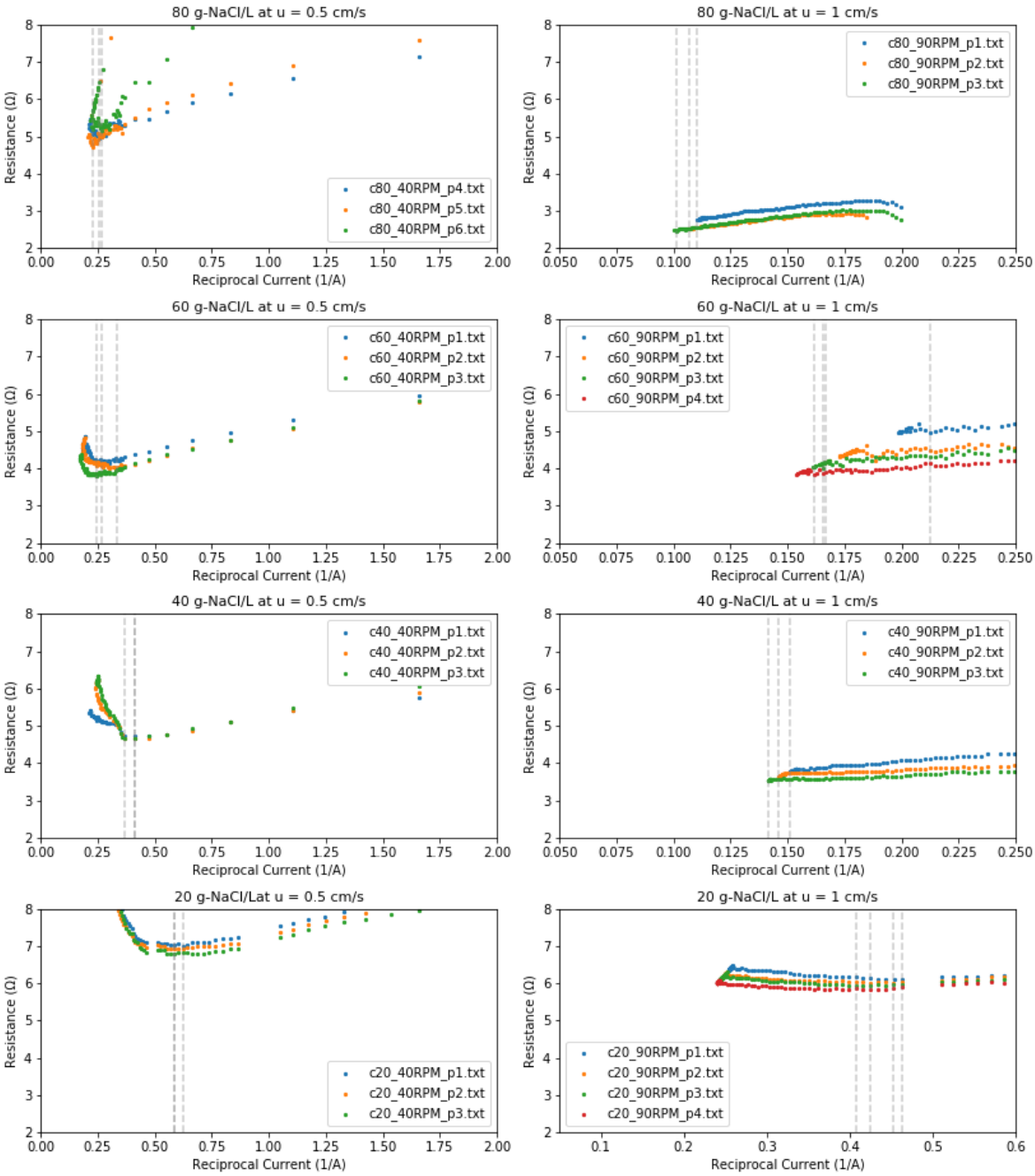

20 g-NaCl/L							
$v_{cross-flow} = 0.5\ cm/s$				$v_{cross-flow} = 1\ cm/s$			
Experiment	$R_{min}[\Omega]$	$1/I\ (R_{min})\ [A^{-1}]$	$I\ (R_{min})\ [A]$	**Experiment**	$R_{min}[\Omega]$	$1/I\ (R_{min})\ [A^{-1}]$	$I\ (R_{min})\ [A]$
P1	7.01	0.623	1.60	**P1**	6.1	0.464	2.16
P2	6.93	0.586	1.71	**P2**	6.02	0.453	2.21
P3	6.78	0.586	1.71	**P3**	5.95	0.407	2.46
				P4	5.82	0.424	2.36

40 g-NaCl/L							
$v_{cross-flow} = 0.5\ cm/s$				$v_{cross-flow} = 1\ cm/s$			
Experiment	$R_{min}[\Omega]$	$1/I\ (R_{min})\ [A^{-1}]$	$I\ (R_{min})\ [A]$	**Experiment**	$R_{min}[\Omega]$	$1/I\ (R_{min})\ [A^{-1}]$	$I\ (R_{min})\ [A]$
P1	4.72	0.415	2.41	**P1**	3.78	0.151	6.62
P2	4.65	0.415	2.41	**P2**	3.65	0.146	6.86
P3	4.65	0.369	2.71	**P3**	3.54	0.142	7.06

60 g-NaCl/L							
$v_{cross-flow} = 0.5\ cm/s$				$v_{cross-flow} = 1\ cm/s$			
Experiment	$R_{min}[\Omega]$	$1/I\ (R_{min})\ [A^{-1}]$	$I\ (R_{min})\ [A]$	**Experiment**	$R_{min}[\Omega]$	$1/I\ (R_{min})\ [A^{-1}]$	$I\ (R_{min})\ [A]$
P1	4.11	0.270	3.70	**P1**	4.95	0.212	4.71
P2	4.01	0.333	3.00	**P2**	4.17	0.167	5.99
P3	3.79	0.247	4.06	**P3**	4.00	0.166	6.04
				P4	3.84	0.161	6.19

C80 g-NaCl/L							
$v_{cross-flow} = 0.5\ cm/s$				$v_{cross-flow} = 1\ cm/s$			
Experiment	$R_{min}[\Omega]$	$1/I\ (R_{min})\ [A^{-1}]$	$I\ (R_{min})\ [A]$	**Experiment**	$R_{min}[\Omega]$	$1/I\ (R_{min})\ [A^{-1}]$	$I\ (R_{min})\ [A]$
P4	4.94	0.256	3.90	**P1**	2.75	0.110	9.09
P5	4.71	0.230	4.36	**P2**	2.52	0.107	9.35
P6	5.17	0.266	3.75	**P3**	2.47	0.101	9.85

B.4. Effect of volume ratio on concentration factor and energy consumption

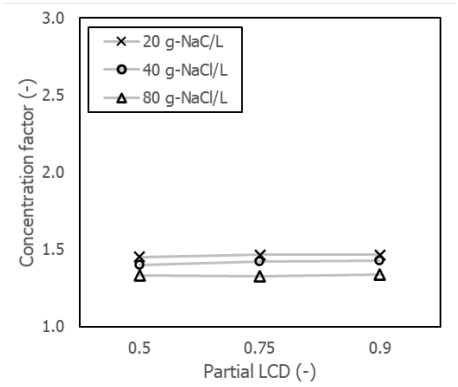

(a) Φ_1

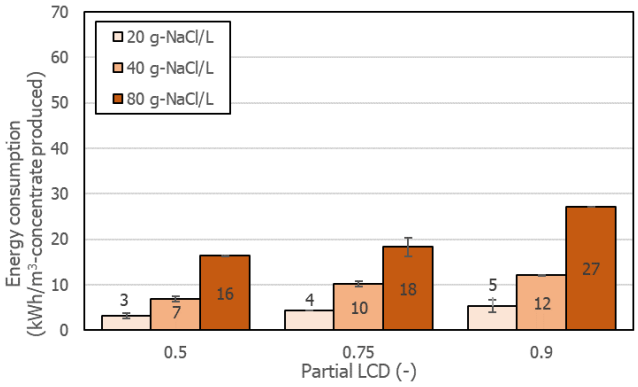

(b) Φ_1

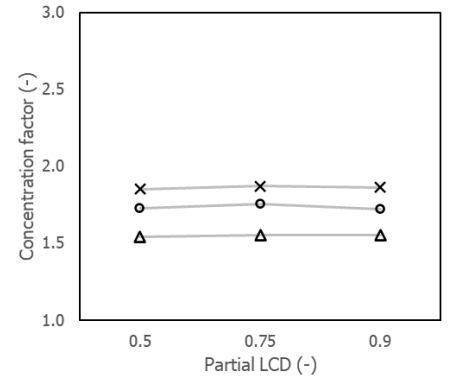

(c) Φ_2

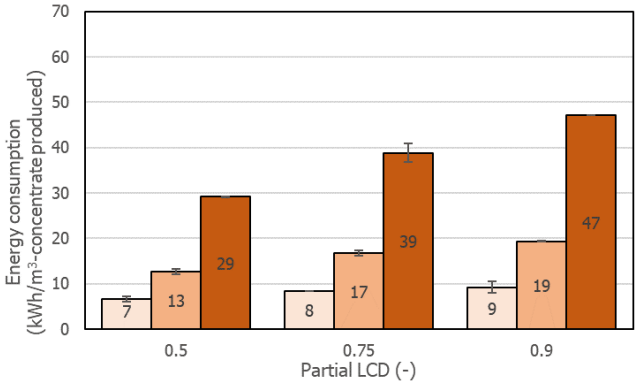

(d) Φ_2

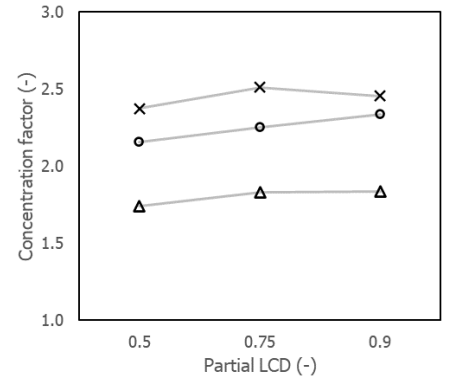

(e) Φ_4

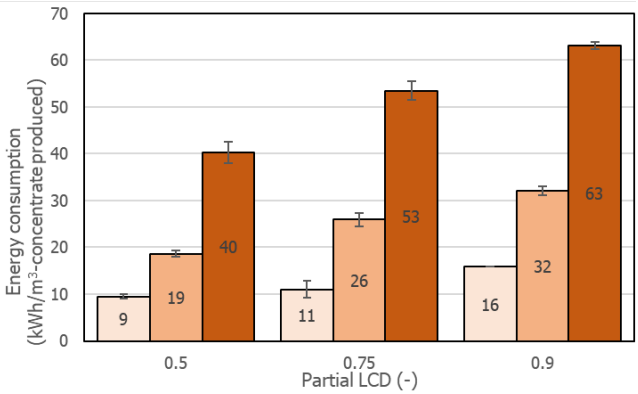

(f) Φ_4

B.5. Experimental configuration: laboratory set-up

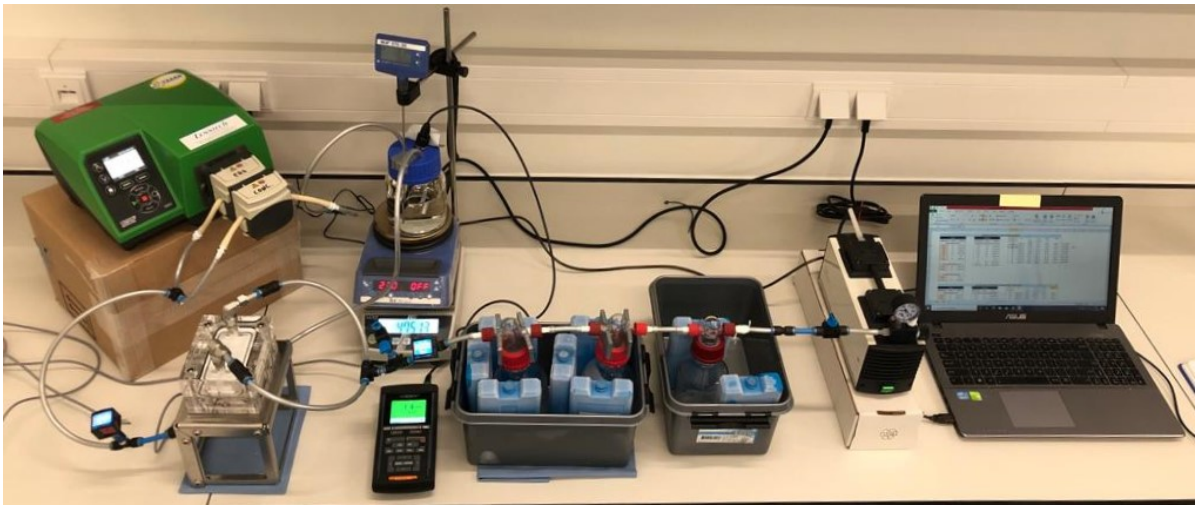

Figure B.4: Vacuum MD configuration at laboratory scale, Lenntech (Delfgauw).

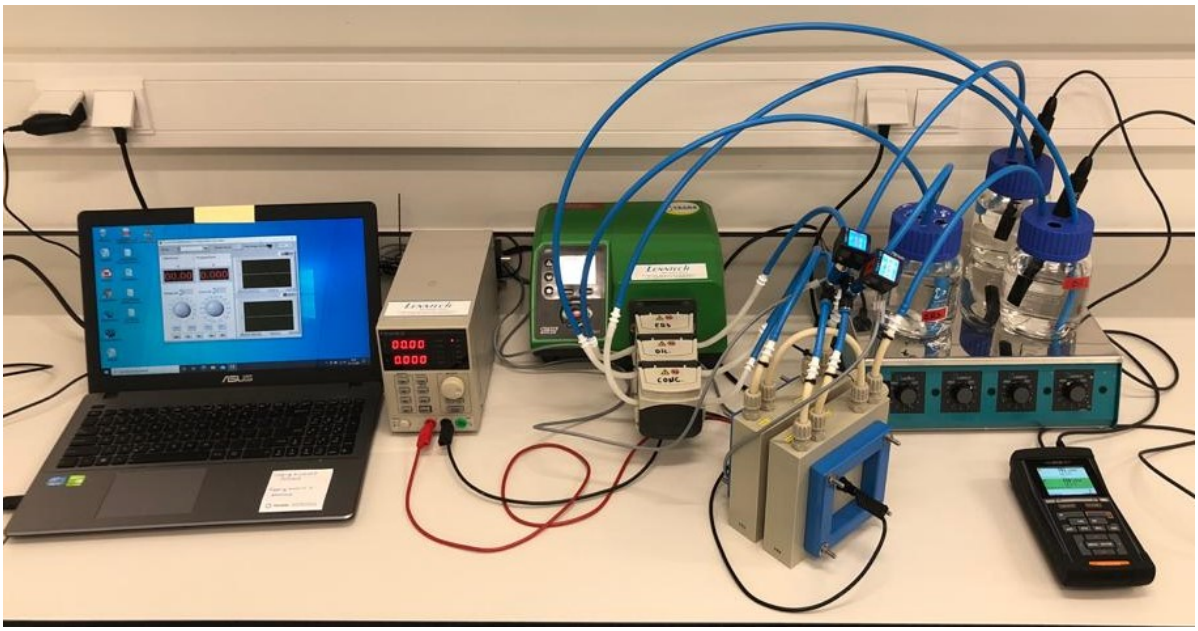

Figure B.5: Conventional ED configuration at laboratory scale, Lenntech (Delfgauw).

B.6. Superheated steam

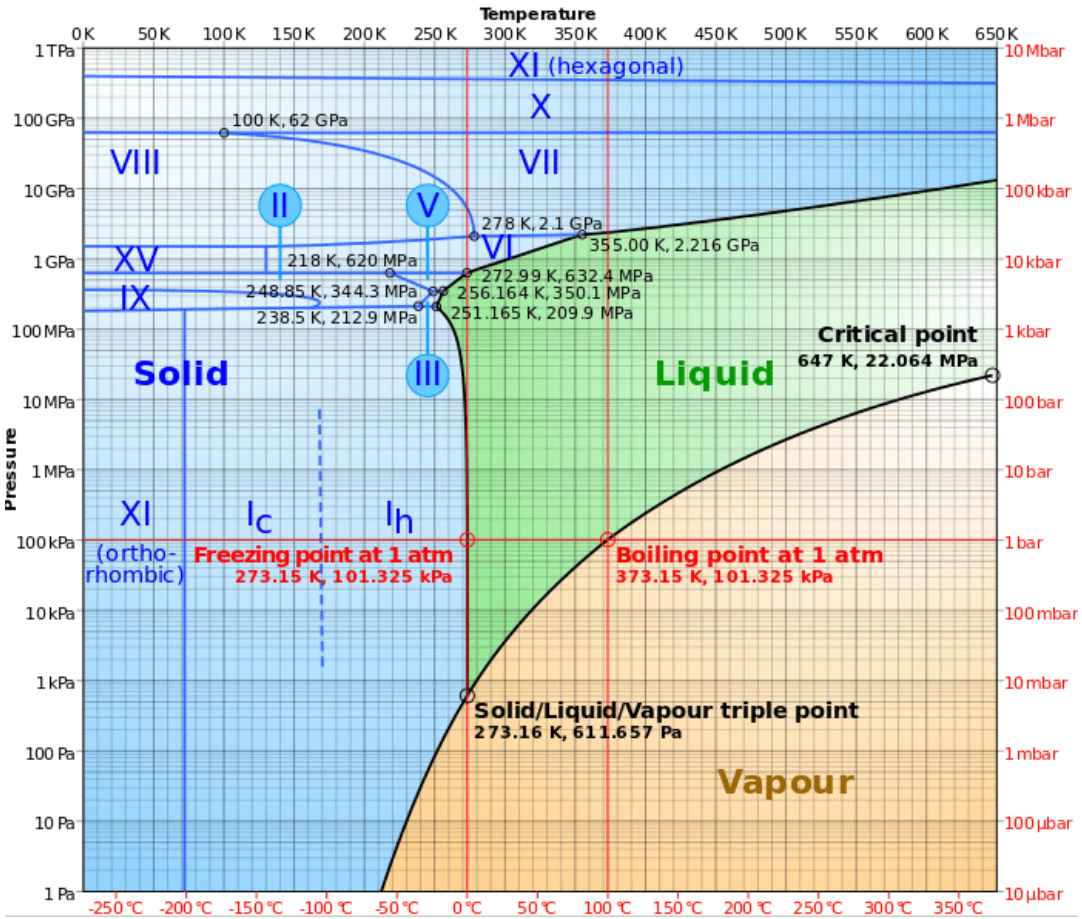

Figure B.6: Phase diagram of water. Source: *wikipedia.org CC BY-SA*

Property	Value	Unit
medium :	saturated steam	
pressure :	0.015	[bar]
boiling temperature : (calculated)	13.019743284254	[Celsius]
density water :	999.329177838	[kg / m^3]
density steam :	0.011368533417849	[kg / m^3]
dynamic viscosity water :	0.0011998809805655	[Pa s]
kinematic viscosity water :	1.2006864276308	[10^{-6} m^2 / s]
dynamic viscosity steam :	9.539518923182E-6	[Pa s]
kinematic viscosity steam :	839.11605592018	[10^{-6} m^2 / s]
specific inner energy water:	54.683642407219	[kJ / kg]
specific inner energy steam:	2392.8061314443	[kJ / kg]
specific enthalpy water :	54.685143414128	[kJ / kg]
specific enthalpy steam :	2524.7492717657	[kJ / kg]
specific entropy water :	0.19557296085579	[kJ / kg K]
specific entropy steam :	8.8270497446019	[kJ / kg K]
specific isobar heat capacity water: cp	4.191669686631	[kJ / kg K]
specific isobar heat capacity steam: cp	1.8984945323197	[kJ / kg K]
specific isochor heat capacity water: cv	4.1819050392351	[kJ / kg K]
specific isochor heat capacity steam: cv	1.4301870869614	[kJ / kg K]
isentropic exponent steam : kappa	1.325998019802	
thermal conductivity water :	0.58565954684022	[W / m K]
thermal conductivity steam :	0.017798548750692	[W / m K]
speed of sound steam :	418.27749936928	[m / s]

Figure B.7: Calculation of steam properties at 1500 Pa noa [6].